Microtubules as target of new herbicides

Zur Erlangung des akademischen Grades eines

DOKTORS DER NATURWISSENSCHAFTEN

(Dr. rer. nat)

von der KIT-Fakultät für Chemie und Biowissenschaften des Karlsruher Instituts für Technologie (KIT) genehmigte

DISSERTATION

Von

M.Sc. Kai Miadowitz

1. Referent: Prof. Dr. Peter Nick

2. Referent: Prof. Dr. Reinhard Fischer

Tag der mündlichen Prüfung: 11. Dezember 2024

Die vorliegende Dissertation wurde am Joseph Gottlieb Kölreuter Institut für Pflanzenwissenschaften (JKIP) des Karlsruher Instituts für Technologie (KIT), Lehrstuhl I für molekulare Zellbiologie, im Zeitraum von Juni 2021 bis Oktober 2024 angefertigt.

Statement

Hiermit erkläre ich, Kai Miadowitz, dass ich die vorliegende Dissertation, abgesehen von der Benutzung der angegebenen Hilfsmittel, selbständig verfasst habe. Alle Stellen, die gemäß Wortlaut oder Inhalt aus anderen Arbeiten entnommen sind, wurden durch Angabe der Quelle als Entlehnungen kenntlich gemacht. Diese Dissertation liegt in gleicher oder ähnlicher Form keiner anderen Prüfungsbehörde vor.

Zudem erkläre ich, dass ich mich beim Anfertigen dieser Arbeit an die Regeln zur Sicherung guter wissenschaftlicher Praxis des KIT gehalten habe, einschließlich der Abgabe und Archivierung der Primärdaten, und dass die elektronische Version mit der schriftlichen übereinstimmt.

Karlsruhe, den 30. Oktober 2024

Kai Miadowitz

Acknowledgement

I would like to sincerely thank …

… Prof. Dr. Peter Nick, who gave me the opportunity to do this work within his laboratory and for his constant support and important feedback. I would also like to express my thanks for his patience and help in times of crisis.

... I would like to express my gratitude to Prof. Dr. Reinhardt Fischer for agreeing to act as coreferent for this study.

… Bayer Crop Science and, in particular, to members of the KIT-Bayer Cooperation, for providing invaluable experience and the opportunity to work with this promising and fascinating substance.

... Professor Dr. Vaidurya Sahi, had I not had the opportunity to meet you, my life might have taken a different course.

... my brother, Jens, for providing me with a source of entertainment during periods of frustration..

… My father, Heinz Miadowitz, he was a great source of support for me, and I know I can always rely on him, no matter what.

… Lisa, you're the one and only.

… my mother, Andrea Miadowitz, for all the important lessons she taught me for my future. I miss you.

… Paula and Joachim for their high energy and motivation to contribute to this study. Best Bachelor students ever.

... David, for staying with the project even if results need their time, sometimes ;).

… My dear lab colleagues who keep lab life entertaining, interesting and family-like: Michael, Jathish, Nitin, Nathalie, Chris, Noemi, Wengjin, Manuel, Toranj, Javier, Nasim, Kunxi and all the others.

… Sabine and the lab’s Azubis for their constant effort to keep the lab organised.

… Pete, Jathish and Lukas for proofreading this thesis.

Stay as you are!

In the following, the AI-supported online tool DeepL (www.deepl.com, DeepL SE) was employed to rectify grammatical and orthographic errors, as well as to enhance the written presentation through partial rephrasing of the text created by me. It should be noted that the tool did not alter the content or meaning of the text given for corrections.

Zusammenfassung

Die Entdeckung von Herbiziden revolutionierte die Herangehensweise zur modernen Unkrautbekämpfung. Die hohe Effizienz und geringere Kosten führten zu exzessiver Nutzung einer Vielzahl von kommerziell erhältlichen Substanzen. Der daraus resultierende Selektionsdruck förderte die Entwicklung von Herbizidresistenzen bei Unkräutern, ein globales Problem von wachsender Bedeutung. Zur selben Zeit kam die Entwicklung neuer Herbizide mit neuen Wirkmechanismen aufgrund von Marktsättigung für die letzten 30 Jahre zum vollständigen Erliegen. Um diesem Problem entgegenzuwirken, ist eine Wiederaufnahme der Herbizidforschung unerlässlich, da bis zum heutigen Tag keine Methode mit vergleichbar hoher Effektivität bekannt ist. In dieser Arbeit wurde Icafolin, ein neues Herbizid, das von Bayer CropScience entwickelt und in naher Zukunft veröffentlicht wird, hinsichtlich seines Effekts und seines Wirkmechanismus auf zellulärer Ebene untersucht. Durch den Einsatz von Tabak-BY-2-Zellkulturen, die entweder GFP-markiertes α-Tubulin 3 oder β-Tubulin 6 überexprimieren, konnte eine schnelle und effektive Depolymerisation von Mikrotubuli bei einer geringeren Konzentration als bei herkömmlichen Mikrotubuli-Giften gezeigt werden. Nach der Entfernung von Icafolin können die Zellen in Abhängigkeit von der Expositionsdauer und der ursprünglichen Wirkstoffkonzentration Mikrotubuli regenerieren. Der Regenerationszeitraum bis zur vollständigen Wiederherstellung der Mikrotubuli ist jedoch bei Icafolinexposition deutlich länger im Vergleich zu bereits bekannten irreversibel bindenden Mikrotubuli-Hemmstoffen. Icafolin führt außerdem zum Verlust der Zellaxialität, zu radialem Anschwellen und kann die Mortalität der Zellen signifikant erhöhen. Durch Affinitätschromatographie konnten acht mikrotubuliassoziierte Proteine neben α- und β-tubulin identifiziert werden, und es wurde eine fast irreversible Bindung von Icafolin an seinen Interaktionspartner nachgewiesen. Die erhaltenen Ergebnisse deuten darauf hin, dass Icafolin einen anderen Wirkmechanismus besitzt als herkömmliche Anti-Mikrotubuli Wirkstoffe. Daher könnte die Aufklärung dessen möglicherweise zusätzlich zu einem tieferem Verständnis von Mikrotubuli und deren regulatorischem System führen. Auf Grundlage der in dieser Arbeit erhaltenen Ergebnisse werden mögliche Modelle für den Wirkmechanismus von Icafolin diskutiert.

Abstract

The discovery of herbicides revolutionised modern weed control management. The high efficacy and low costs led to excessive use of a diverse repertoire of commercially available substances. The resulting selective pressure promoted the development of herbicide-resistance in weeds, a global problem of increasing significance in recent years. Simultaneously, the development of herbicides harboring novel modes of action came to a full stop due to market saturation for the last 30 years. To be able to cope with herbicide-resistance in weeds, a revival of herbicide development is necessary, as no equally effective alternative for weed control is currently available. In this study, Icafolin, a novel herbicide developed by Bayer Crop Science and soon to be released, was investigated for its effects and cellular mode of action. Using tobacco BY-2 cell cultures expressing either GFP-tagged α-tubulin3 or β-tubulin6, Icafolin demonstrated rapid and effective microtubule depolymerisation at a threshold lower than that of common anti-microtubule agents. Removal of Icafolin allows the cells to recover from its effects, depending on exposure time and concentration, but regeneration takes longer compared to other reportedly reversible tubulin-binding agents. Exposure to Icafolin leads to a loss of cell polarity, radial swelling, and a significant increase in cell mortality, indicating herbicidal properties. To further understand the mode of action of Icafolin, affinity chromatography using agarose-coupled Icafolin was performed and revealed eight microtubule-associated proteins, alongside α- and β-tubulin, and demonstrated almost irreversible binding properties to its interaction partner. The results obtained during this study suggest for a mode of action located rather in microtubule regulation than tubulin dimer sequestration, which is the common mode of action of other anti-microtubule agents. Therefore the unraveling of the mode of action of Icafolin might also lead to a deeper understanding of microtubules and their regulatory system. Based on findings obtained during this study, potential models for the mode of action of Icafolin will be discussed.

Table of contents

Abbreviations

2,4-D 2,4-Dichlorophenoxyacetic Acid

AI Artificial Intelligence

DMSO Dimethyl sulphoxide

DTT Dithiothreitol

EPC Ethyl-N-phenylcarbamate

FABD2 aa 325–687 of *A. thaliana* fimbrin 1

FPLC Fast protein liquid chromatography

GCP γ-tubulin complex protein

GFP Green fluorescent protein

HR Herbicide-resistance/Herbicide resistant

HRAC Herbicide-resistance Action Committee

MAP microtubule-associated protein

MS Mass spectrometry

MT Microtubule

NB-Icafolin Nile Blue-Icafolin

PMSF Phenylmethylsulfonyl fluoride

PPB preprophase band

PVDF polyvinylidene fluoride

SEC Size exclusion chromatography

TCA Trichloroacetic acid

Tobacco BY-2 Tobacco Bright yellow clone 2

γTuRC γ-tubulin-containing ring complex

γTuSC γ-tubulin-containing small complex

List of Figures

List of Tables

1 Introduction

1.1 Weeds in agriculture

Weeds are in a constant competition with crop plants for nutrients, sunlight and water (Zimdahl 2013),which negatively affects the crop's growth and development (Rajcan and Swanton 2001).Weeds cause an even larger impact in terms of yield loss than all other major biological pests (**Fig.1**) (Oerke, Dehne et al. 2012). In important agronomic crops, the potential loss of crop production reaches 23 % for wheat, 30 % for potatoes, 36 % for cotton, 37 % for soy beans, 37 % for rice and 40 % for maize (Oerke 2006).Thus,sustainable weed management is important for present agriculture to prevent negative effects on yield. Common strategies to reduce the impact of weeds include the usage of herbicides, mechanical weeding and hand weeding. Hand weeding is a wide-spread technique to remove weeds, but it comes with a huge workload since it must be performed several times during growing period and is therefore difficult to apply in large scale agriculture (Jabran, Mahajan et al. 2015, Orlando, Alali et al. 2020) and returning to mechanical strategies creates losses in soil health structure. Therefore, for large scale agriculture only the usage of herbicides is a valid option in the short-term due to the lower labor cost and higher effectiveness.

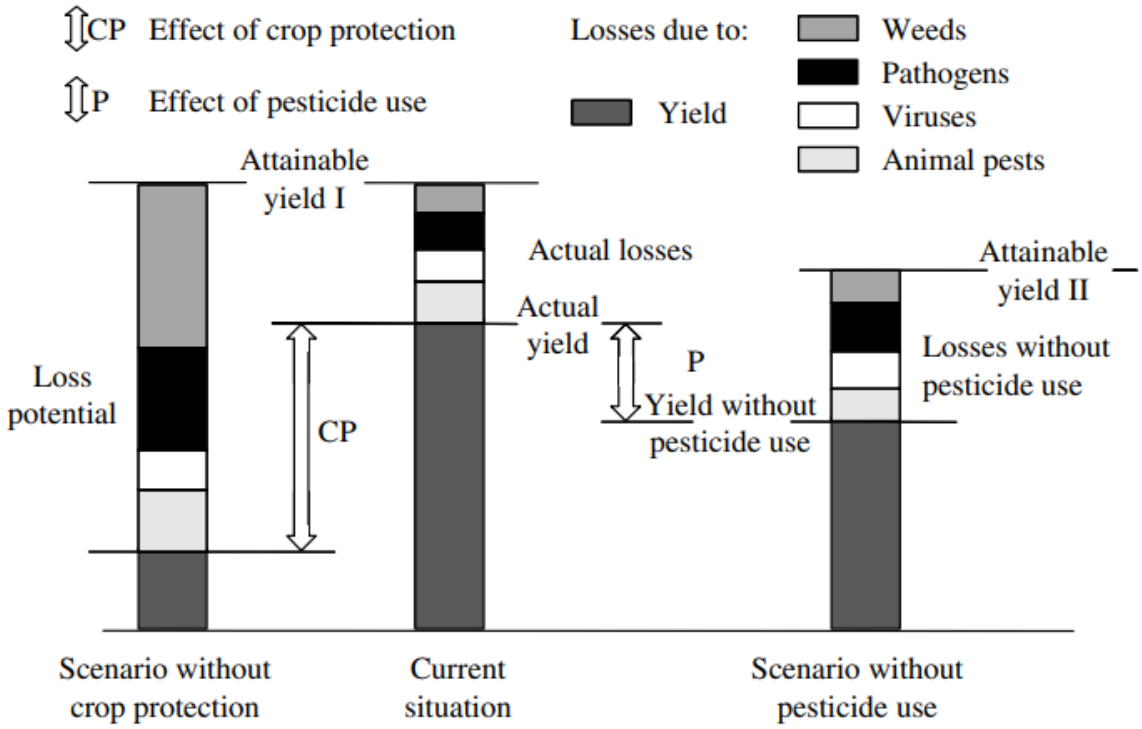

Fig. 1: Crop losses and yield levels. *The figure shows the potential loss of yield by different factors and compares it to actual losses in modern days by the use of pesticides and crop protection (reproduced with permission of Cambridge University Press from Oerke, 2006)*

1.2 Synthetic herbicides

1.2.1 History

The usage of substances to suppress the growth of unwanted plants is not an invention of modern agriculture. Already ancient Romans used, in addition to religion and witchcraft, natural compounds like salt and waste products of oil production for crop protection (Smith and Secoy 1975). In literature, the timestamp to modern herbicides is often marked by the introduction of 2,4-D (2,4-Dichlorophenoxyacetic Acid) in the 1940s (Shaner 2014). But solutions containing 6 % copper sulfate were already used in the 19th century to selectively prevent charlock (*Brassica kaber*) growth in cereal fields and sodium arsenide can be considered as the first commercially available herbicide (Mesnage, Szekacs et al. 2021). Nevertheless, the introduction of 2,4-D brought a revolution to the future usage of agrochemicals. While previous herbicides were poorly adopted by farmers due to high costs and insufficient efficacy, 2,4-D was able to overcome those issues, and the herbicide market experienced enormous growth (Peterson 1967). In the subsequent decades, a plethora of different herbicides were developed, facilitating the coverage of a broad variety of modes of action and becoming available for commercial use. Especially in the 1970s and 1980s, progress in herbicide development was achieved (Kraehmer 2012) with ten new modes of action introduced from

1970-1985 and another five between 1985 and 1991 (Schulte 2005). Afterwards, herbicide invention slowed down due to market saturation and therefore lower market potential (Rüegg, Quadranti et al. 2007, Kraehmer 2012). The cost-profit ratio seemed to be unattractive for companies. Unfortunately, herbicide development was strongly focused on the most valuable crops like maize, rice or wheat. Crops placed in smaller market niches were only covered as byproducts of those big market rulers. This could be overcome with the introduction of Herbicide-resistant crops (HR crops) in 1996. Using genetic engineering, crop plants could be protected from the toxic effects of the applied herbicide (Duke and Powles 2008). Especially Glyphosate became popular among consumers due to its broad range, high efficacy and low cost. HR crops therefore delivered efficient weed control combined with maximum convenience (Benbrook 2012). Glyphosate and Glyphosate resistance crops therefore quickly dominated the market, making Glyphosate the most successful herbicide of modern times (Duke and Powles 2008). Although the discovery of novel modes of action is stagnating, the release of substances within already-known modes of action keeps going. The focus now was not to find new chemical classes for weed suppression, but the improvement of already established ones by minor modifications or the use of crop safeners (substances to weaken the herbicidal effect on crop plants)(Green 2014). In the present day, there are 361 different herbicides distributed over a classification of 25 different modes of action (Herbicide-resistance Action Committee (HRAC), accessed 13.06.24).

1.2.2 Herbicide-resistance in weeds

While herbicides provide an easy and effective way to suppress weed growth in agriculture, excessive use also creates massive selective pressure on treated weeds and leads to herbicide-resistance (Délye, Jasieniuk et al. 2013). Although the evolution of herbicide- resistant weeds takes rather long due to the long life cycle, the first well-documented case of herbicide-resistance in weeds can be traced back to 1968 (Ryan 1970, Heap 2014). Herbicide-resistance, in general, is a natural process, where weeds undergo random mutations and eventually gain tolerance for specific herbicides. Further use of the same herbicide then generates selection for biotypes being the most tolerant up to the point at which the herbicide is no longer effective at reasonable concentrations (Heap 2014).

In general, it is possible to distinguish between five different types of herbicide-resistance:

1) Alterations in the target site of the herbicide: Mutations that alter the binding site of the herbicide, which causes lesser or lost affinity to the target. Resistance against Acetolactate synthase (ALS) inhibitors, Acetyl-CoA Carboxylase (ACCase) inhibitors and Dinitroaniline and Triazine herbicides is often facilitated by target site mutations (Powles and Yu 2010, Avila-Garcia, Sanchez-Olguin et al. 2012, Beckie and Tardif 2012, Délye, Jasieniuk et al. 2013, Heap 2014).
2) Enhanced metabolism: By enhanced metabolism of the herbicide, resistance can be achieved by fast degradation of the bioactive substance, leading to high tolerance. This resistance mechanism seems to be one of the major causes of resistance against ACCase and ALS inhibitors (Powles and Yu 2010, Beckie and Tardif 2012, Délye, Jasieniuk et al. 2013, Heap 2014).
3) Decreased absorption and translocation: By altering the rate of absorption or hindering the herbicide from reaching its target, tolerance can be gained. This seems to be the case, especially for cases of resistance to Glyphosate and Photosystem I inhibitors (Délye, Jasieniuk et al. 2013, Heap 2014).
4) Compartmentalisation: Sequestering of the active compound by specific proteins can cause herbicide-resistance in weeds (Yuan, Tranel et al. 2007, Délye, Jasieniuk et al. 2013, Heap 2014).
5) Overexpression: By altering the expression and translation level of the target protein, higher quantities of herbicides are needed to achieve the same inhibitory effect. Therefore, overexpression can lead to herbicide tolerance (Heap 2014).

As mentioned above, mechanisms of herbicide-resistance are diverse. While target site-specific alterations (1;5) can lead to tolerance against a single herbicidal mode of action, the development of non-target site-based resistance (2-4) can affect the efficiency of even more than one herbicide at once, including the market dominant Glyphosate (Pratley, Urwin et al. 1999, Heap and Duke 2018). Herbicide-resistant weeds have become a serious issue for future agriculture, and at the time of this study, 531 cases of resistance against several herbicides have been documented (**Fig. 2, Fig. 3**) (www.weedscience.org, accessed 14.06.24).

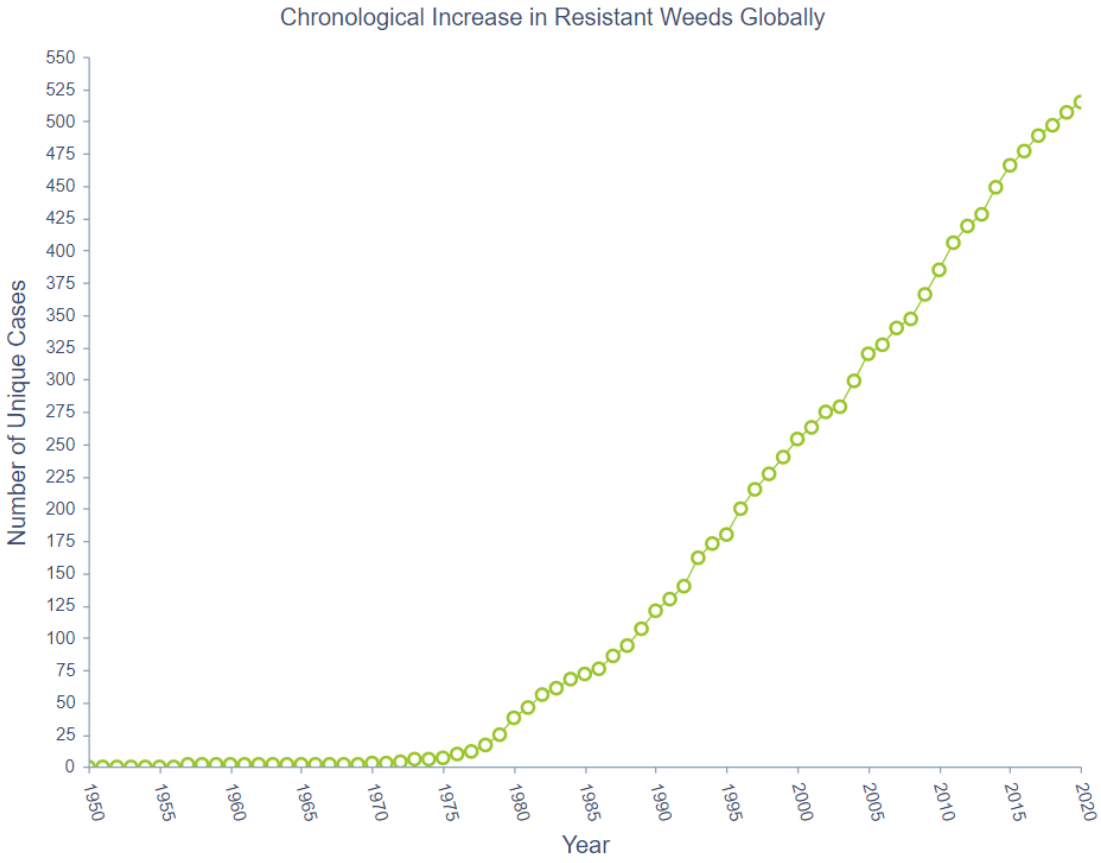

Fig. 2: Chronological Increase in Resistant Weeds Globally. *Documentation about the number of weed species resistant against one or more herbicide classes from 1950 until 2020 (reproduced with permission of Dr. Ian Heap, www.weedscience.org, accessed 15.06.24).*

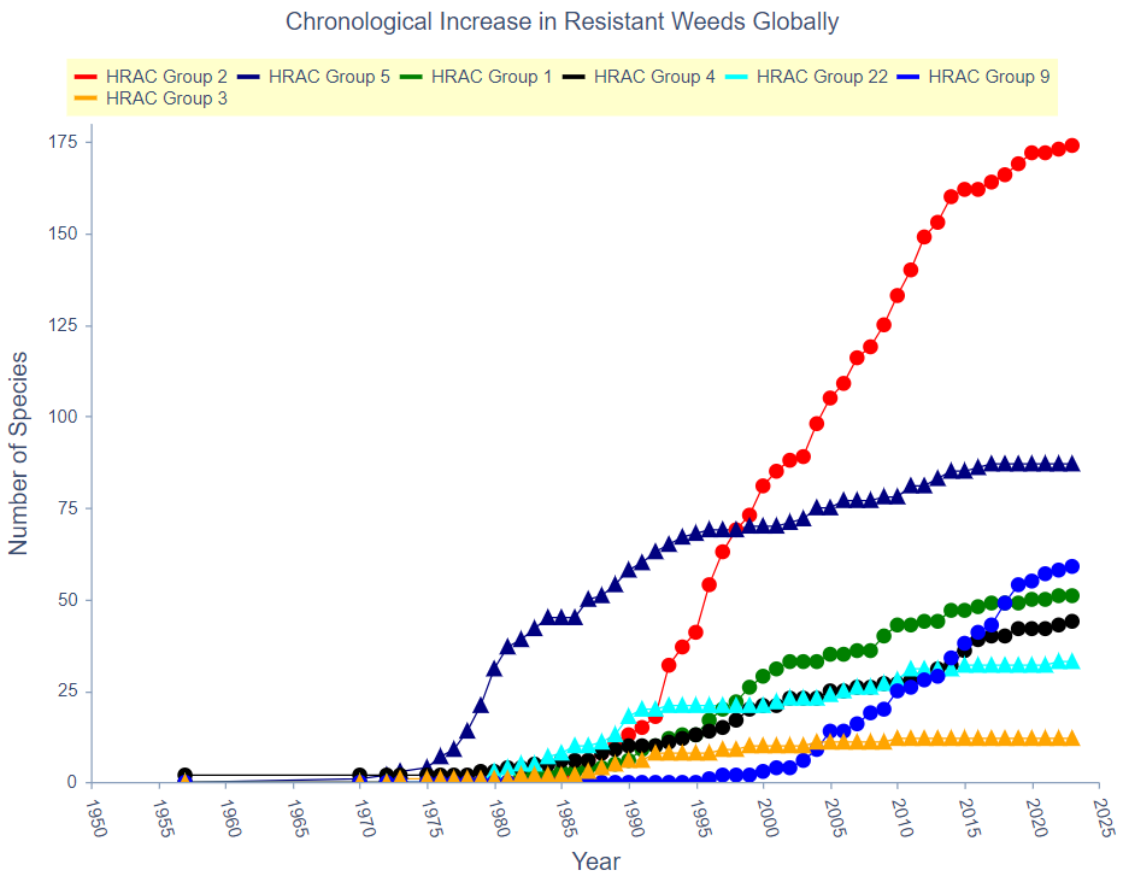

Fig. 3: Chronological Increase in Resistant Weeds Globally. *In this chart, the number of individual herbicide-resistance cases about specific HRAC modes of action can be observed (reproduced with permission of Dr. Ian Heap, www.weedscience.org, accessed 15.06.24).*

1.2.3 Need for novel herbicide mode of actions and criteria to be met

As mentioned before, the boom of herbicide invention can be dated to the 1970s and 1980s. Afterwards the identification of new chemical classes inhibiting critical biological processes in plants slowed down and came to an end in 1991. In 30 years, only a single new mode of action could be introduced and classified by HRAC in 2021 (**Fig. 4**) (www.weedscience.org accessed 15.06.24). However, the rise in numbers of herbicide-resistant weeds becoming resistant to more and more herbicide classes has caused a demand for novel modes of action to cope with them (Qu, He et al. 2021). In the meantime, the high efficiency of herbicides led to a great loss of knowledge when it comes to weed control strategies of growers abroad herbicides due to lack of necessity in practicing other strategies than herbicidal ones (Heap 2014). The use of one single herbicide year after year was successful for quite a long time but eventually led to the selection of more and more herbicide-resistant weeds. One possible approach for the future could be to use herbicide mixtures in agriculture, but the used herbicides would have to be equally efficient in the present weed to suppress HR evolution in weeds (Heap 2014, Hachisu 2021, Ofosu, Agyemang et al. 2023). Since this would also cause higher costs for farmers, it is not adopted easily. Additionally, it would need to involve

different weed control strategies complementing herbicide usage (Ofosu, Agyemang et al. 2023), and farmers would require re-education and easy access to information on strategies to suppress the evolution of herbicide-resistance in weeds (Heap 2014). The revival of the search for new modes of action for herbicides has already started, and investments in herbicide research and development are increasing (Hachisu 2021). Nevertheless, there are also high expectations new herbicides must meet to be successful. A promising herbicide should be highly selective for plants, should be target-specific, maintain low toxicity, act in low concentrations and have a low impact on the environment (Qu, He et al. 2021).

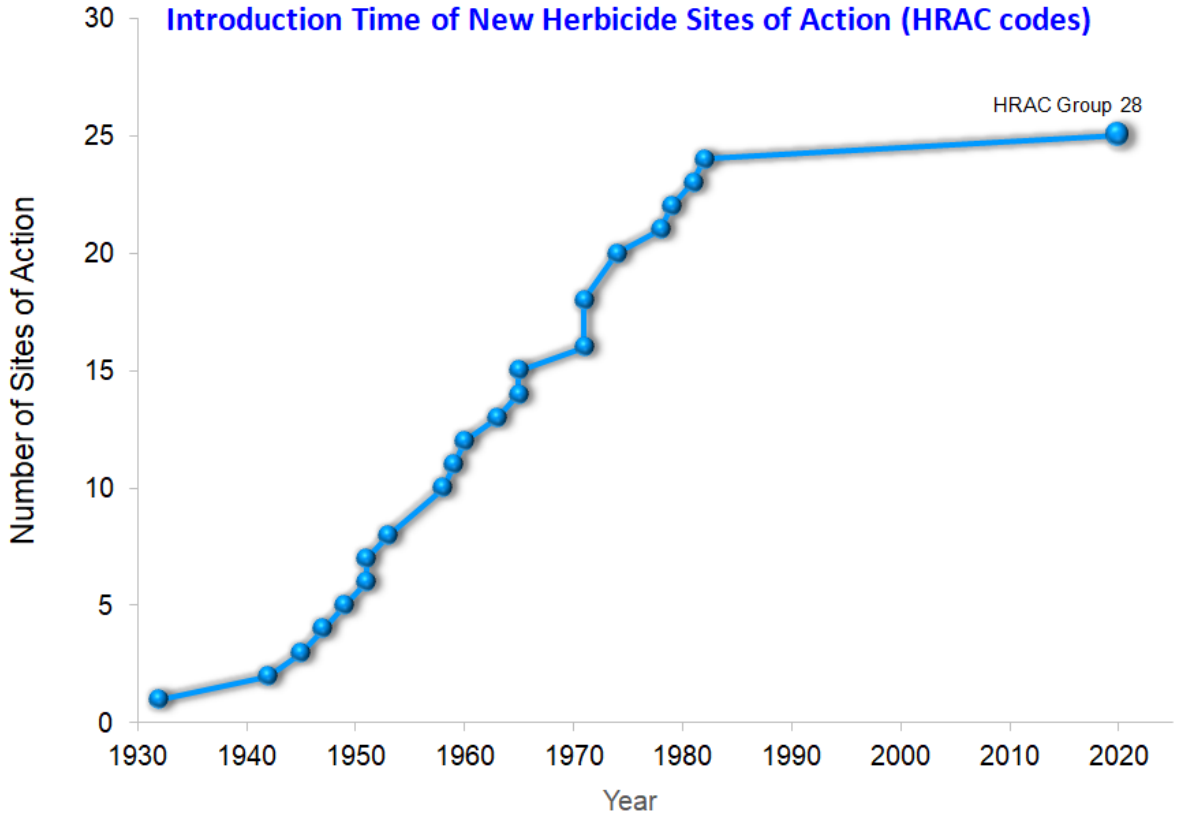

Fig. 4: Introduction Time of New Herbicide Sites of Action (HRAC codes). *Introduction of new herbicide modes of action slowed down and eventually stopped completely. The company FMC with Tetfluorpyrolimet could achieve the first discovery of a new herbicide mode of action for 30 years in 2021, classified by HRAC as HRAC Group 28 (reproduced with permission of Dr. Ian Heap , www.weedscience.org, 2021).*

1.2.3.1 Icafolin

The characterisation of Icafolin (**Fig. 5**) will be the aim of this work. As mentioned before, the industry has begun a renewed investment in herbicide research and development. Also, Bayer Crop Science is involved in this process and was able to develop a new herbicide called Icafolin-Methyl. Bayer reported a high efficiency of Icafolin-Methyl during field testing and observed high efficiency even at extremely low concentrations. The mode of action is hypothesised to be microtubule-related, but evidence is lacking. Although there are other anti-microtubule agents, like Dinitroanilines, Carbamates, Phosphoroamidates, and Pyridines, the mode of action for Icafolin-Methyl could be a different one than identified in those.

As stated by Bayer, Icafolin-Methyl is absorbed by the plant cell and quickly metabolised to its active form, Icafolin, which is the acidic metabolite of Icafolin-Methyl, which is hypothesized to cause alterations in the microtubule behavior.

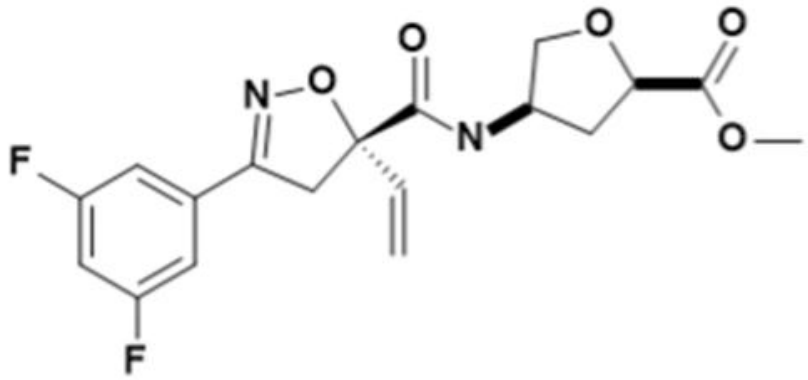

Fig. 5: Structure of Icafolin-Methyl. *Novel substance designed by Bayer Crop Science for herbicidal purposes. The mode of action is not clear to the present day, but it is hypothesised to act against microtubules.*

1.3 Microtubules

Microtubules are thin, hollow structures with a diameter of 25 nm. Together with actin filaments, microtubules are a component of the plant cytoskeleton. Intracellular mechanisms, involving microtubules are quite diverse, making microtubules critical structures for cell health and functionality. This Chapter will give information about microtubules in general, from historical research to intracellular function and the consequences if microtubule integrity is inhibited.

1.3.1 Microtubules in plants – a summary of discovery

Already in 1888, pictures of microtubules were obtained by Ballowitz, who detected "Elementarfibrillen" in partially dissociated flagella of bird sperm (**Fig. 6**) (Ballowitz 1888). For plant cells, the first detection can be traced back to the year 1950, when Irene Menton investigated cilia of sperm cells of the moss *Sphagnum acutifolium* and visualised them by ultraviolet microscopy, revealing they are bundles of threads, numbered to be roughly ten (Manton 1950). It was also Menton, together with Clarke, who were able to obtain the first electron microscopy pictures of plant microtubules, although they did not recognise them as such (Manton and Clarke 1952). In 1962, Paul Green predicted, due to indirect observations of the mechanism of plant cell elongation, the involvement of proteins located at the plant cell cortex in the control of the orientation of cellulose fibres (Green 1962). Shortly after, Ledbetter and Porter were able to visualise and describe thin, hollow structures in the mitotic spindle and the cortex of plant cells by electron microscopy and named those microtubules (Ledbetter and Porter 1963). They observed the occurrence of sub-units within a microtubule and shortly after were able to visualise 13 protofilaments, assembling the structure of a single microtubule (Ledbetter and Porter 1964). Ledbetter and Porter were able to show the occurrence of microtubules at the mitotic spindle apparatus during cell divison. Therefore Colchicine, known to inhibit proliferation of cells by disruption of the spindle apparatus, was used to identify the composition of those protofilaments on the protein level. By affinity approaches, α- and β-tubulin were identified as the heterodimer forming the building blocks of microtubular protofilaments (Weisenberg, Broisy et al. 1968).

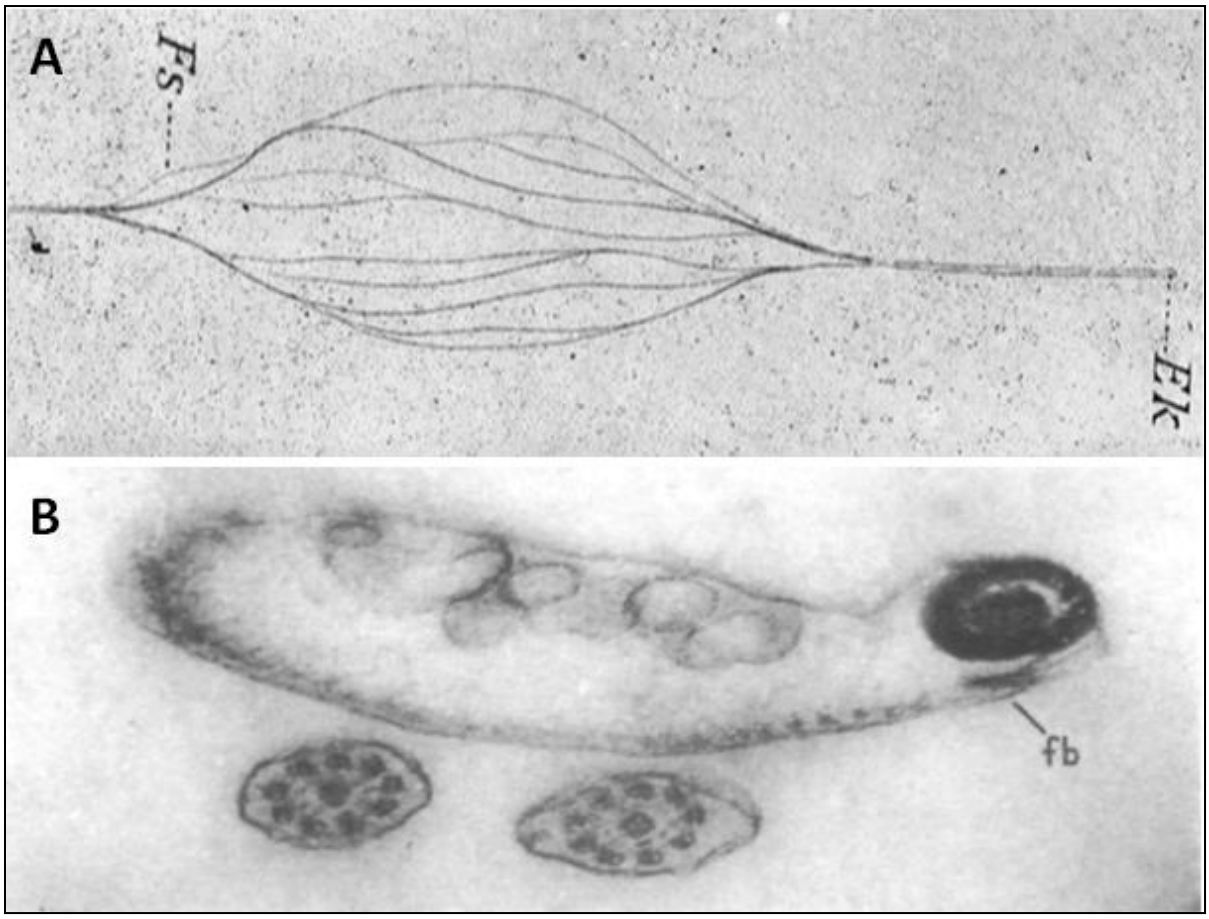

Fig. 6: Early observations of microtubules. *A: Microtubules observed by Ballowitz in dissociated flagella of bird sperm (Ballowitz 1888). B: Early electron microscopy images of microtubule cross Chapters from moss sperm cell cilia (reproduced with permission of Oxford University Press from Manton (Manton 1957).*

1.3.2 Microtubules – Structure

Microtubule structures can be broken down into (1) the polymerised tubules with an average diameter of 25 nm, which is a hollow cylindric structure consisting of 13 parallel aligned protofilaments (2) (Ledbetter and Porter 1964). Protofilaments again are assembled by dimers of α- and β-tubulin sub-units (3) (Weisenberg, Broisy et al. 1968). Additionally, microtubules maintain a polarity, which is defined as a positive and negative end, whereby the end exposing the β-tubulin sub-unit is considered as positive (“plus end”) and contrary, exposing the α-tubulin sub-unit as the negative end (“minus end”) (Hashimoto 2015). When protofilaments align to form the microtubule cylinder, they produce a B-Type lattice, meaning lateral interactions between protofilaments are mediated by α-tubulin – α-tubulin or respective β-tubulin – β-tubulin forming helices with a seam (**Fig.7**).

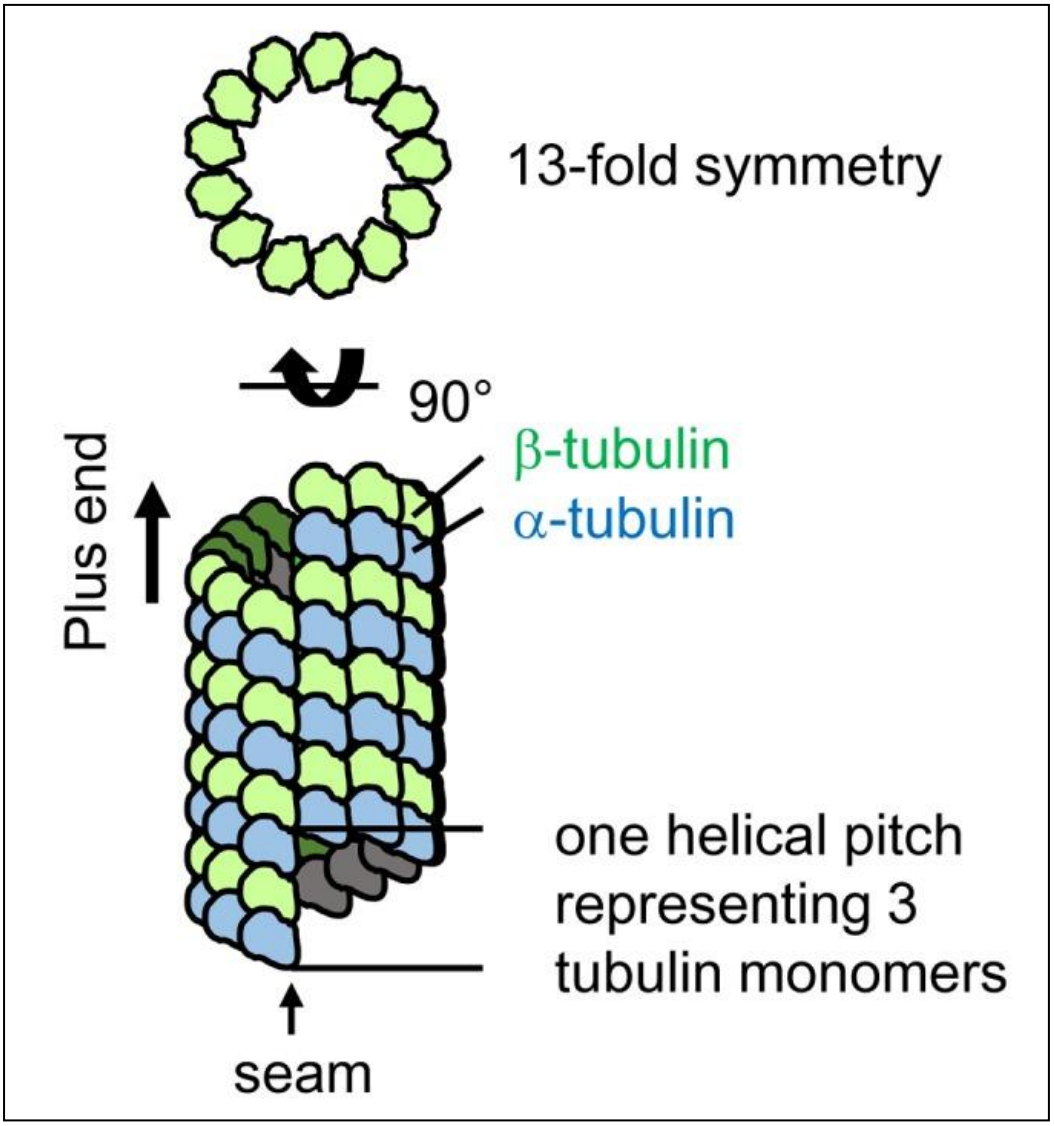

Fig. 7: Microtubule structure. *Eukaryotic microtubules are commonly composed of 13 parallely aligned protofilaments, forming a symmetric cylinder. Protofilaments are assembled by α- and β-tubulin dimers. The polarity of microtubules is defined by the exposure of the respective tubulin subunit, whereby β-tubulin marks the plus end and α-tubulin the minus end. Lateral interactions of protofilaments are mediated by α-tubulin – α-tubulin or respective β-tubulin – β-tubulin interactions, which are arranged in helical pitches. (reproduced with permission of Hasimoto 2015).*

Commonly in eukaryotes, there are 13 protofilaments assembling to a microtubule. However, variable numbers of protofilaments in the range of 8-20 could be observed *in vitro* (Böhm, Vater et al. 1984, Chrétien and Wade 1991) as well as *in vivo* (Dallai and Afzelius 1990, Dallai, Lupetti et al. 2006). It is assumed that the possibility of incorporating different numbers of protofilaments enables the microtubule to bend due to lateral deformation (Sui and Downing 2010).

Since microtubules are part of the cytoskeleton, one could imagine they appear as static structures within the cell, although the separation of chromosomes by the spindle apparatus indicated a dynamic nature already. With the introduction of fluorescently labeled proteins, evidence for the dynamic nature of microtubules could be achieved *in vitro* (Horio and Hotani

1986) as well as *in vivo* (Sammak and Borisy 1988). Microtubules undergo cycles of polymerisation and depolymerisation events, referred to as the dynamic instability model postulated by Kirschner (Mitchison and Kirschner 1984).

Protofilaments are assembled by the addition of tubulin dimers. The tubulin dimer itself is composed of a α-tubulin and a β-tubulin sub-unit. Each of the sub-units can interact with one GTP. For α-tubulin, the GTP is bound at the interaction site with its respective β-tubulin sub-unit (N-Site) (Nogales, Wolf et al. 1998). This GTP molecule is not exchangeable and is considered to play a critical role in the dimer's structure. GTP bound to β-tubulin is located at the outer surface of the protein (E-Site). This GTP is exchangeable, and in the state of a free tubulin dimer (not polymerised in a microtubule), GDP is quickly exchanged with GTP. When it comes to a polymerisation event, α-tubulin interacts with the GTP located at the E-site of the protofilaments plus end β-tubulin, mediating a GTPase activating function, which leads to hydrolysis of the E-site GTP to GDP after contact. In this way, a GTP cap at the plus end of protofilaments and microtubules is maintained (**Fig. 8**) (Hashimoto 2015). Altering the GTPase activating properties of α-tubulin by mutation leads to highly stable microtubules, which indicates hydrolysis of GTP to GDP is linked to microtubule depolymerisation due to a small conformational change which strains the microtubule lattice (Ishida, Kaneko et al. 2007). Therefore, the plus-end GTP cap contributes to microtubule stabilisation. In growing microtubules, GTP hydrolysis slightly lags the incorporation of new tubulin dimers, and the GTP cap can be maintained. If the cap is lost due to paced-out hydrolysis or stochastic dissociation of GTP, the microtubule becomes unstable and depolymerises rapidly (Mitchison and Kirschner 1984). In dynamic microtubules, the depolymerising state can be rescued, and a shrinking microtubule is stochastically able to switch back to a growing status. Dimitrov *et al.* were able to show that not all GTP molecules along the microtubule are hydrolysed to GDP. This could be shown *in vitro* as well as *in vivo*. Those GTP remnants are located in a spot-like manner along the microtubule longitudinal axis and are considered to trigger the rescue event when reached by a shrinking microtubule (**Fig. 8**) (Dimitrov, Quesnoit et al. 2008).

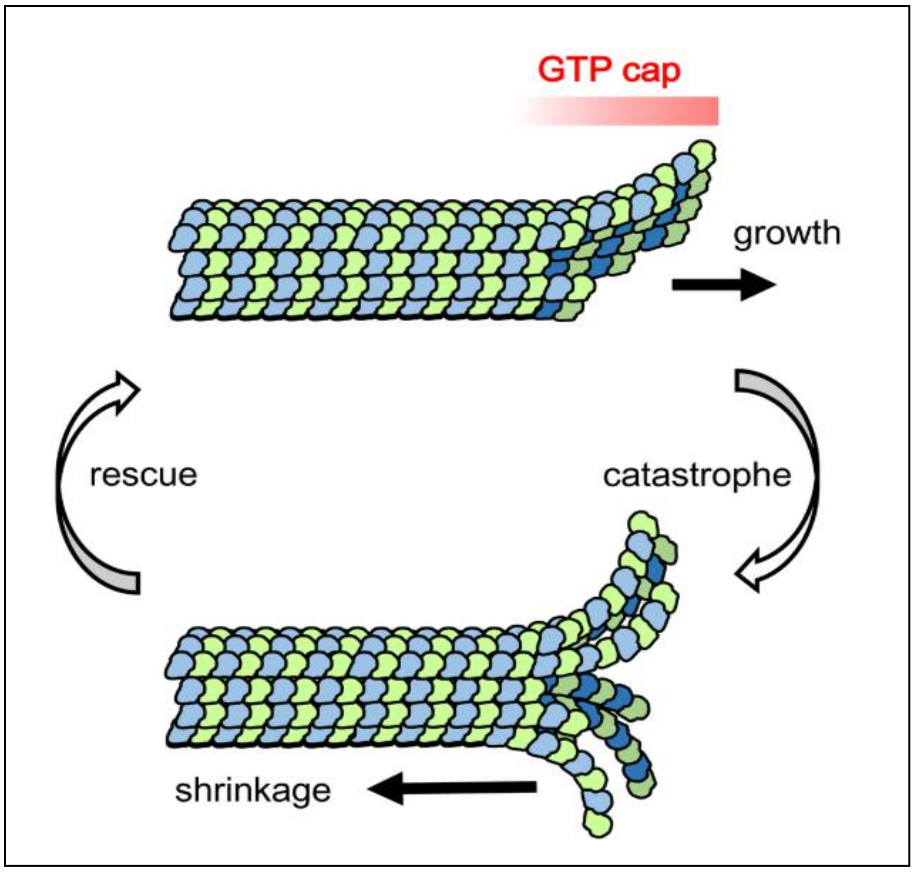

Fig. 8: Dynamic instability of microtubules. *At the same time, the GTP cap is maintained by the progressive addition of GTP-tubulin. If the GTP cap is lost, small conformational changes lead to strain in the microtubule lattice and result in rapid depolymerisation. If the GTP cap can be restored, the microtubule growth is rescued, and the transition back to a growing state is achieved (reproduced with permission of Hashimoto 2015).*

1.3.3 Important plant microtubule arrays

1.3.3.1 Cortical microtubules

In interphase plant cells, the most prominent microtubule population is located close to the plasma membrane at a distance of several nanometers (Ledbetter and Porter 1963). This microtubule array is commonly referred to as cortical microtubules. One major function of those cortical microtubules is the guidance of the cellulose synthase complex, which moves along cortical microtubules while synthesising β-1,4-glucan chains (Paredez, Somerville et al. 2006), which subsequently combine to cellulose microfibrils when hydrogen bonds are formed between them. The orientation of these microfibrils guides plant cell growth direction during cell elongation by reinforcement of the cell wall along the longitudinal growth axis, preventing radial expansion of the cell (Baskin 2001) during water uptake. If cortical microtubules lose their integrity, for example, due to microtubule destabilising drug treatment, cells are not able to maintain their growth axis, resulting in immense cell swelling (Noodén 1971).

1.3.3.2 Mitotic microtubules

During mitosis, a whole set of microtubule arrays are formed, orchestrating crucial tasks necessary for successful cell division (**Fig. 9**). Cortical microtubules disassemble during preprophase and relocate to a specific site in a ring structure, slightly offset to the nucleus' periphery, forming the preprophase band (PPB) (Hashimoto 2015). The nucleus then migrates towards the PPB to become centred within the PPB ring. During this process, PPB microtubules could be observed to connect to the nuclear envelope (Granger and Cyr 2001). In cells dividing symmetrically, the PPB is commonly located at the cell's equator, determining the future division plane of the cell (Rasmussen, Humphries et al. 2011). This procedure is dependent on the nucleus' position, as experiments relocating the nucleus intentionally lead to the following of the PPB (Burgess and Northcote 1968). For asymmetrically dividing cells, polarity is generated by actin-dependent mechanisms before mitosis, which overrides the rules applied for symmetrically dividing cells (Rasmussen, Humphries et al. 2011). Migration of the nucleus is mediated by actin filaments and centring of the nucleus in the PPB plane is not necessary (Kennard and Cleary 1997).

Upon reaching prophase, microtubules form the perinuclear spindle after nuclear envelope breakdown and just before the PPB starts to disassemble. When the PPB disassembles, it leaves behind molecular markers at its original position. Those markers will remain at their location during cytokinesis and guide the centrifugal expansion of the cell plate in later stage (Van Damme 2009).

After PPB disassembly, the mitotic spindle apparatus is formed perpendicular to the prior PPB plane. The spindle polarity is defined by the microtubule minus ends, which are overlapping but not connected to a specialised organising centre as found in animal cells. During anaphase, spindle microtubules are disassembled, forming a bipolar microtubule array at the spindle midzone when late anaphase to telophase is reached, separating the daughter chromosomes by pulling them towards the spindle poles (Hashimoto 2015).

In telophase, the spindle microtubules transform into another microtubule array, the phagmoplast, which is involved in synthesising the cell plate (Lee and Liu 2013). During cell plate synthesis, a sub-population of microtubules located at the division site overlaps, stabilising the whole phagmoplast array (Ho, Hotta et al. 2011) while the Golgi-derived vesicles are transported along the structure to deliver cell wall material. During this procedure, the phragmoplast expands in a centrifugal manner towards the molecular markers left behind by the PPB earlier. During this process, the expanding phragmoplast is stabilised by novel polymerised overlapping microtubules in the phragmoplast periphery while microtubules at the centred phragmoplast structure are disassembled (Murata, Sano et al. 2013).

After the generation of the cell plate, the phragmoplast disassembles, and novel cytoplasmic microtubules are promoted by the nuclear envelope of the newborn daughter cell. Those microtubules then extend to the plasma membrane to form new cortical microtubule arrays (Ambrose and Wasteneys 2014).

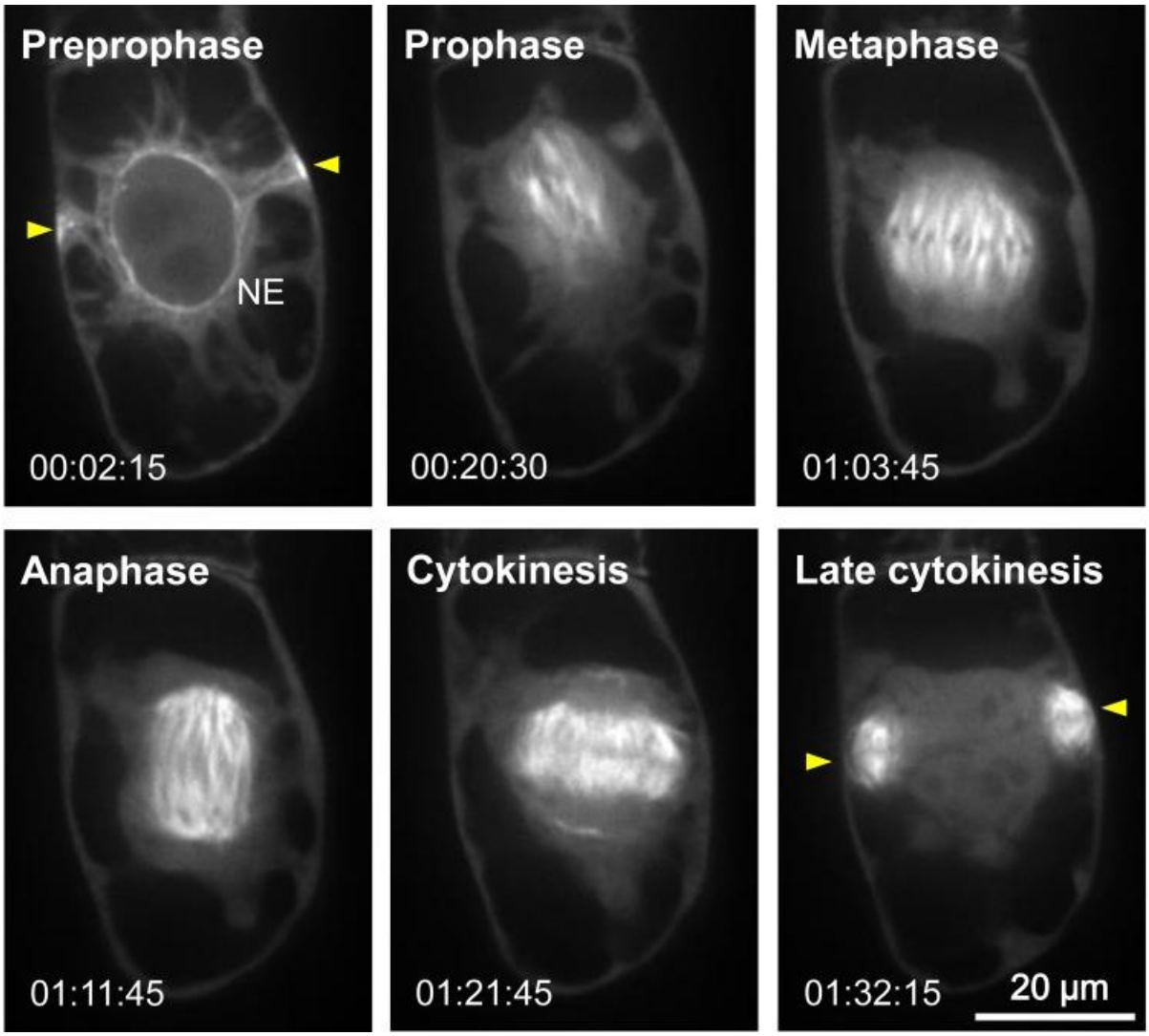

Fig. 9: Microtubules in cell division. *During preprophase, cortical microtubules disassemble, and the PPB is formed near the nuclear envelope, predicting the future division plane already (yellow arrowheads). At prophase, PPB disassembles, and perinuclear spindle microtubules are established perpendicular to the division plane. In metaphase, the mitotic spindle matures and aligns with corresponding chromosomes in the spindle centre. Spindle microtubules then disassemble during anaphase, separating the daughter chromosomes towards the respective spindle pole. Reaching cytokinesis, spindle microtubules transform into the phragmoplast array, guiding Golgi-derived vesicles to the division plane to establish the cell plate. The phragmoplast expands centrifugally until it eventually reaches the position specified by the PPB earlier (yellow arrowheads) (reproduced with permission of Hashimoto 2015).*

1.3.4 Microtubule nucleation in plants

In contrast to animal cells, microtubule (MT) nucleation in plants takes place without the presence of centrosomal nucleation centres but is located at particular nucleation sites. In general, three nucleation sites are common in plants. In interphase cells, nucleation mainly occurs at pre-existing cortical microtubules, resulting in microtubule branching. Branching site daughter microtubules can spread at an angle of up to 40°, but a parallel course of mother and daughter MT can also be observed, resulting in microtubule bundling. Additional nucleation sites in plants are the nuclear envelope (for example, during the transition of the mitotic array to the cortical right after mitosis; see **Chapter 1.4.3.2**) or the plasma membrane.

Although MT nucleation in plants differs from that in animals, the protein complex mediating nucleation events remains similar. The γ-tubulin-containing ring complex (γTuRC) consists of γ-tubulin and up to five distinct proteins called γ-tubulin complex proteins (GCPs) (Kollman, Merdes et al. 2011). Within this complex, GCP2 and GCP3 interact with one γ-tubulin molecule each and form the smaller sub-complex γ-tubulin-containing small complex (γTuSC). In models, GCP2 and/or GCP3 can be replaced by other GCP proteins (GCP4-6), resulting in several γTuSC-like varieties (Kollman, Merdes et al. 2011). Seven γTuSC or γTuSC-like complexes then assemble helically to γTuRC. The first and seventh sub-units of the γTuRC each overlap half in their width, creating a perfect template for microtubules consisting of 13 protofilaments and their three monomer offset (resulting from the helical twist) at the minus pole (**Fig.10**) (Hashimoto 2015). The presence of γTuRC is crucial for cell viability, as loss of function in Arabidopsis leads to lethality and partial knock-down of specific complex components cause inhibition of MT nucleation (Hashimoto 2013).

Although γTuRC is the priming complex for MT nucleation and can be found in most nucleation events in plants, its positioning and activation have to be regulated to prevent uncontrolled MT generation within the cell, and those processes are hypothesised to be connected (Kollman, Merdes et al. 2011, Kollman, Greenberg et al. 2015). One of the most studied γTuRC regulators is Augmin, which is a protein complex consisting of eight distinct proteins and is known to increase MT quantity independent of centrosomes in the mitotic spindle in animals (Goshima , Mayer et al. 2008). In *Arabidopsis thaliana* cells, homologs and functional homologs of proteins present in the animals' Augmin complex are required for MT-dependent nucleation in the spindle, the phragmoplast (Kimmy Ho, Hotta et al. 2011) and branching events in interphase cortical microtubules (Liu, Tian et al. 2014).

Furthermore, the interaction between γTuRC and Augmin is mediated by NEDD1 (Neural precursor cell expressed, developmentally down-regulated protein 1) (Goshima and Kimura

2010), and the presence of NEDD1 is required for MT assembly in the spindle apparatus, the phragmoplast and cortical microtubules (Zeng, Lee et al. 2009).

Another regulating protein is an 8kD protein called Mitotic-spindle organising protein associated with a ring of γ-tubulin 1 (MOZART1). MOZART1 is necessary for MT nucleation in fission yeast (Masuda, Mori et al. 2013), humans (Hutchins, Toyoda et al. 2010) as well as in *Arabidopsis thaliana* (Janski, Masoud et al. 2012, Nakamura, Yagi et al. 2012). In fission yeast, the absence of MOZART1 does not impede the formation of γTuRC. MOZART1, therefore, is likely active in the peripheral regulation of γTuRC (Hashimoto 2015).

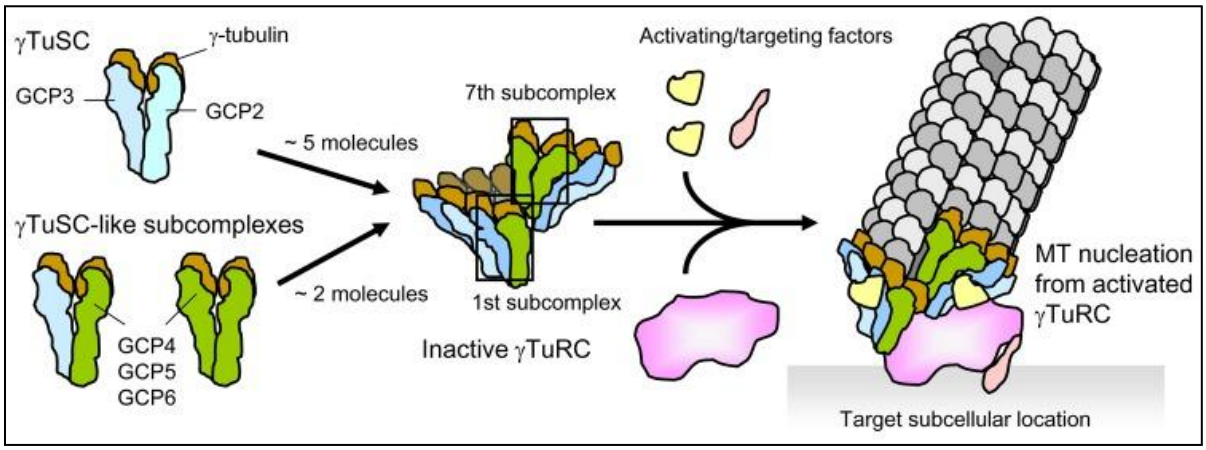

Fig. 10: γTuSC , γTuRC and microtubule nucleation. *The smaller subcomplex γTuSC is commonly composed of GCP2 and GCP3, with one of each binding one single γ-tubulin. The exchange of one or both GCP2 or GCP3 results in γTuSC-like subcomplexes, delivering variety. Seven of γTuSC or γTuSC-like subcomplexes assemble helically to the bigger complex γTuRC, whereas the first and seventh subcomplex are shifted by half of their width, providing a perfect template for a standard 13 protofilament microtubule. Nucleation activity is mediated by additional regulatory proteins like the Augmin complex, NEDD1 or MOZART1 (reproduced with permission of Hashimoto 2015).*

1.3.5 Microtubule-associated proteins

As illustrated before, microtubules are essential for the maintenance of crucial intracellular processes. Therefore, a strict and constant regulation of microtubule organisation must be performed by the cell. One major part of microtubule regulation takes place by interaction with microtubule-associated proteins (MAPs), which are involved in orchestrating microtubule dynamics (Umeyama, Okabe et al. 1993), interaction with other cell organelles (Leterrier, Linden et al. 1990) or other parts of the cytoskeleton (reviewed by Mohan (Mohan and John 2015)), crosslinking (resulting in bundling) (Gaillard, Neumann et al. 2008), microtubule protection (Goodwin and Vale 2010), intracellular transportation (reviewed by Sweeney (Sweeney and Holzbaur 2018)), signalling (reviewed by (Nick 2013)) and microtubule assembly (Desai and Mitchison 1997). While fundamental MAPs are shared within eukaryotes

and are highly conserved, there are unique MAPs in plants, which are adapted to their specific physiology and morphology (Gardiner 2013).

A large number of MAPs are located at the MT lattice, and binding is, on the one hand, thought to be mediated by an enrichment of basic amino acid residues in their MT binding domain, which can interact with the highly acidic C-terminus of tubulin (Paschal, Obar et al. 1989), but a wide variety of MAPs is also able to bind to the MT surface by other, unrelated binding modes (Hashimoto 2015). The importance of MAPs for cell viability and development becomes clear when knockout experiments of different MAPs are performed. For a short impression, complete knockout of the Kinesin ATK5 leads to spindle defects during mitosis (Ambrose and Cyr 2007), temperature-sensitive mutants of MOR1 (member of the XMAP215 family) in *Arabidopsis thaliana* show defects in cortical microtubule organisation (Whittington, Vugrek et al. 2001), and the homozygous MOR1 mutant *Gemini pollen 1* (*gem1*) causes lethality which is hypothesised to be connected to impeded cytokinesis (Twell, Park et al. 2002). Therefore, the alteration of the set of microtubule-associated proteins by interaction with novel herbicides could lead to effective growth inhibition caused by the disturbance of microtubule regulation. Additionally, targeting plant-specific MAPs would deliver specificity to the herbicide.

1.3.6 Microtubule affecting drugs and consequences for cell viability

Drugs targeting microtubules are commonly used in cancer treatment as well as weed control. They can be categorised by their function as either microtubule stabilising or destabilising agents. Microtubule stabilisers, like Taxol, for instance, act via enhancement of lateral interactions of protofilaments or prevention of microtubule curvature after hydrolysis of GTP-tubulin to GDP-tubulin leading to a lower concentration of tubulin needed to promote microtubule assembly (Field, Díaz et al. 2013).

Depolymerising agents, on the other hand, promote microtubule disassembly by inducing microtubule curving or inhibiting a straight MT lattice (Hashimoto 2015). Additionally, the binding site of dinitroaniline herbicides like Oryzalin could be found to bind the αβ-tubulin dimer at the respective α-tubulin, preventing further incorporation of Oryzalin- αβ-tubulin complexes into growing microtubules by sequestering and therefore limiting the pool of tubulin available for microtubule assembly. Another chemical class which binds tubulin are benzamides, including the herbicide Propyzamide. These molecules can bind at the β-tubulin interface of the αβ-tubulin dimer.

Disturbance of the microtubule network in plants results in spectacular phenotypic effects. Since microtubules are necessary for proper cellulose fibre organisation, loss of microtubules due to depolymerising agents leads to malfunction of the cell wall and subsequent cell swell-

ing during cell elongation (Baskin, Wilson et al. 1994). Of course, due to the high importance of microtubules in cell division processes, high-proliferating plant regions harbouring meristems, like root tips, are typically more severely affected (Morejohn, Bureau et al. 1987), resulting in the breakdown of plant viability.

1.4 Aim of the work

As illustrated, the usage of herbicides and the evolvement of herbicide resistance in weeds are closely connected. To be able to provide a sufficient food supply for future generations, food production must be maintained. In modern times, synthetic herbicides are commonly used to reduce weed infestation in agriculture, which has the potential to cause up to 30 % losses in yield due to competition for nutrition, space and sunlight. Due to the excessive use of only a small fraction of very effective herbicides, weeds developed resistances, which now have to be overcome by the discovery of novel herbicide modes of action and a more sustainable usage thereof. Additionally, environmental criteria must be met by novel developed herbicides.

Microtubules have already been an effective target for, on one hand, specific and, on the other hand, effective growth inhibitors for plants. Disturbance in microtubule structure leads to critical defects in plant development due to the inhibition of proper cell wall synthesis or inhibition of mitotic processes during cell proliferation. Also, the strict regulation of microtubules by MAPs and the specificity provided by MAPs uniquely expressed in plants offer an additional target spectrum for future herbicidal effectors.

Therefore, this study is trying to characterise Icafolin concerning:

1. Its effects on microtubules *in vivo*.
2. The growth success of plant cells after Icafolin application and concentration dependency
3. Identification of potential Icafolin interacting proteins

Experiments are performed using tobacco BY-2 as a major model organism due to its high proliferation rate, complete known genome sequence, easy maintenance and, most importantly, its changing behaviour from proliferating cells in the early days after sub-cultivation and the transition to elongating ones in later stages of the cultivation cycle. Since already-known anti-microtubule agents show significant phenotypes for either one or both of these cell stages, it is an optimal organism to investigate the effects of potential anti-microtubule herbicides.

2 Material and Methods

2.1 Tobacco BY-2 cell culture

Tobacco BY-2 cells (*Nicotiana tabacum cv. 'Bright Yellow'*) (Nagata, Nemoto et al. 1992) were cultivated in Murashige-Skoog media. Subcultivation was performed weekly, transferring 1,5 ml from a mother culture in fresh media as described previously (Maisch and Nick 2007). For visualising microtubules, two additional cell lines overexpressing either the α-tubulin NtTuA3 fused to GFP (Green fluorescent protein) (Kumagai, Yoneda et al. 2001); Brevario, Linss, Nick, 2001) or the β-tubulin AtTub6 (Hohenberger, Eing et al. 2011). Both overexpressor lines are driven by the *Cauliflower mosaic virus* (*CaMV) 35S* promotor. For transgenic lines, the media was supplemented with 50 mg l^{-1} kanamycin, and the weekly subculture volume was adapted to 2 ml.

2.2 Preparation of Icafolin

Icafolin was provided by Bayer CropScience. The solid powder was dissolved in DMSO (Dimethyl sulphoxide, Roth, Germany) to reach a stock concentration of 100 mM. For experimental setups, the stock solution was diluted in DMSO to obtain a working concentration of 10 mM. Solutions were stored at -20°C until use.

2.3 Cultivation of Arabidopsis thaliana seedlings

For the visualisation of microtubules, a transgenic *A. thaliana* line overexpressing the β-tubulin AtTub6 (Nakamura, Naoi et al. 2004) was used. For the investigation of actin filaments in vivo, a transgenic line overexpressing FABD2 (aa 325–687 of *A. thaliana* fimbrin 1), an actin binding protein part decorating actin filaments, fused to GFP (Voigt, Timmers et al. 2005) was chosen. To prevent contamination, seeds were transferred into a reaction vessel and covered with 80 % Ethanol for 1 min under continuous inversion and subsequently washed 3 times with distilled water. After this, 1.5 ml of a sterilisation mixture containing 9,375 % sodium hypochlorite was filled into the vessel and incubated for 20 min under continuous shaking at room temperature. After the incubation, the seeds were washed under sterile conditions with autoclaved water until the chlorine odour vanished completely.

To keep sterile conditions, a round filter paper was transferred to a Petri dish and autoclaved subsequently. Then, 10-30 sterilised seeds were placed on the filter paper, and 3ml of autoclaved water was added. The Petri dishes were closed, sealed by Parafilm and subsequently placed in a 12 h photoperiod growth chamber at 27°C for 7 days.

2.4 Generation of tobacco BY-2 protein extracts of the soluble fraction

Tobacco BY-2 cell cultures were cultivated as described in Chapter 2.1. After 5 days of cultivation, cells and media were separated by filtration. Obtained cells were immediately transferred and well closed in aluminium foil and frozen in liquid nitrogen. For further processing, cells were disrupted in a frozen state using pre-cooled mortar and pestle, and subsequently, 300 mg cell mass was transferred into a pre-cooled 2 ml reaction vessel. On the ice, 1:1 v/v cold 5x extraction buffer (25 mM MES, 5 mM EGTA, 5 mM $MgCl_2 \cdot 6H_2O$, pH 6,9 adjusted by KOH, 1 mM DTT and 1 mM PMSF) was added, and samples were allowed to thaw under vigorous mixing. To further protect proteins from proteolysis, 5 µl Protease Inhibitor Cocktail (Sigma-Aldrich, München, Germany) was added, and cell debris was sedimented using a cooling centrifuge at 4°C at 17000g for 15min. The resulting supernatant, containing the soluble protein fraction, was transferred into a fresh pre-cooled 2 ml reaction vessel and used immediately for subsequent experiments or was stored at -20°C for short-term use.

2.5 SDS-PAGE

Protein samples were concentrated by Trichloroacetic acid (TCA) precipitation. To enhance protein solubilisation, 1:100 vol. of a 2 % sodium deoxycholate solution was added, and samples were incubated at 4°C for 30 min. After incubation, 1:10 vol. of Trichloroacetic acid was added, and mixed and protein precipitation was allowed to complete overnight at 4°C followed by a 15 min centrifugation at 17000 g at 4°C. The supernatant was removed, and the pellet was resuspended in 10 µl l 3x SDS-loading buffer (**Table 1**), 10 µl distilled water and 10 µl 1 M sodium chloride to neutralise possible remaining acid.

Concentrated samples were loaded on a 10 % Polyacrylamide gel (**Table 2**) in a Mini Gel Tank (Life Technologies, Thermo Fisher Scientific), and gel electrophoresis was performed at a current of 25 mA. Obtained gels were either stained by Coomassie brilliant Blue staining (**Chapter 2.5.1**), silver staining (**Chapter 2.5.2**), or further processed for western blot analysis (**Chapter 2.6**).

Buffer	Components	Concentration
3x loading buffer	Bromphenolblue	0.05 % (w/v)
	Stacking gel buffer	48 % (w/v)
	DTT	300 mM
	SDS	6 % (w/v)
	Glycerol	30 % (w/v)
	Milli Q water	To 10 ml

Table 1: Composition of the 3x loading buffer used for SDS-PAGE sample preparation.

Stock	Components	Seperation gel (10 %)	Stacking gel (4 %)
30 % Acrylamide/Bis-solution	30 % (w/v) Acrylamid and 0.8 % (w/v) Bisacrylamid	8.2 ml	1.3 ml
Separation gel buffer	1.5 M Tris-HCl (pH=8.8) and 0.6 % (w/v) SDS	6.2 ml	-
Stacking gel buffer	0.5 M Tris-HCl (pH=6.8) and 0.6 % (w/v) SDS	-	2.3 ml
ddH2O		10.3 ml	6.3ml
TEMED	N,N,N',N'-Tetramethylethylendiamin	108 µl	52.8 µl
APS	10 % (w/v) ammonium sulphatein milli Q water	215.9 µl	105.7µl

Table 2: Composition of a 10 % Polyacrylamide gel used for SDS-PAGE.

2.5.1 Coomassie brilliant Blue staining

For the visualisation of proteins following SDS-PAGE protein separation, polyacrylamide gels were placed in a bath containing Coomassie brilliant blue dye solution (**Table 3**) for a period of 24 hours at room temperature with constant agitation. Coomassie brilliant blue stains proteins non-specifically by binding to alkaline amino acid side chains. To remove any excess stain, the gel was transferred into a bath containing a destaining solution (**Table 3**), which removed any unbound Coomassie brilliant blue, thus revealing observable protein bands in the gel.

Buffer	Components	Concentration
Coomassie Brilliant Blue solution	Coomassie Brilliant blue R250	0.04 % (w/v)
Destainer solution	Methanol Ethanol Acetic acid	40 % (w/v) 10 % (w/v) 30 % (w/v)

Table 3: Composition of solutions necessary for Coomassie Brilliant Blue in-gel protein staining.

2.5.2 Silver staining

Since Coomassie brilliant blue staining of Polyacrylamide gels is a convenient method, it lacks sensitivity, which can lead to insufficient visualisation of proteins in the gel. To overcome this limitation, a silver staining protocol was used, which harbours the capability to visualise proteins to a limit of detection of 0.5-5 ng. To be able to analyse the protein contained in obtained bands, a silver staining protocol by Blum (Blum, Beier et al. 1987), slightly modified and optimised for MS analysis by Mortz (Mortz, Krogh et al. 2001), was chosen.

Obtained SDS-Page gels were fixed in Fixer solution (**Table 4**) for 1 h, washed three times with distilled water with a subsequent bath in distilled water overnight at room temperature. On the following day, the gel was transferred into a sensitising solution (**Table 4**) for exactly 1 min and washed again three times with distilled water and incubated in pre-cooled 0.1 % silver nitrate solution (**Table 4**) for 20 min at 4°C under continuous shaking followed by three times washing with distilled water and subsequent transfer into a fresh container for an additional 1 min incubation in distilled water. To visualise bands, the gel was exposed to developer solution (**Table 4**) supplemented with 0.05 % formaldehyde. When a sufficient staining level was reached, the reaction was washed for 20 seconds with distilled water, and the reaction was terminated by the addition of a 5 % acetic acid solution for 5 min. Relevant bands visualised were cut and sent for MS analysis in a vessel containing 1 % acetic acid.

Buffer	Components	Concentration
Fixer solution	Ethanol Acetic acid Distilled Water	40 % 10 % 50 %
Sensitizing solution	Sodium thiosulfate	0.02 %
Silver nitrate solution	Silver nitrate Formaldehyde (add before use)	0.1 % 0.02 %
Developer	Sodium carbonate Formaldehyde (add before use)	3 % 0.05 %
Terminating solution	Acetic acid	5 %

Table. 4: Solutions required for the MS optimized silver staining protocol according to Mortz (Mortz, Krogh et al. 2001).

2.6 Western Blot

For visualising tubulin, the stacking part of the polyacrylamide gels obtained from Chapter 2.5 was removed, and the remaining gel, containing the separated proteins, was blotted on a polyvinylidene fluoride (PVDF, Pall Gelman Laboratory, Dreieich, Germany) membrane. To achieve this, two filter papers (Whatman, Dassel, Germany) were cut to the size of the gel and soaked in transfer buffer (14.4 g/L glycine, 12.07 g/L Tris-HCl and 20 % [v/v] MeOH) and placed on the anode of a Trans-Blot® Semi-Dry Transfer (Bio-Rad) blotting device. A piece of PVDF membrane was activated in methanol (Roth, Germany) for 30 s and placed on top of the filter papers, followed by the polyacrylamide gel, two additional, presoaked pieces of filter paper and the lid of the device (cathode). Blotting was performed at a constant current of 25 V for 1.5 h. After the blotting process, the PVDF membrane was washed twice for 10 min with TBS buffer (20 mM Tris-HCl, pH 7.6 and 150 mM NaCl) and subsequently incubated in blocking buffer (5 % milk powder in TBS) for one h at room temperature at constant shaking. After blocking, the membrane was washed twice with TBST buffer (TBS supplemented with 0.1 % Tween-20) and twice in TBS buffer for 10 min for each washing step, followed by overnight incubation in the primary antibody solution (DM1A, diluted to 1:3000 in TBS) at 4°C under continuous shaking. On the next day, the membrane was washed twice with TBST and once with TBS buffer for 10 min each washing step and incubated in the secondary antibody solution (anti-mouse IgG, alkaline phosphatase-conjugated. diluted to 1:30000 in TBS) for 1 h at room temperature and constant shaking. Before development, the membrane was again washed four times with TBST buffer for 10 min each washing step and

subsequently developed using 1 ml of a NBT/BCIP (Sigma, Germany) solution. The developing reaction was stopped by several washing steps with distilled water.

2.7 Live cell imaging

Microscopical approaches were performed under the Zeiss Cell Observer Spinning Disc (Zeiss, Jena, Germany) equipped with a cooled digital CCD camera (AxioCamMRm) and a spinning-disc device (YOKOGAWA CSU-X1 5000) microscope, using a 63x oil immersion objective. To obtain the fluorescent signal, GFP fusion proteins were excited with the blue line (488 nm) of an Ar-Kr laser (Zeiss, Jena, Germany), and 561 nm for Nile-Blue Icafolin or Synaptored experiments. Exposure time was set to 300 ms, and laser intensity was 80 %. Pictures were created by capturing Z-stacks in an interval of 0,5 µm. Pictures were stacked to generate a geometrical projection.

2.8 Icafolin Effects and dose-response Microscopy

In order to employ microscopic approaches, tobacco BY-2 cells that overexpress either GFP-tagged α-tubulin3 or GFP-tagged β-tubulin 6 were utilised. A 1 ml sample of the respective cell line was transferred into a 2 ml reaction vessel and subsequently exposed to the respective test concentration of Icafolin. Samples were incubated for one hour at 28°C on a horizontal shaker at 180 rpm. Following incubation, 40 µl of the cell suspension was transferred onto a microscopy slide and mounted for live cell imaging, as described in Chapter 2.7.

2.8.1 Taxol-induced microtubule stabilisation

For observation of a possible impact of a slowed-down microtubule turnover on the effectivity of Icafolin, Taxol was used to stabilise microtubules. 1 ml samples of TuA3 cell culture were transferred to a 2 ml reaction vessel and incubated with 10 µM Taxol for 30 min before Icafolin treatment in a concentration of 10 µM for an additional hour at 28°C on a horizontal shaker at 180 rpm. Effects were observed as described in Chapter 2.7.

2.9 Nile Blue Icafolin

In the experiments described in this Chapter, Icafolin was replaced with a fluorescently tagged Icafolin derivative, Nile Blue-Icafolin (NB-Icafolin). NB-Icafolin was provided by Bayer Crop Science and synthesised by extending the original Icafolin molecule with a linker. The resulting derivative (linker-Icafolin) was subjected to biological activity testing (**Chapter 5.1**), by methods described in Chapters 2.8 and 2.7. Once verification was complete, the fluorophore was added to create the finalised NB-Icafolin substance. In addition to its intrinsic fluorescent properties, the molecule is hypothesised to exhibit a quenching effect, which is re-

leased if the Icafolin part binds to its target. This results in a significant increase in the fluorescent signal if bound, in contrast to unbound NB-Icafolin.

2.9.1 NB-Icafolin localization

1 ml TuA3 cell culture was transferred into a 2 ml reaction vessel and treated with 100 µM NB-Icafolin for 1 h at 28°C on a horizontal shaker at 180 rpm. The fluorescent signal obtained by NB-Icafolin was detected, as described in Chapter 2.7.

2.9.2 Endocytosis assay

To investigate possible uptake of Icafolin by endocytosis, 1 ml tobacco BY-2 wildtype cell culture was transferred into a 2 ml reaction vessel and treated with 10 µM of the endocytosis blocker Ikarugamycin for 24 h before treatment and incubation for 1 h with either 100 µM Nile Blue-Icafolin or 10 µM Synaptored, a membrane-impermeable dye which enters the cell by endocytosis. The fluorescent signal was detected as described in Chapter 2.7.

2.9.3 NB-Icafolin as sensor

Protein extracts of the soluble fraction (Chapter 2.4) were separated by isocratic size exclusion chromatography at 4°C using an FPLC device (ÄKTApure 25^{TM}, Cytiva, Marlborough, Massachusetts, USA). Samples were concentrated by ultrafiltration (Amicon Ultra 2 ml, Merck, Germany), and 500 µl of the concentrated extract was used for fractionation at an isocratic flow of the mobile phase (80 mM PIPES- di-natrium-salt, 1 mM $MgCl_2$,200 mM NaCl, pH 6.8). Separation was performed by the Superdex™ 200, 10/30 SEC column (Citiva, Marlborough, Massachusetts, USA. Fractions were collected in volumes of 0,5 ml. Obtained samples were transferred to a 96-well plate (Greiner,No.655077). 300 nM NB-Icafolin was added in each well, mixed and incubated for 15 min. The fluorescent signal was detected by a plate reader device (CLARIOstar, BMG Labtech).

2.10 Microtubule Recovery Assay

To obtain information about the reversibility of Icafolin effects, 1 ml of tobacco BY-2 TuA3 cell culture was transferred into a 2 ml reaction vessel. Icafolin was added to reach respective test concentrations, and samples were incubated according to the respective impulse duration at 28°C under continuous shaking on a rotary shaker at 180 rpm. After incubation, media was removed from samples and substituted by fresh media not containing any additives to wash out Icafolin. The washing process was repeated three times, and samples were subsequently transferred into 30 ml fresh media and further incubated according to the usual tobacco BY-2 cultivation protocol (**Chapter 2.1**). Samples were checked for microtubule recovery after a regeneration time of 24 h, 48 h and 72 h by the method described in Chapter 2.7.

2.10.1 Inhibition of translation

For investigating the necessity of protein *de novo* synthesis for microtubule recovery, 100 µM Cycloheximide was added to the samples 1 h before the start of the Icafolin impulse to inhibit protein synthesis. To make sure cells can achieve full microtubule recovery within 24 h, Icafolin concentration was set to 50 nM with an impulse duration of 1 h. After incubation, samples were further treated as described in Chapter 2.7.

2.11 Growth curve

The cell lines were subcultured in accordance with the methodology outlined in Chapter 2.1. The respective test concentrations of 10 nM, 20 nM, 30 nM, 40 nM, and 50 nM were achieved through the supplementation of Icafolin. To monitor cellular proliferation, 500 µl of the culture medium was analysed for its sugar content using a refractometer (HI96801 Refractometer, Hanna instruments, Germany). The results obtained in %Brix were normalised against the respective initial value of the sample to generate a 100 % baseline, and the progressive reduction in sugar concentration was tracked over a seven-day period.

2.12 Mortality Assay

To track cell mortality over time, tobacco BY-2 cells of the respective cell line were subcultures according to Chapter 2.1. Icafolin was supplemented to reach the test concentration of 10 µM. Cell mortality was tracked in a 24-hour interval by the Evans Blue staining technique (Gaff and Okong'O-Ogola 1971). Evans blue is a non-permeable dye which can enter the cell after plasma membrane degradation occurs, resulting in deep blue staining of the whole cell. To achieve sufficient staining, 100 µl of cell suspension was filtered to remove excess media and transferred into a vial containing a solution of 2,5 % Evans-Blue dye. After 5 min incubation, cells were washed 3 times with distilled water. The visualisation was performed under an Apotome microscope (Zeiss Axio Imager Z1, Apotom, Axiocam 503 mono, Zeiss, Germany) with a magnification of 100x.

Data was analysed by an artificial intelligence (AI) model trained for the detection of stained cell corpi (dead) and unstained cell nuclei (living). The AI model was created by the Apeer online tool provided by Zeiss (Carl Zeiss Microscopy, 2023). For extremely deformed cells, the AI was not able to detect nuclei anymore. In this case, AI results were human-curated using the software ImageJ as a counting platform.

2.13 Approaches of tubulin isolation: Ultracentrifugation

Purification of tubulin was attempted by a modified ultracentrifugation approach described by Krtková et al. (Krtková, Zimmermann et al. 2012). Protein extracts derived from tobacco BY-2 wildtype cell culture were supplemented with 40 µM Taxol and incubated at 35°C for 1 h to allow in vitro microtubule polymerisation. Samples were transferred on a 20 % sucrose cushion in 5x extraction buffer and centrifuged at 100.000 g at 25°C for 1 h (L8-70M Ultracentrifuge, Beckman). The supernatant was removed, sedimented microtubules were resuspended in 3x loading buffer and containing proteins were separated by SDS-PAGE as described as in Chapter 2.5. Purity was analysed by Coomassie brilliant blue staining (**Chapter 2.5.1**), and the presence of tubulin was verified by western blotting (**Chapter 2.6**).

2.14 Approaches of tubulin isolation: EPC-Sepharose affinity chromatography

Another attempt at tubulin purification was performed utilising the α-tubulin binding property of EPC (ethyl-N-phenylcarbamate). To generate an affinity matrix, carboxy- ethyl-N-phenyl carbamate was synthesised and coupled to activated Sepharose 4B (Amersham Pharmacia, Freiburg, Germany) according to the method of Mizuno ((Mizuno, Koyama et al. 1981). The generated affinity matrix was transferred into custom-made filter inlets for 2 ml reaction vessels. 500 µl of the respective samples' soluble protein fraction (**see Chapter 2.4**) was loaded, incubated for 10 min on ice to achieve sufficient binding and subsequently centrifuged at 15000 g for 1 min. Following this procedure, samples were washed three times by TBS (20 mM Tris-HCl, pH 7.6 and 150 mM NaCl) and subsequently eluted over a KCl (potassium chloride) gradient starting at 0 M KCl up to 1 M KCl in 0.05 M steps. In the case of TuA3 or TuB6 samples, a fluorescent signal originating from the GFP-tagged tubulin expressed was checked for each fraction before further downstream experiments using a Fluorimeter (Jasco FP 8300 Fluorimeter, Jasco). Obtained fractions were concentrated using TCA precipitation (**see Chapter 2.4**), and proteins were separated by SDS-PAGE (**Chapter 2.5**). Proteins in gel were visualised either using Coomassie Brilliant Blue staining (**Chapter 2.5.1**) or, for more sensitive staining, the silver staining technique (**Chapter 2.5.2**). For the detection of tubulin, western blotting was used (**Chapter 2.6**).

2.15 Icafolin affinity chromatography

To generate an Icafolin affinity matrix, the linker-Icafolin derivate (see Chapter 2.9) was coupled to agarose beads by CarboxyLink™ Immobilization Kit (Thermo Fisher, Waltham, Massachusetts, USA). The resulting 2 ml gravity column was loaded with the respective protein extract of the soluble fraction (**see Chapter 2.4**) and incubated for 15 min to allow complete binding. The column was washed with three column volumes of TBS (20 mM Tris-HCl, pH 7.6 and 150 mM NaCl) before elution and was subsequently eluted over a KCl salt gradient ranging from 0 M KCl up to 3 M KCl in 0,1 M steps in a volume of 2 ml (one column volume) per step. Fractions were collected in a 2 ml reaction vessel, concentrated by the TCA precipitation protocol described in Chapter 2.5 and subsequently subjected to protein separation by SDS-PAGE (**Chapter 2.5**). The resulting polyacrylamide gel was stained using the silver staining technique described in Chapter 2.5.2. Since higher affinity should require higher ionic pressure to be eluted from the affinity resin, protein bands obtained from higher salt fractions were cut and sent for MS/MS analysis performed by Bayer Crop Science. To assess non-elutable proteins still bound to the resin, the resin was removed from the column, transferred into a 2 ml reaction vessel and subsequently boiled at 98°C for 10 min to achieve protein denaturation and release from the affinity matrix. Obtained samples were sent for MS/MS analysis.

3 Results

3.1 Icafolin eliminates microtubules rapidly, efficiently, and independently of tubulin type.

In order to ascertain whether Icafolin indeed targets microtubules, the response to 10 µM of Icafolin was assessed in tobacco BY-2 cells overexpressing green fluorescent protein (GFP) fusions of either tobacco α-tubulin 3 (TuA3) or *Arabidopsis thaliana* β-tubulin 6 (TuB6) after 1 h by spinning-disk confocal microscopy. While untreated cells displayed a network of intact cortical microtubules for both TuA3 (**Fig. 11A**) and TuB6 (**Fig. 12A**), the majority of these microtubules had disappeared after treatment with Icafolin (**Figs. 11B, 11B**). Only a small proportion of the shorter microtubules could be discerned (**see Figs. 11B and 12B, indicated by white arrows**). Instead, a diffuse fluorescent background was observed in the cytoplasm surrounding non-fluorescent small particles that, in terms of size and shape, resembled mitochondria and plastids. A similar response was observed using Oryzalin as a positive control. Once more, the microtubules were largely degraded, resulting in a diffuse cytoplasmic signal and the presence of only a few remaining microtubules (**Figs. 11C, 12C, white arrows**). In a few cells, fluorescent dots were observed, occasionally linked with short rods of microtubules, suggesting that the microtubules had shrunk to a minimal length.

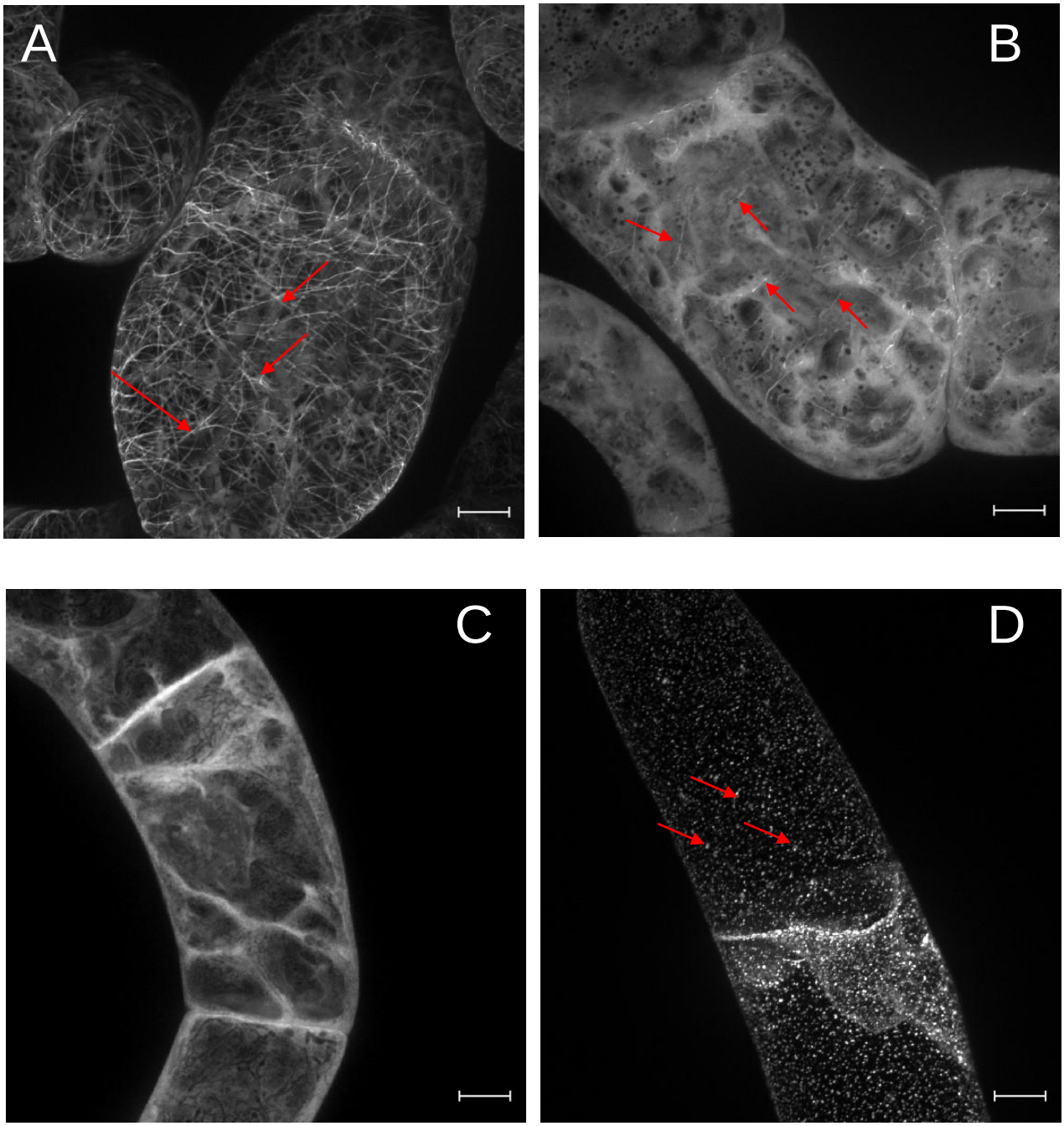

Fig.11: Effect of Icafolin on microtubules in TuA3 cells. *Images show representative geometric projections from confocal z-stacks collected in the cortical region of either untreated cells (A), cells exposed to 10 µM Icafolin for 1h (B), or cells treated with 10 µM Oryzalin for 1 h (C, D). For Oryzalin treatment, either cells with a diffuse fluorescence (C) or with fluorescent speckles (D) were observed. Arrows are indicating microtubules or microtubule residues for treated cells. Scalebar represents 10 µm.*

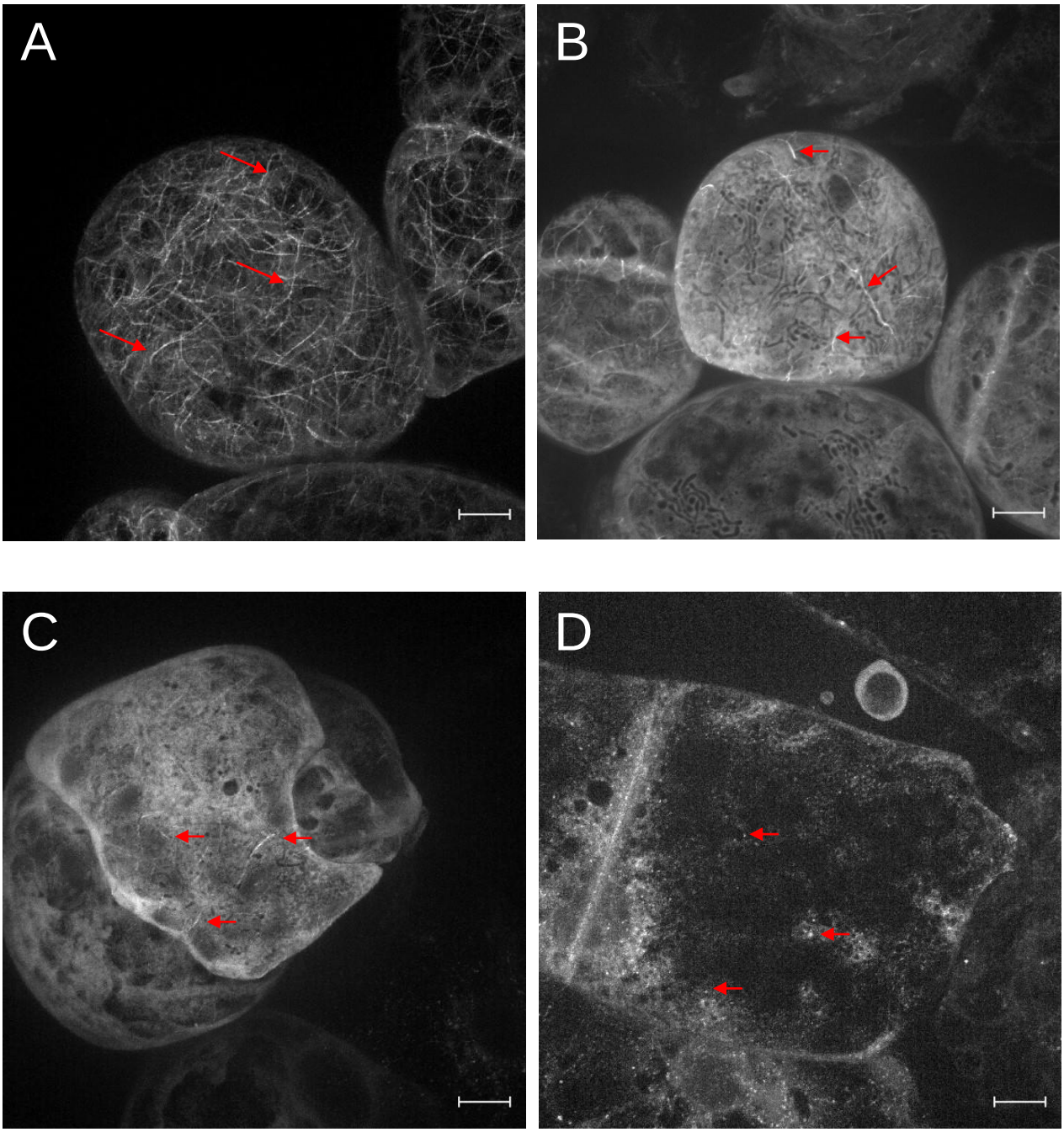

Fig.12: Effect of Icafolin on microtubules in TuB6 cells. *Images show representative geometric projections from confocal z-stacks collected in the cortical region of either untreated cells (A), cells exposed to 10 µM Icafolin for 1 h (B), or cells treated with 10 µM Oryzalin for 1 h (C, D). For Oryzalin treatment, either cells with a diffuse fluorescence (C) or with fluorescent speckles (D) were observed. Arrows are indicating microtubules or microtubule residues for treated cells. Scalebar represents 10 µm.*

3.2 Live Cell Imaging: *A. thaliana* seedlings

To gain insight into the effects on microtubules next to cell culture, *A. thaliana* seedlings overexpressing GFP-TuB6 were cultivated for five days and subsequently treated with 10 µM Icafolin for 1 h prior to observation. Images were captured from cotyledons and hypocotyl cells and compared to samples that had not been treated. The results demonstrate that the microtubular network in control cotyledons and hypocotyl cells is intact (**Fig. S1: A; B**). Following treatment with 10 µM Icafolin for 1 h, microtubules begin to depolymerise, resulting in the formation of short microtubule residues within the cells (**Fig. S1: C; D**).

Given that microtubules and actin filaments are both components of the cytoskeleton, it was investigated whether the observed depolymerising effect on microtubules is also present for actin filaments when Icafolin is applied. To this end, *A. thaliana* seedlings overexpressing GFP-FABD2 were cultivated for a period of five days and subsequently treated with 10 µM Icafolin for 1 h prior to observation. The results demonstrate the presence of intact actin filaments in *A. thaliana* cotyledons and hypocotyls (**Fig. 14: A and B**). In Icafolin-treated cells, no depolymerising effect was observed after 1 h (**Fig. 14: C and D**), suggesting that the phenomenon may be microtubule-specific with regard to cytoskeletal effects.

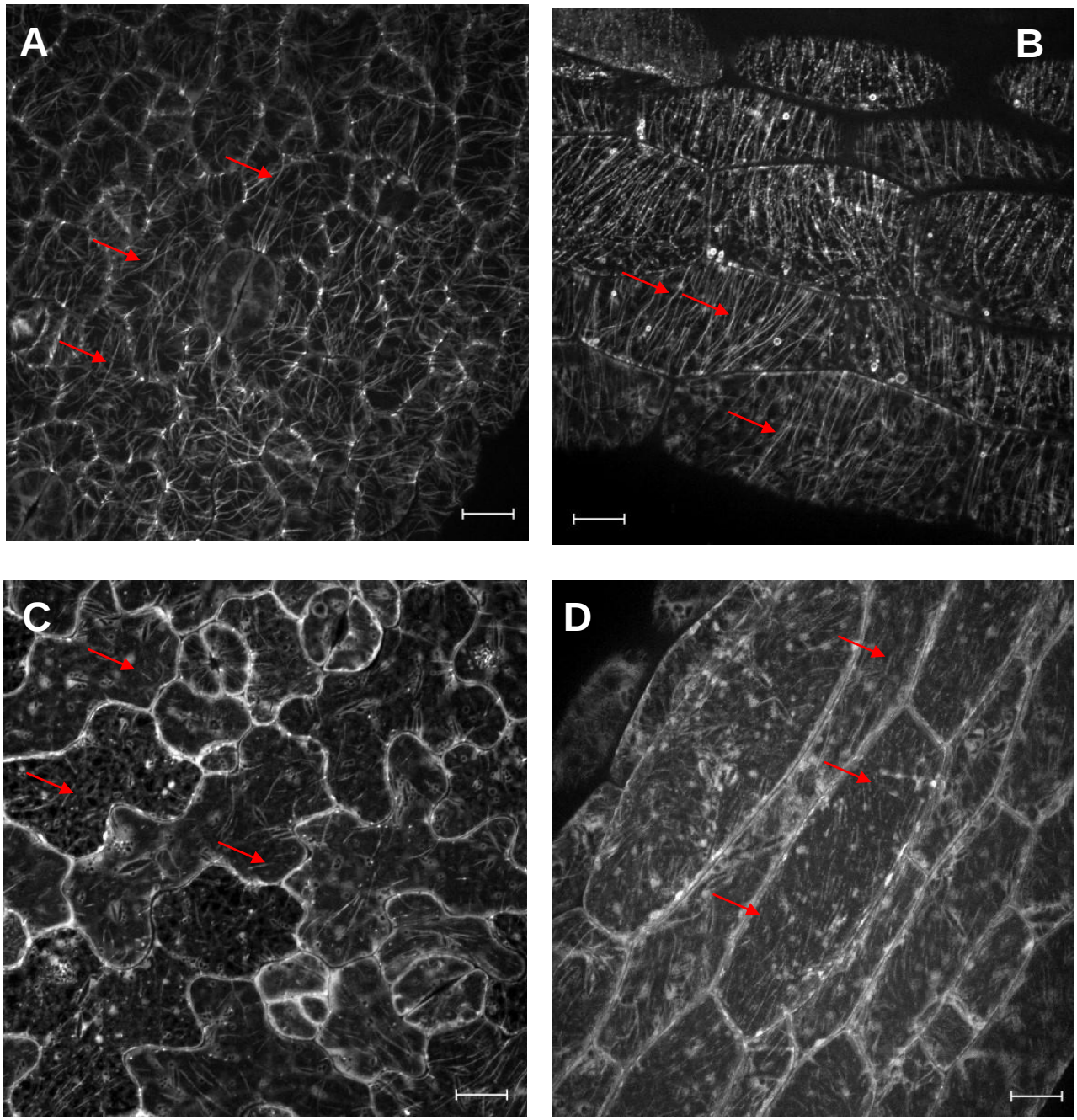

Fig.13: Effects of Icafolin on microtubules in A. thaliana seedlings overexpressing GFP-TuB6. *A: Live cell Imaging of untreated A. thaliana cotyledons. B: Live cell imaging of untreated A. thaliana hypocotyl. C: Live cell imaging of A. thaliana cotyledons after 1h 10 µM Icafolin treatment. D: Live cell imaging of A. thaliana hypocotyls after 1h 10 µM Icafolin treatment. Arrows are indicating intact microtubules for control cells and microtubule residues for Icafolin treated cells. Scalebar represents 10 µm.*

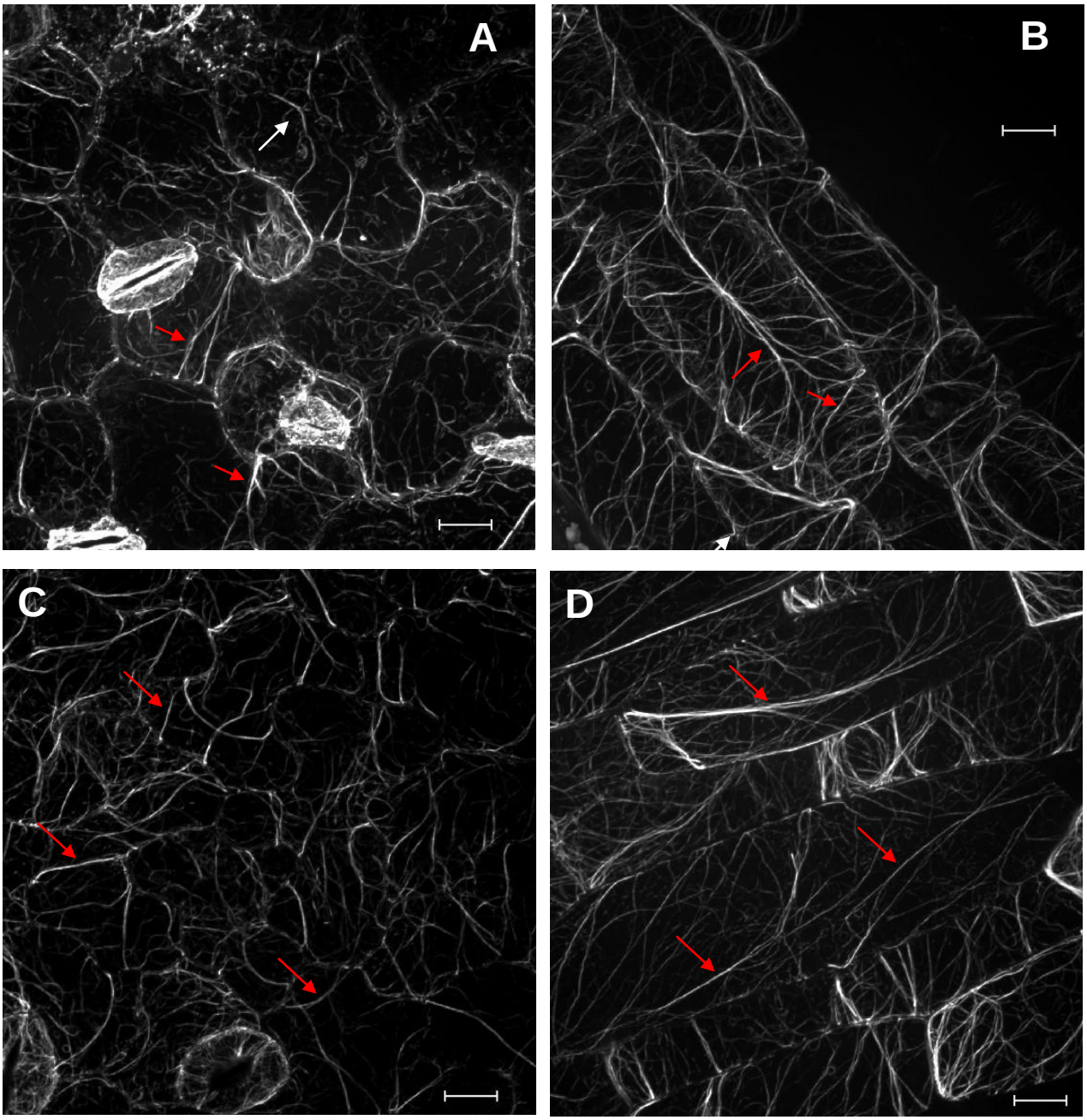

Fig.14: Effects if Icafolin on actin filaments, visualised by overexpressing GFP-FABD2 in A. thaliana seedlings. *A: A: Live cell Imaging of untreated A. thaliana cotyledons. B: Live cell imaging of untreated A. thaliana hypocotyl. C: Live cell imaging of A. thaliana cotyledons after 1 h 10 µM Icafolin treatment. D: Live cell imaging of A. thaliana hypocotyls after 1 h 10 µM Icafolin treatment. Arrows are indicating actin filaments. Scalebar represents 10 µm.*

3.3 Icafolin eliminates microtubules at a threshold of 100 nM

Given that other anti-microtubule agents, such as Propyzamide, necessitate concentrations in the micromolar range to induce notable microtubule defects, the threshold of sensitivity for Icafolin-mediated microtubule elimination was subjected to scrutiny. To investigate this, cells were incubated with Icafolin at concentrations ranging from 50 nM to 100 µM for a period of 1 h, after which their responses were assessed through the use of spinning disc confocal microscopy.

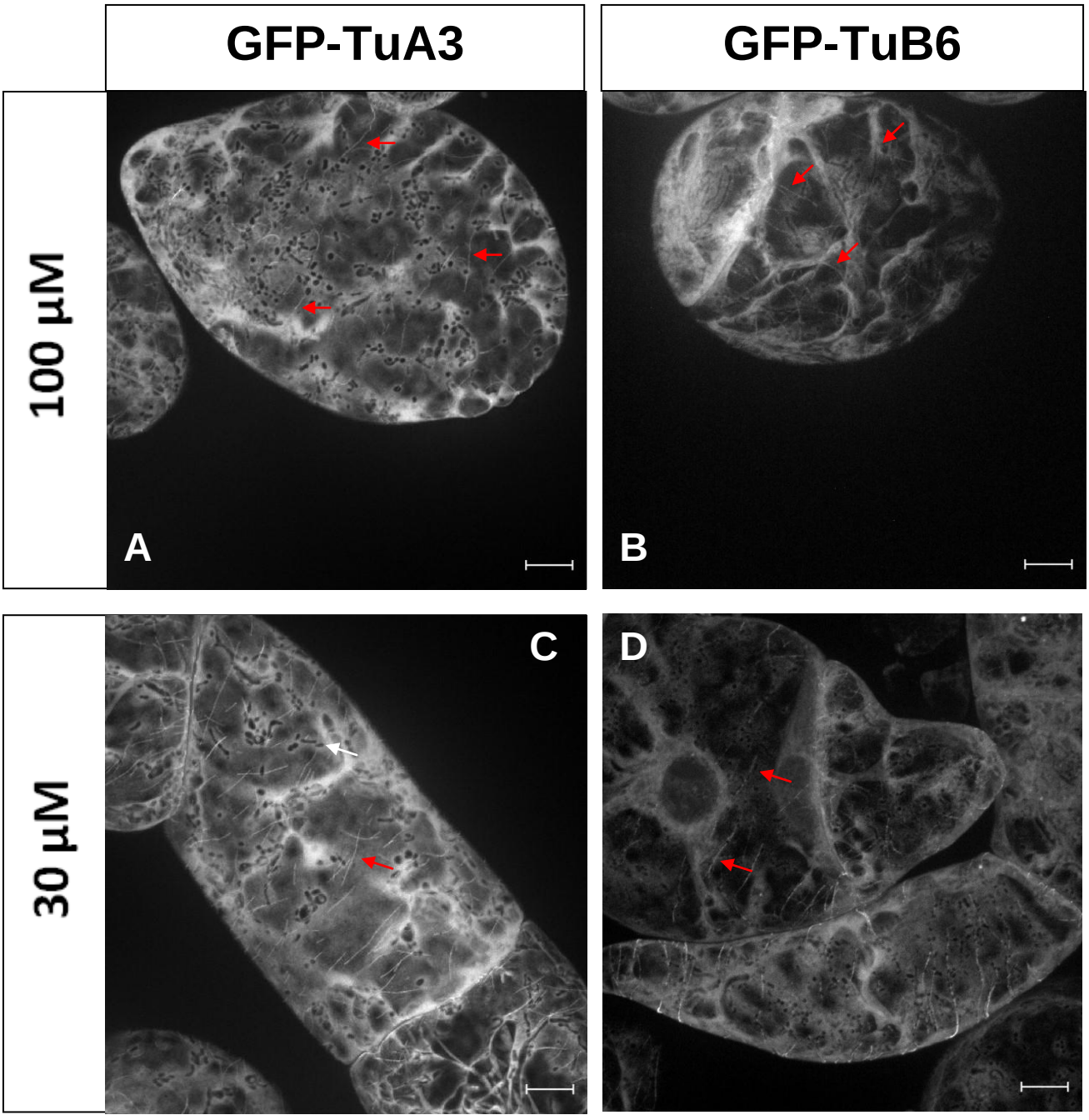

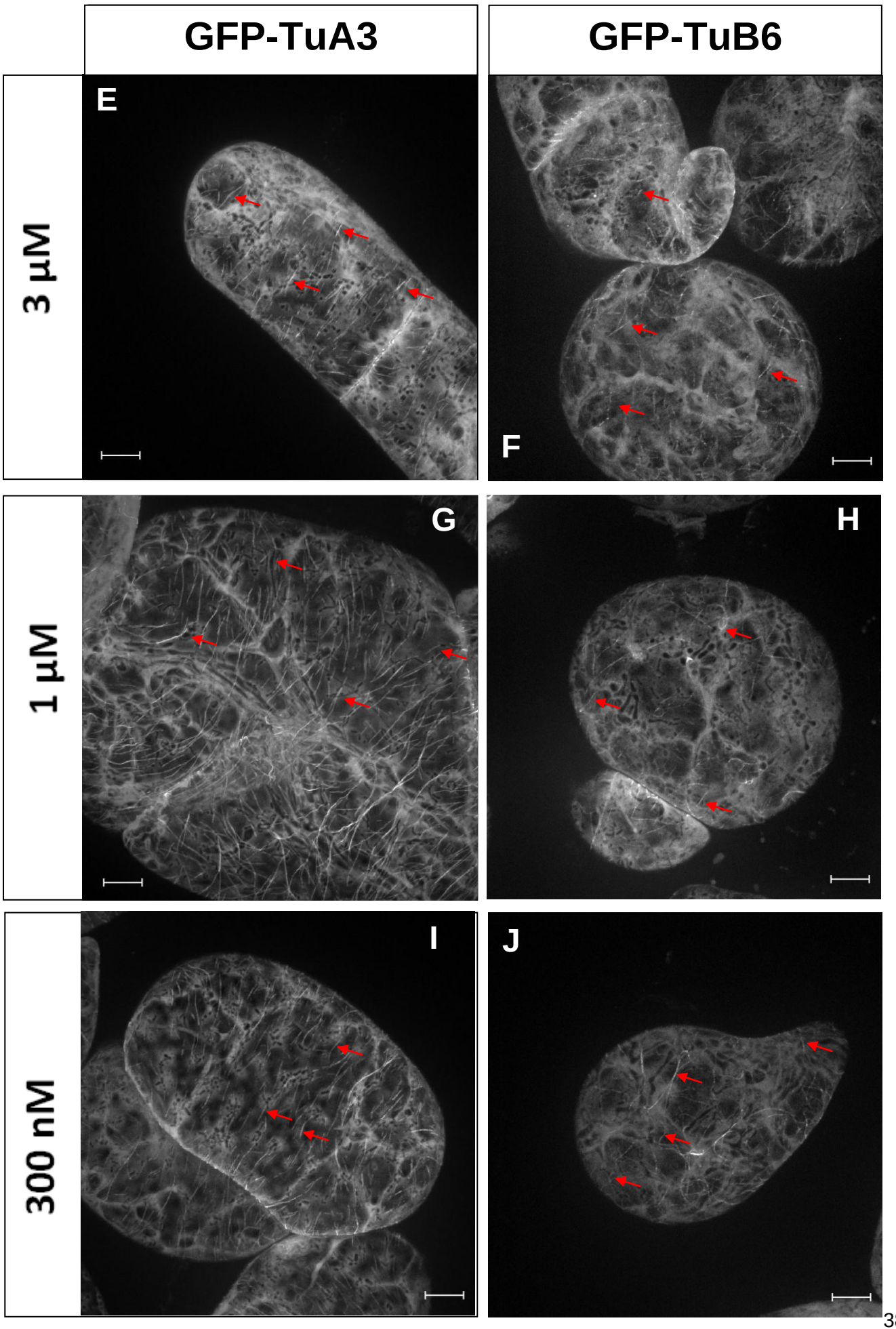
GFP-TuA3
GFP-TuB6
3 µM
1 µM
300 nM
E
F
G
H
I
J

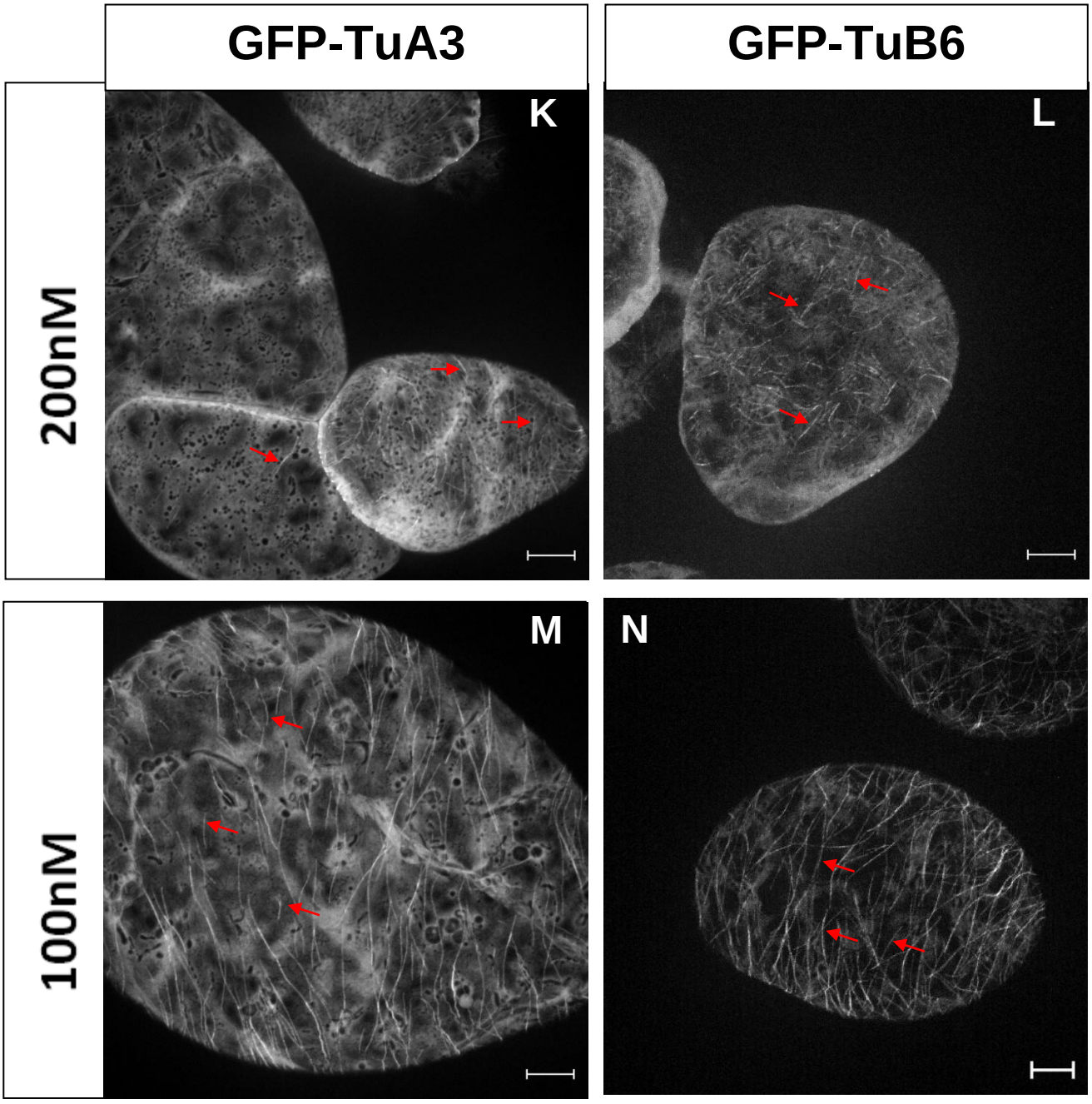
GFP-TuA3
GFP-TuB6
200nM
100nM
K
L
M
N

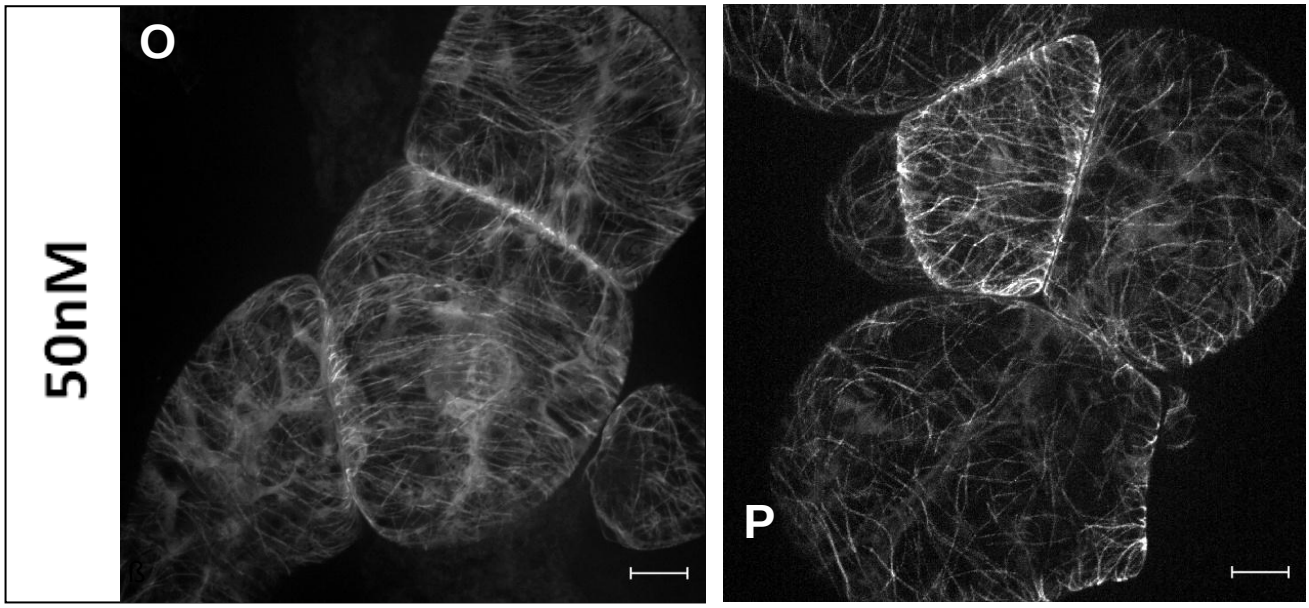

Fig.15: Dose dependency of the microtubular response to Icafolin in TuA3 and TuB6 cells. *Images show representative geometric projections from confocal z-stacks collected in the cortical region after 1 h incubation with 100 µM (A, B), 30 µM (C, D), 3 µM (E, F), 1 µM (G, H), 300 nM (I, J), 200 nM (K, L), 100 nM (M, N), or 50 nM (O, P) of Icafolin, either in TuA3 (A, C, E, G, I, K, M, O) or in TuB6 (B, D, F, H, J, L, N, P). The scalebar represents 10 µm. Arrows indicate microtubules or microtubule remnants.*

To test whether the effect can be amplified at higher concentrations, Icafolin was evaluated at 100 µM (**Fig. 15A, B**) and 30 µM (**Fig. 15C, D**). Nevertheless, a residual number of microtubules were observed, irrespective of whether TuA3 or TuB6 were taken into account. Therefore, 10 µM is sufficient to elicit the maximum response. When concentrations were reduced to levels below 3 µM, the elimination of microtubules was less pronounced, accompanied by a reduction in the intensity of the diffuse cytoplasmic signal. The response of TuB6 appeared to be more sensitive than that of TuA3, particularly at 1 µM of Icafolin (**Fig. 15G, H**). Conversely, at the lowest concentrations tested (200 nM and 100 nM, respectively), TuA3 demonstrated a more pronounced elimination of microtubules in comparison to TuB6. At a concentration of 50 nM (**Fig. 15, K, L**), no significant difference was observed in comparison to the untreated control cells (**Fig. 11A, 12A**). Therefore, the threshold for the Ifacolin effect is as low as 100 nM.

3.4 Icafolin blocks cell expansion depending on α-tubulin

The elimination of cortical microtubules should result in the disruption of cell axiality. It is possible that this will result in impaired cell expansion; however, this is not a certainty. To address this aspect, a comprehensive analysis of cell growth throughout the entire cultivation cycle in response to varying concentrations of Icafolin was conducted. In addition to the non-transformed tobacco BY-2 wildtype, the responses of TuA3 cells were also tested, given that microtubule responses had previously been observed in those cells due to the presence of the GFP tag. Given the extended duration of the treatment, the concentration range was reduced in comparison to the short-term experiments previously described. To monitor the cell response non-invasively, sugar concentration in the medium was measured over time, as reported by Kaźmierczak et al. (Kaźmierczak, Siatkowska et al. 2023). The residual sugar concentration in the supernatant was followed over the entire cultivation cycle in response to different concentrations of Icafolin added at the start of the cultivation cycle.

A notable reduction in sugar consumption was observed from day 4 onwards, which coincides with the transition from mitotic activity to cell expansion (Huang, Maisch et al. 2017). The threshold of activity was identified as 30 nM for non-transformed wildtype cells (**Fig. 16A**). The inhibition observed at 30 nM was more substantial for TuA3 cells (**Fig. 16B**). However, at 50 nM, sugar consumption was reduced to approximately one-third of the value seen in untreated cells in both cases.

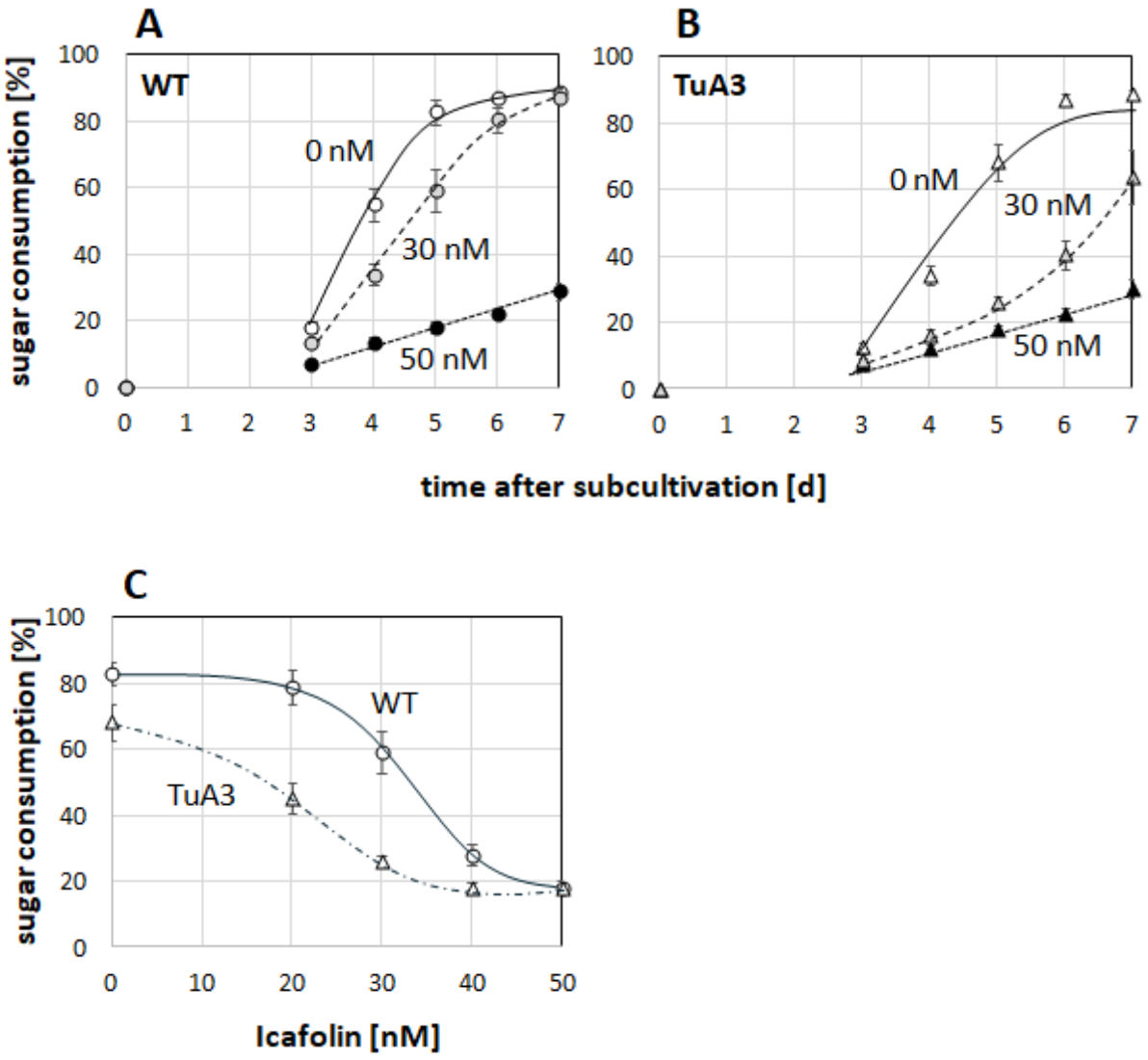

Fig.16: Time course and dose dependency of sugar consumption in WT and TuA3 cells. *Sugar consumption as readout for culture growth was followed from day 3 after the addition of different concentrations of Icafolin to either the non-transformed BY-2 WT (A) or the TuA3 strain expressing a GFP fusion of tobacco α-tubulin 3 (B). The dose-response relations in the linear phase of sugar consumption, at day 5, is given in C. Data represent mean and standard error from three independent experimental series.*

A comparison of the dose-response relations for the two cell lines (**Fig. 16C**) revealed that the curve for the TuA3 line was shifted to lower concentrations of Icafolin. The shift was in the range of 1.5-fold, indicating that TuA3 cells are more sensitive to Icafolin than non-transformed cells. This finding is consistent despite a slight reduction in ground-level sugar consumption in TuA3 (by approximately 15 %) compared to the WT. Despite this minor difference in amplitude, both curves reached saturation at 20 % sugar consumption, indicating that this represents the maximal effect that can be achieved.

3.5 Exposure to Icafolin leads to cell swelling and, eventually, cell death

In order to understand whether the elimination of microtubules and the inhibition of sugar consumption are reflected by differences in cellular morphology and viability, viability was followed in response to 10 µM Icafolin by means of the Evans Blue Dye Exclusion Assay. Evans blue is a deep blue membrane-impermeable dye that is excluded from viable cells. In the event of plasma membrane compromise due to cell death, the dye can enter the cell, resulting in blue staining of the entire cell. Obtained samples was analysed by differential interference contrast microscopy and mortality was quantified by a human-curated AI system that had been trained to detect intact nuclei in living cells and (stained) cell corpses for dead cells (**Fig. 18**). While control cells retained the elongate cylindrical morphology characteristic of a well-curated tobacco BY-2 cell culture (**Fig. 17A, B**), cells treated with Icafolin after one day exhibited localised losses of axiality at the terminal cells of a file, manifesting as lateral bulging (**Fig. 17C**).

On the subsequent day, the majority of cells were observed to exhibit misshapen morphology (**Fig. 17D**). From day 3 onwards, cells displayed a rounded appearance (**Fig. 17E**). From day 4 onwards, a significant proportion of the cells were stained blue, indicating that they had died (**Fig. 17F**). The application of an AI-based approach to the tracking of cell viability enabled the measurement of large populations of cells with a high degree of reproducibility across independent experimental series (**Fig. 18**). It was observed that mortality in non-treated cells was negligible, with a rate of less than 5 % across all cell lines (WT, TuA3, TuB6). In response to Icafolin, mortality was significantly increased from day 3, and increased progressively, mainly up to day 4, while additional increases during the expansion phase (after day 4) were less substantial. The mortality of TuA3 cells was reduced substantially to almost half of the value seen in the WT, while TuB6 cells displayed a mortality that was around 50 % higher than in the WT.

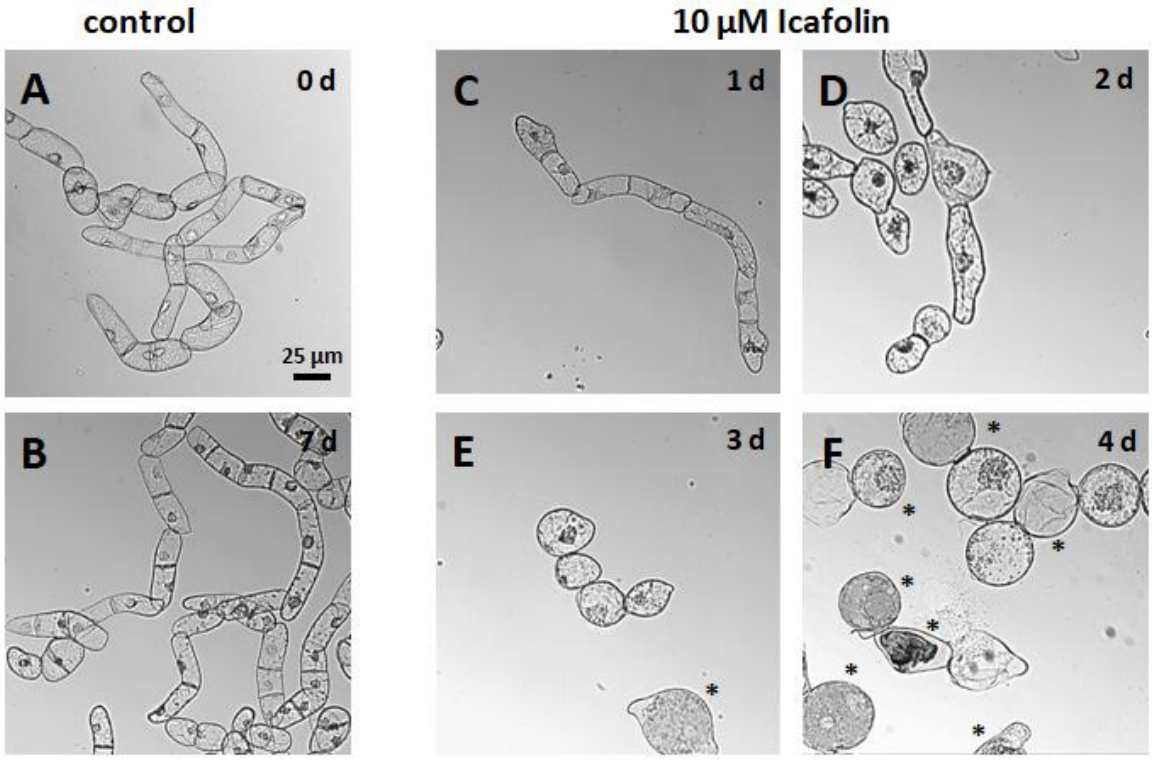

Fig.17: Effect of Icafolin on cell shape and viability in WT and TuA3 cells. *Representative images from a time-course experiment upon staining with the membrane-impermeable dye Evans Blue are shown. Control cells are shown for day 0 (A) and day 7 (B). Cells treated with 10 µM Icafolin are shown for day 1 (C), day 2 (D), day 3 (E), and day 4 (F). Asterisks indicate dead cells stained in blue due to lost membrane integrity.*

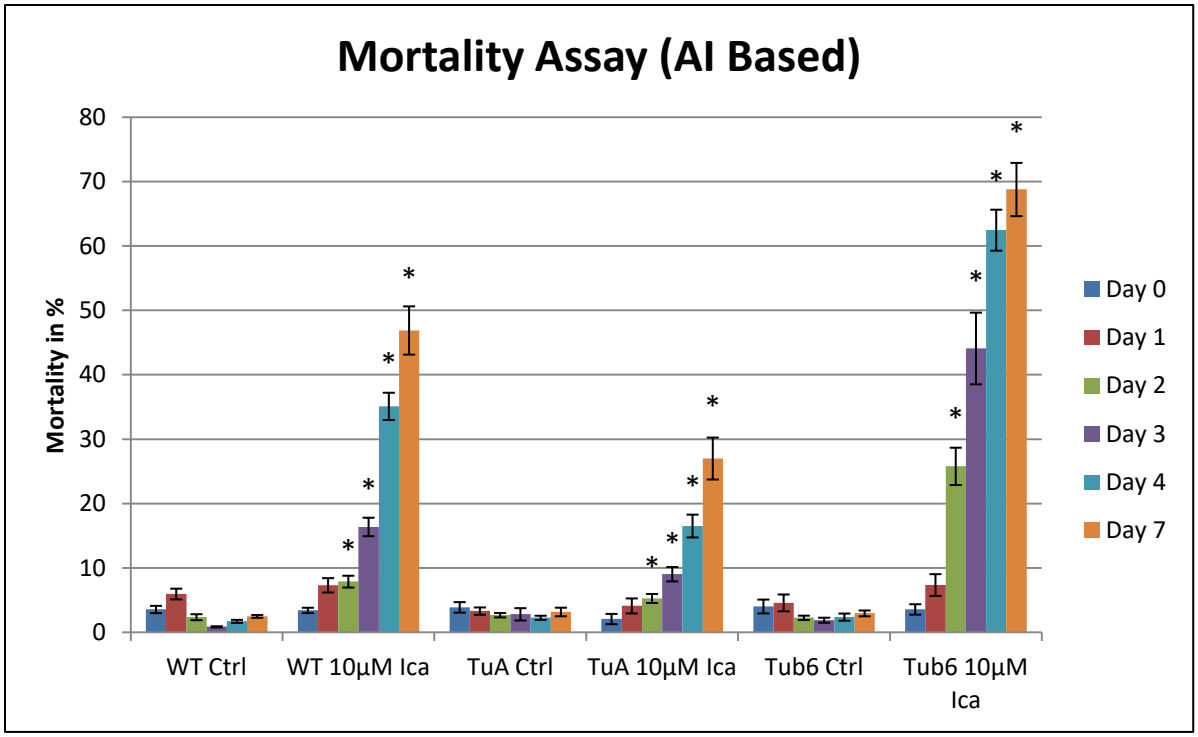

Fig.18: AI-based Mortality Assay of Tobacco BY-2 wildtype/TuA3/TuB6 cells. *Cells were incubated in 10 µM Icafolin for 7 Days. A portion of dead cells was counted by an AI trained to differentiate between living and dead cells. Asterisks indicate statistical significance at the 0.01 level between treated samples and their respective controls, derived from a one-tailed t-test. Error bars represent the standard error of the mean from three independent experimental series.*

3.6 Microtubules can recover in an Icafolin pulse-chase experiment

It is conceivable that Icafolin may eliminate microtubules by means of irreversible sequestration of tubulin heterodimers. To address this issue, a pulse-chase experiment was conducted using the TuA3 cell line. Cells were exposed to either 50 nM or 10 µM of Icafolin for 1 h, after which they were washed several times to remove unbound Icafolin. Subsequently, the cells were transferred into fresh medium to allow for the observation of the subsequent response of the microtubules.

While a 1 h treatment was sufficient to completely eliminate microtubules for both concentrations (**Fig. 19A, B**), recovery was observed after one day. For the low concentration of 50 nM, recovery was already complete (**Fig. 19D**), whereas for the saturating concentration of 10 µM, some cells had not yet reformed a complete array of cortical microtubules (**Fig. 19C**). However, at 48 h post-washout, microtubules had reformed for both concentrations (**Fig. 19E and F**). Furthermore, they persisted subsequently (**Fig. 19G, H**), and in some cells, even mitotic arrays, such as a phragmoplast (*Fig. 17H*), could be observed. The microtubule array of these recovered cells did not exhibit any significant differences with the untreated control group (**Fig. 19I**).

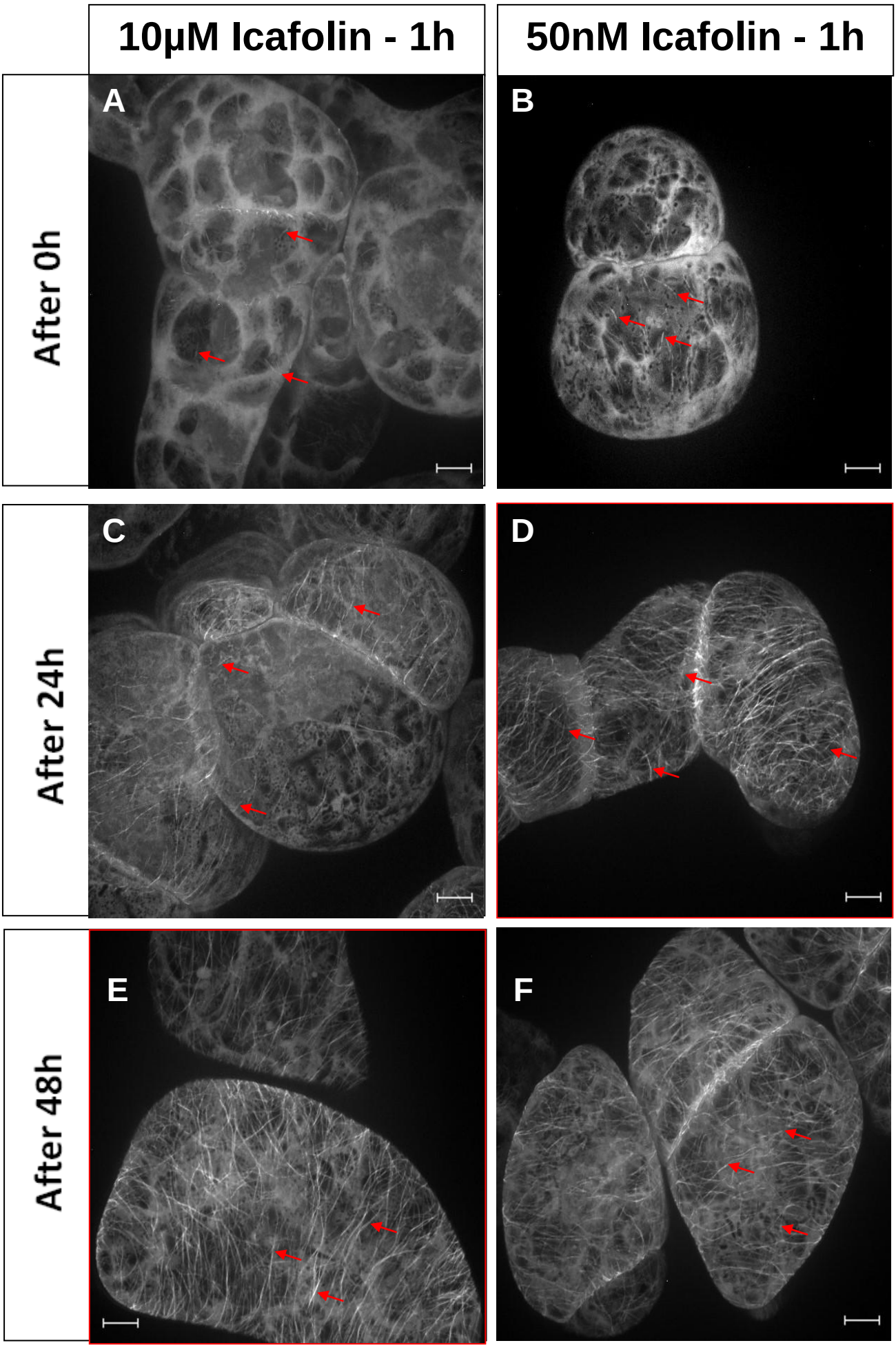
10µM Icafolin - 1h
50nM Icafolin - 1h
After 0h
After 24h
After 48h
A
B
C
D
E
F

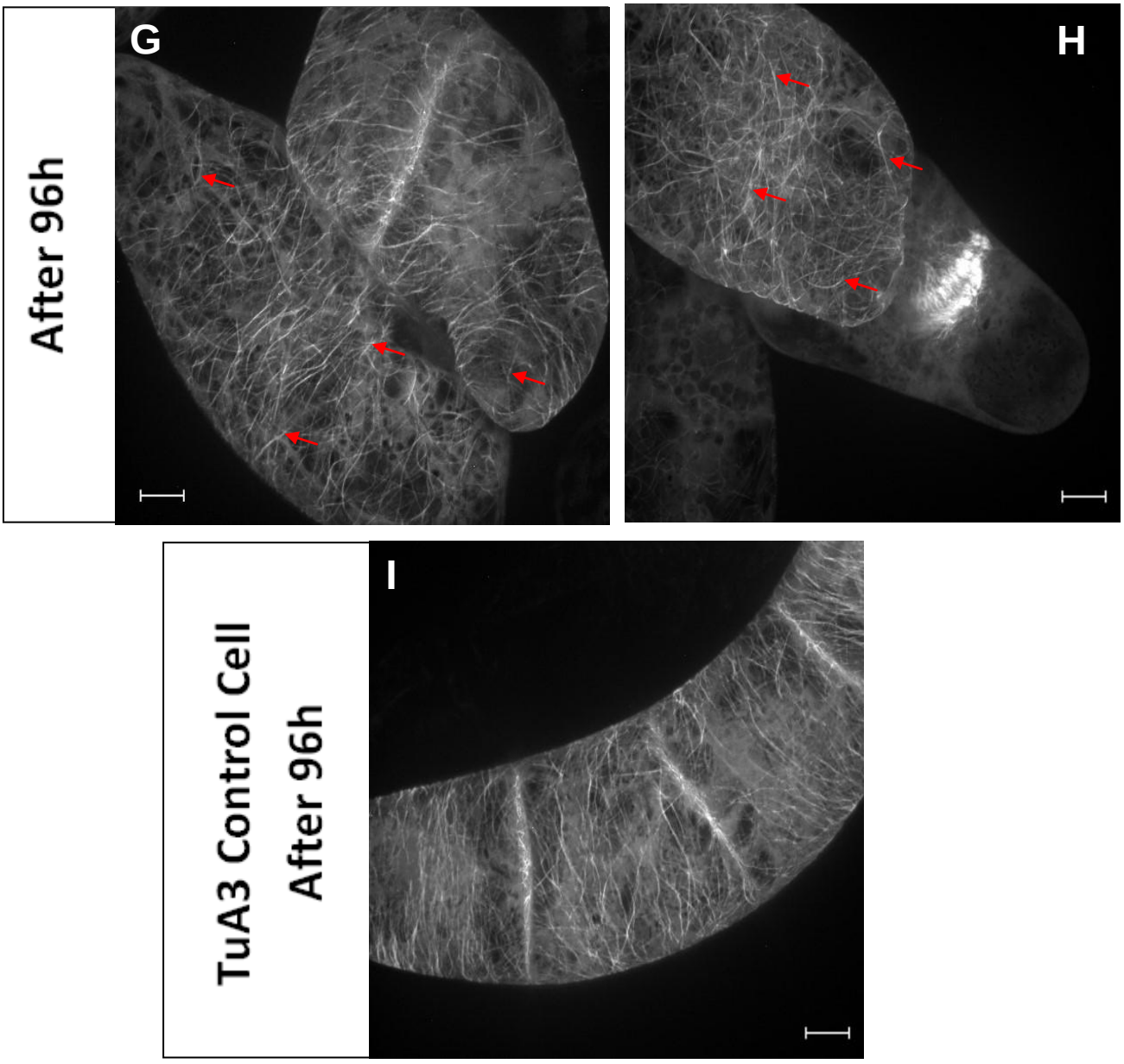

Fig.19: Microtubule recovery assay. *TuA3 cells were exposed to 10 µM (A, C, E, G) or 50 nM (B, D, F, H) of Icafolin for a period of 1 h before Icafolin was washed and microtubules monitored either at 0 h after washout (A, B), 24 h (C, D), 48 h (E, F), or 96 h (G, H). I: TuA3 control cell without any herbicidal treatment. Arrows indicate recovering microtubules. The scalebar represents 10 µm.*

3.7 *De novo* synthesis of tubulin is not necessary for microtubule recovery

The complete recovery may be attributed to the *de novo* synthesis of tubulin, which may compensate for the tubulin sequestered by Icafolin. To investigate this hypothesis, the recovery experiment was conducted in the presence of a saturating concentration (100 µg/ml) of the translation blocker Cycloheximide.

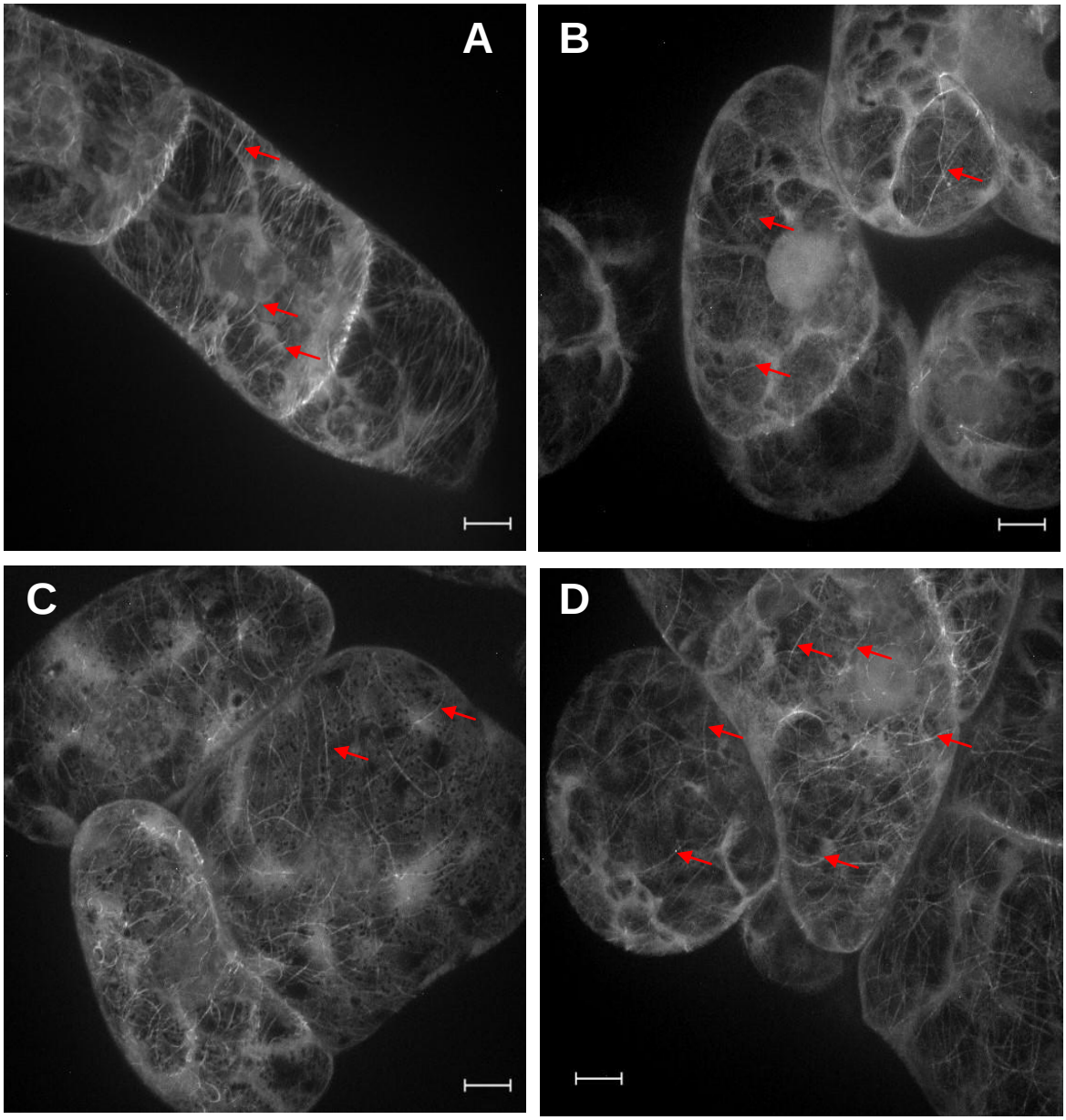

Fig.20: Microtubule recovery under the influence of Cyclohexmide. *A: TuA3 control cell. B: TuA3 treated with 100 µg/ml Cycloheximide for 24 h. C: TuA3 cells after a pulse-chase with 50 nM Icafolin for 1 h and subsequent regeneration without Cycloheximide. D: TuA3 cells after a pulse-chase with 50 nM Icafolin for 1 h and subsequent regeneration in the presence of 100 µg/ml Cycloheximide. Arrows indicate recovering microtubules. The scalebar represents 10 µm.*

In comparison to the untreated control cells (**Fig. 20A**), the 24 h treatment with Cycloheximide resulted in a partial disassembly of microtubules, as evidenced by the thinning and reduction in abundance of microtubule bundles and the emergence of a higher diffuse background in cytoplasmic strands. This phenomenon can be attributed to the elevated steady-state level of GFP-labelled α-tubulin in non-assembled dimers (**Fig. 20B**). This observation demonstrates that the saturating concentration of Cycloheximide had a biological effect. However, the recovery of microtubules following a pulse chase with 50 nM Icafolin for 1 h exhibited no discernible difference between the absence and presence of Cycloheximide at a saturating concentration of100 µg/ml. This suggests that the recovery process is independent of tubulin *de novo* synthesis.

3.8 Microtubule stabilisation leads to a reduction of the phenomenon

In order to obtain information regarding the influence of microtubule dynamics on the efficacy of the substance, Taxol was employed to stabilise (decrease the turnover) the microtubules of TuA3 cells. Prior to the commencement of the experiment, samples were pre-treated with 10 µM Taxol for a period of 30 minutes in order to achieve stability of the microtubules. This was followed by the addition of 10 µM Icafolin for a further hour. The microtubules were visualised by means of spinning-disk confocal microscopy. The results demonstrate the presence of healthy TuA3 cells in the absence of any treatment (**Fig. 21, panel A**). The pre-treatment with Taxol did not result in any impairment of microtubule integrity (**Fig. 21, B**). Following the addition of Icafolin and a 1 h incubation period, microtubules appeared shortened and affected, but the effect was markedly reduced in comparison to Icafolin treatment without microtubule stabilisation (**Fig. 11, B**). The results for cells that were pre-stabilised and treated with Oryzalin, which is known to depolymerise microtubules in a manner that depends on microtubule turnover, were similar (**Fig. 21, D**). The microtubules were shortened, but the effect was reduced in comparison to the treatment that did not involve pre-stabilisation (**Fig. 11, C; D**).

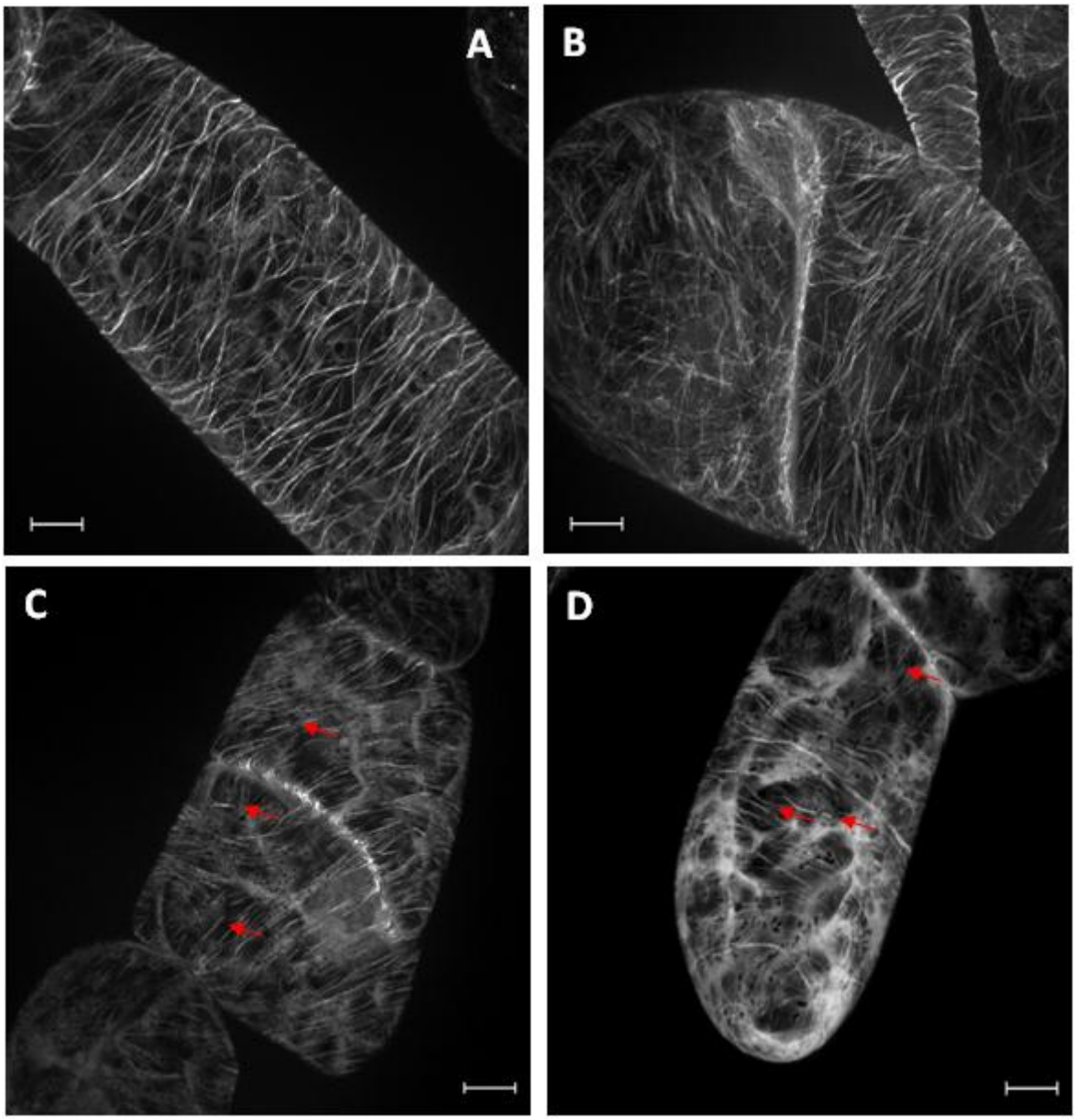

Fig. 21: Taxol rescue experiment. *TuA3 cells were pre-treated with 10 µM Taxol for 30 minutes, and subsequently, 10 µM Icafolin was added and incubated for an additional 1h. A: TuA3 control cell. No treatment was applied. B: TuA3 cell treated with 10 µM Taxol for 30 min. Microtubules are not impeded. C: TuA3 cells pre-treated with 10 µM Taxol for 30 min and 10 µM Icafolin for 1 h. Microtubules show reduced depolymerising effects compared to non-stabilized samples. D: TuA3 cells pre-treated with 10 µM Taxol for 30 min and 10 µM Oryzalin for 1 h. Microtubules show reduced depolymerising effects compared to non-stabilized samples. Arrows are indicating affected microtubules. Scalebar represents 10 µm.*

3.9 Fluorescently labelled Icafolin can enter the cell independent of endocytosis

In order to ascertain the mechanism of uptake of Icafolin, the substance was fluorescently labelled with Nile Blue (**see Chapter 2.9**). The resulting molecule was incubated in a concentration of 100 µM with either Tobacco BY-2 Wildtype or TuA3 cells for one hour. Images were obtained by spinning disk confocal microscopy.

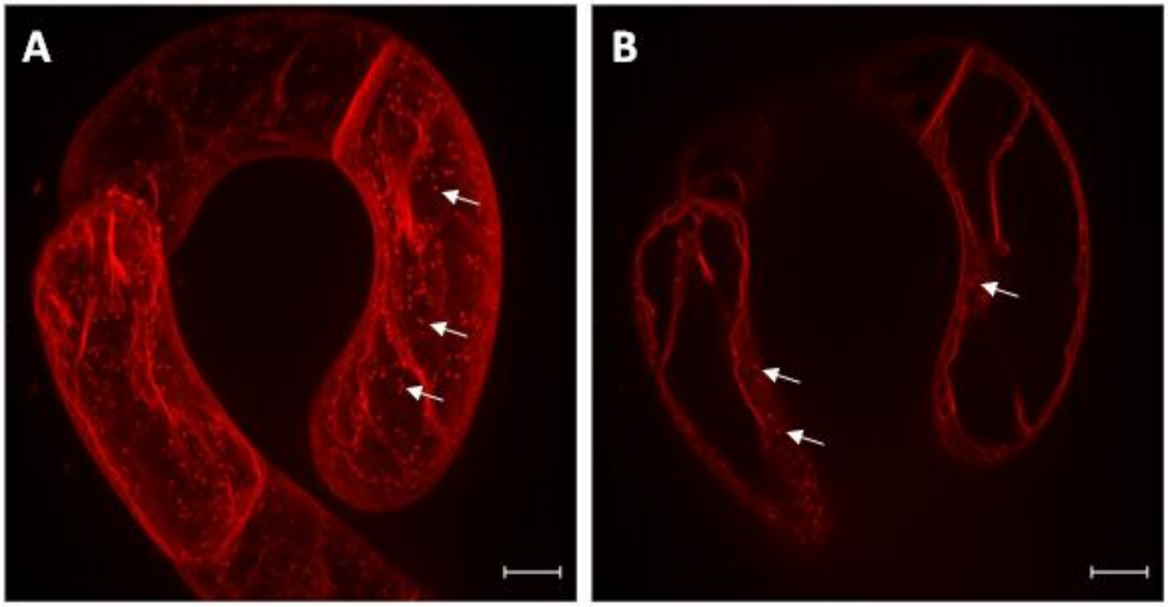

Fig. 22: Nile-Blue Icafolin treatment of Tobacco BY-2 Wildtype cells. *A: Wildtype cell after 1 h incubation with 100 µM Nile-Blue Icafolin. Orthogonal Projection reveals dot-like accumulations within the cell. B: Optical Chapter of the same wild-type cell observed in A. Accumulations of NB-Icafolin are located within the cytoplasm. Arrows are indicating NB-Icafolin accumulations.The scalebar represents 10 µm.*

In wild-type cells, accumulations of the Nile-Blue Icafolin construct are observed as dot-like intracellular structures (**Fig. 22, A**). To gain insight into the subcellular localization of these structures, an optical Chapter of the same wild-type cell was obtained, revealing a cytoplasmic localization of Nile-Blue Icafolin (**Fig. 22, B**). To gain further insight into the potential colocalisation at microtubules, the same treatment was conducted on samples from the TuA3 cell line (**Fig. 23**). In untreated control cells, microtubules are observed as intact network-like structures (**Fig. 23, A**). In contrast, cells treated with 100 µM Nile-Blue Icafolin display shortened and reduced microtubule numbers (**Fig. 23, B**) indicating the bioactivity of the molecule. Nile-Blue Icafolin appears as dot-like accumulations within the cell (**Fig. 23, C**), while a merge of both excitation channels does not reveal an obvious overlap of Nile-Blue Icafolin accumulations and microtubule localization (**Fig. 23, D**).

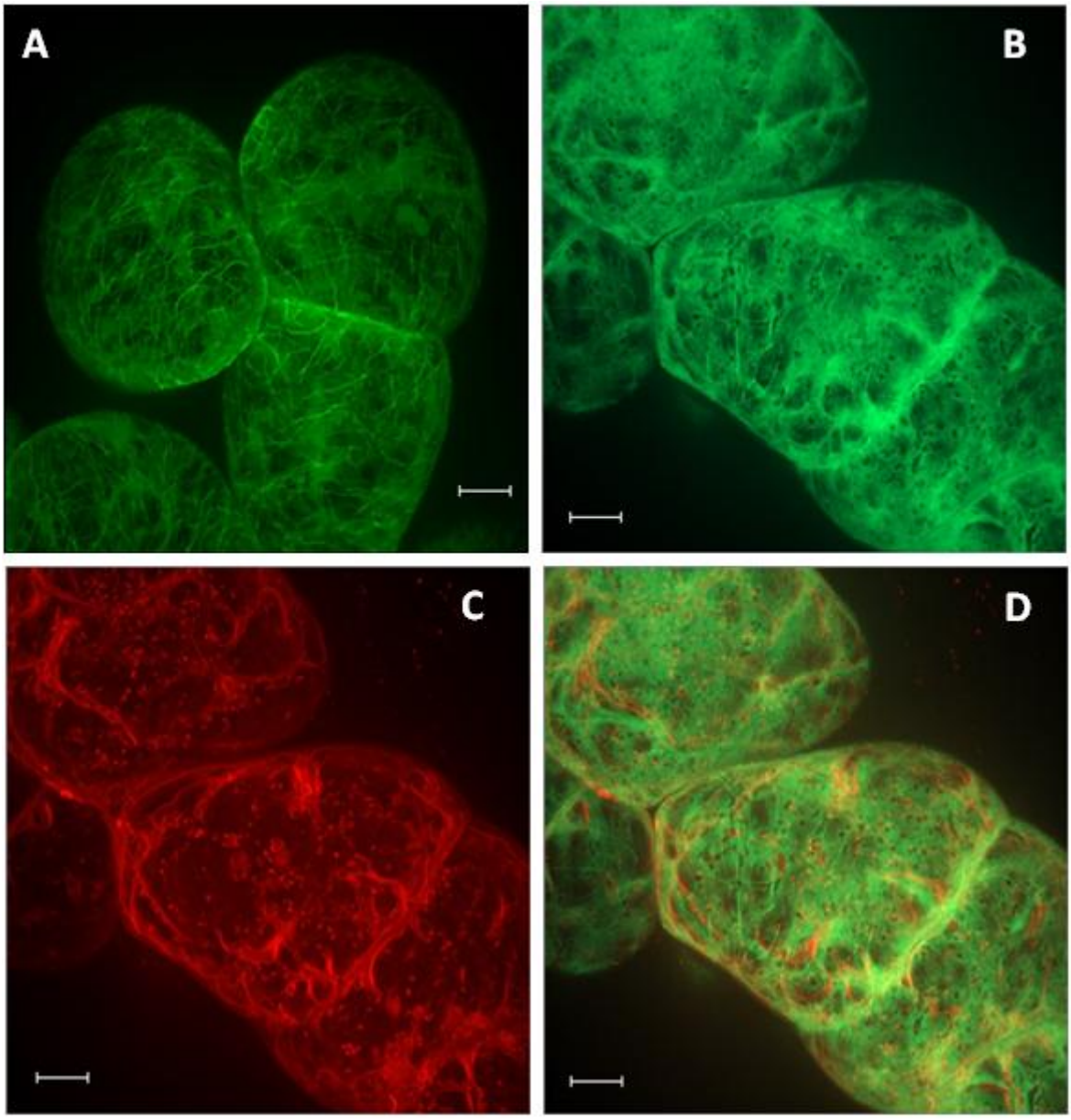

Fig. 23: Nile-Blue Icafolin treatment of Tobacco BY-2 TuA3cells. *A: Untreated TuA3 control cells. Microtubules are intact. B/C/D: TuA3 cells treated with 100 µM Nile-Blue Icafolin with different excitation wavelengths to visualise either tubulin (B), Nile Blue-Icafolin (C) or both (D). B: Microtubules are shortened. C: Dot-like structures can be observed within the cell. D: No obvious colocalisation of remaining microtubules and NB-Icafolin can be observed. The scalebar represents 10 µm.*

To gain further insight into the uptake mechanism, cells were pre-treated with the endocytosis blocker Ikarugamycin at a concentration of 10 µM for 24 h prior to Nile-Blue Icafolin treatment. To confirm the complete inhibition of endocytosis, Synaptored, a dye requiring uptake by this mechanism, was applied. To visualise the uptake success, optical Chapters of treated Tobacco BY-2 Wildtype cells were created. The images obtained demonstrated the effective inhibition of Synaptored invasion into the cell (**Fig. 24A**), whereas treatment with Nile Blue Icafolin resulted in the observation of a fluorescent signal within the cytoplasm (**Fig. 24B**) indicating for a different uptake mechanism than endocytosis.

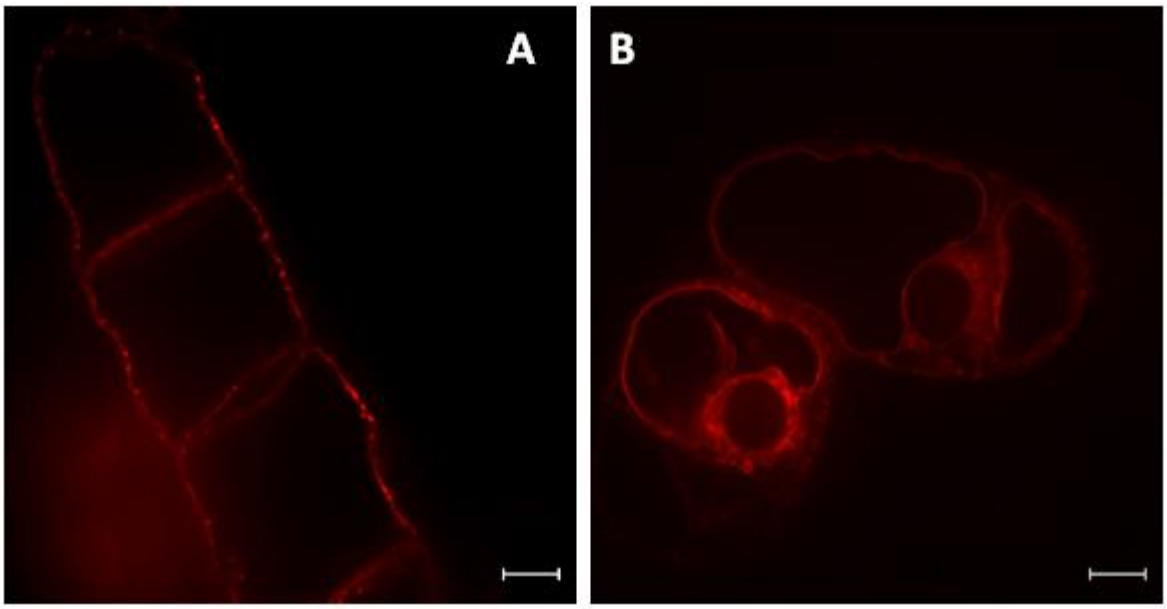

Fig. 24: Nile-Blue Icafolin treatment after endocytosis block. *A: Optical Chapter of a Tobacco BY-2 Wildtype cell treated with 10 µM Ikarugamycin for 24h before treatment with 10 µM Synaptored. The cell is not permeable to the endocytosis-dependent dye. B: Optical Chapter of a Tobacco BY-2 Wildtype cell treated with 10 µM Ikarugamycin for 24 prior treatment with 100 µM Nile-Blue Icafolin. Intracellular fluorescence can be detected. The scalebar represents 10 µm.*

3.10 Approaches of tubulin isolation

Given the evident influence on microtubules, it seems plausible that tubulins may be implicated or even targeted by Icafolin. To substantiate or refute this hypothesis, it is essential to isolate tubulins from crude extracts and examine their interaction properties with Icafolin.

3.10.1 EPC-Sepharose Affinity Chromatography

It has been previously demonstrated that the herbicide ethyl-N-phenylcarbamate possesses the capacity to bind α-tubulins. Consequently, an affinity matrix was constructed and EPC was coupled to Sepharose beads (**see Chapter 2.14**). The resulting affinity matrix was then transferred into custom made filter inlets for 2 ml reaction vessels and loaded with either wild-type, TuA3, or TuB6 crude protein extracts. The washing and elution steps were performed using centrifugal force. Following several washing steps with TBS, the load column was gradient eluted with a rising salt concentration ranging from 0 M to 1 M in 0.05 M steps. To gain initial insight into tubulin elution, samples derived from TuA3 were analysed for fluorescence intensity using a fluorometer for each obtained fraction. The results demonstrated a consistent elution ranging from 0.1 M KCl to 0.3 M KCl (**Fig. 25**).

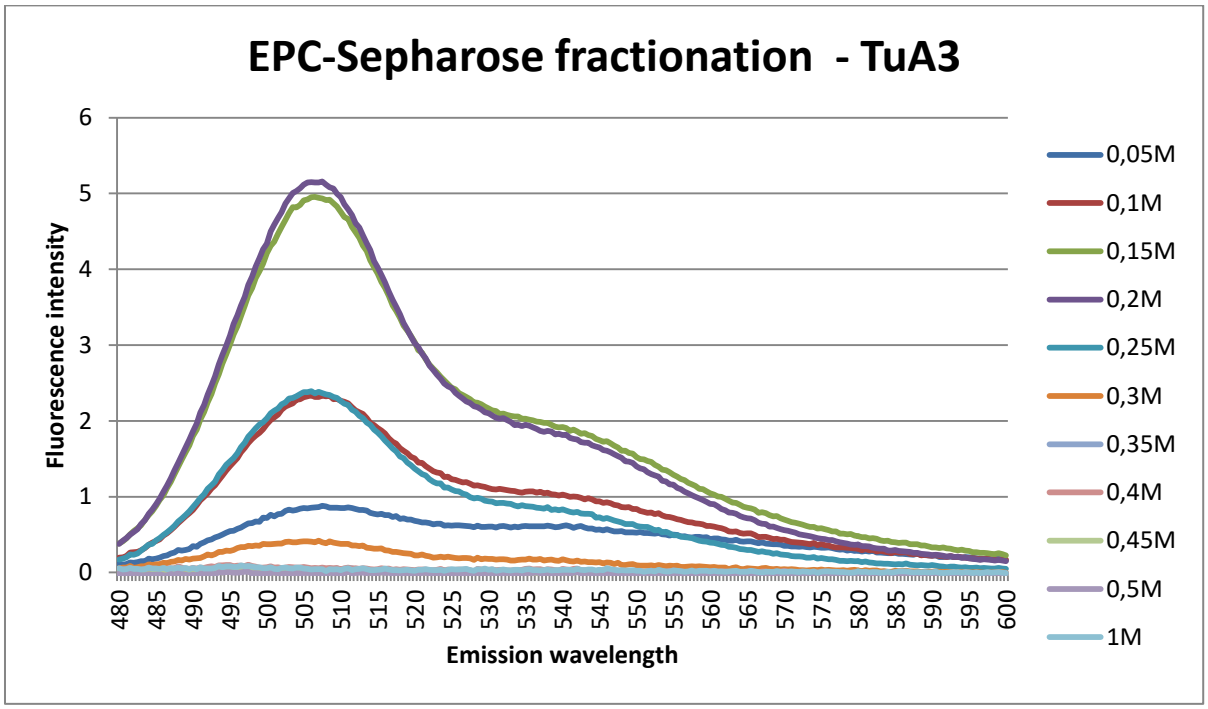

Fig. 25: Fluorometer measurement of fractions obtained by EPC-Sepharose affinity chromatography. *The graph shows the emission spectra of obtained fractions after affinity chromatography. The excitation wavelength was 488 nm. The expected emission peak for GFP is 507 nm.*

To further verify the successful isolation of tubulin and to assess the purity of the fractions, the wild-type fractions were concentrated by TCA precipitation, resuspended in a total volume of 30 µl in 3x loading buffer, and separated by SDS-PAGE in a duplication setup. The

resulting gels were either stained with Coomassie blue to identify any potential protein contamination or used for western blotting to detect α-tubulin. The results demonstrated successful tubulin fractionation and the presence of α-tubulin in fractions that were consistent with the findings of the previous fluorescence assay (**Fig. 25/26, B**). However, the obtained fractions also exhibited a significant presence of impurities (**Fig. 26, A**).

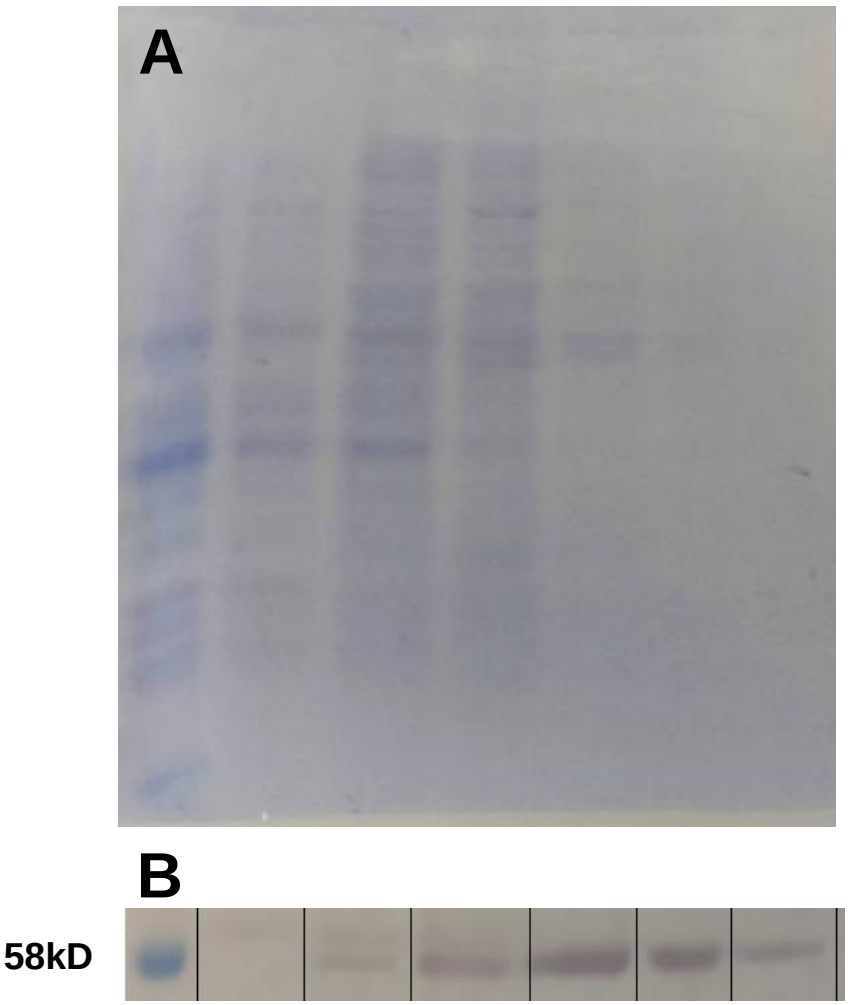

Fig. 26: Stained SDS-PAGE gel and western blot results of EPC fractionated wildtype proteins. *A: SDS-PAGE gel stained with Coomassie Brilliant Blue. Fractions contain less protein content with rising salt concentration during elution. B: Western blot of EPC fractionated wildtype proteins. α-tubulin is detectable in fractions eluted with 0.1 M KCl up to 0.3 M KCl.*

3.10.2 Tubulin isolation by ultracentrifugation

In the subsequent approach for tubulin isolation, a more traditional approach was employed. By leveraging the intrinsic property of free tubulin to spontaneously polymerise into microtubules *in vitro*, it is feasible to separate polymerised microtubules from other soluble proteins through ultracentrifugation along a density gradient. To this end, a 20 % sucrose solutions in TBS was prepared and carefully layered into a 2 ml tube suitable for ultracentrifugation purposes, thereby creating a sucrose cushion when covered with TBS. The protein extracts were incubated in the presence of the microtubule stabilising agent Taxol, which enhanced microtubule polymerisation and stability. Following the incubation period, the protein samples were placed on top of the sucrose gradient tube and ultracentrifuged at 100,000 g for 1 h. This process allowed the polymerised microtubules to sediment, while molecules of lower density were retained by the sucrose cushion. The resulting pellet was resuspended in 30 µl 3x loading buffer and subjected to SDS-PAGE, followed by Coomassie brilliant blue staining and additional western blotting to ascertain the purity of the tubulin.

The western blot results demonstrated the successful detection of tubulin in the investigated sedimentation (**Fig. 27, A**). The Coomassie brilliant blue staining of a polyacrylamide gel containing a sample of the same sedimentation product reveals a plethora of proteins present (**Fig. 27, B**), indicating for insufficient purity. It is noteworthy that the bands observed in the western blot for tubulin are conspicuous in the Coomassie brilliant blue-stained gel (**Fig. 27, A and B, red arrows**), potentially indicative of tubulin degradation products.

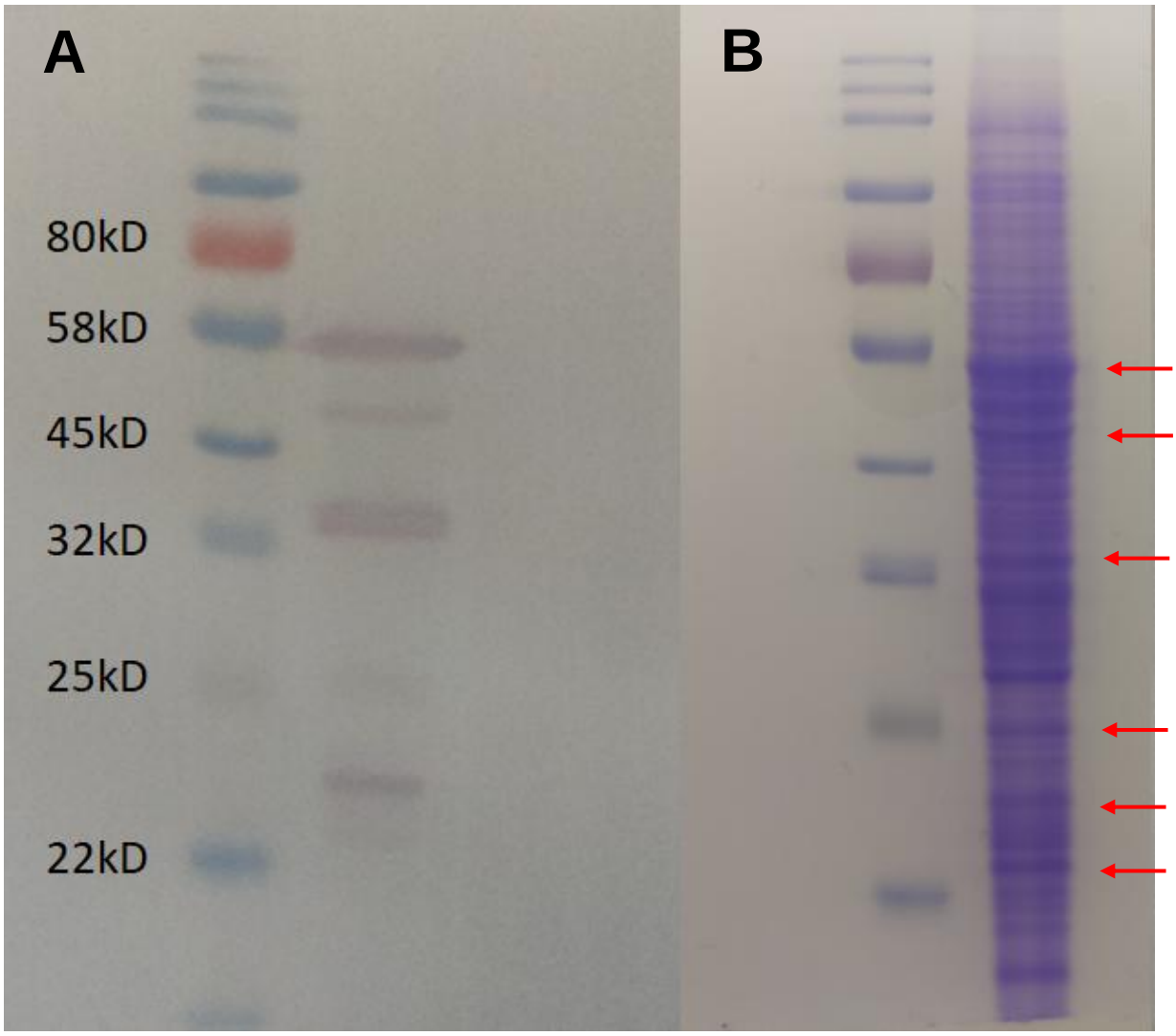

Fig. 27: Tubulin isolation by ultracentrifugation. *A: Polyacrylamide gel stained by Coomassie Brilliant Blue reveals massive impurities in the sample. B: Western blot result aimed at tubulin detection. tubulin can be detected in the sedimented pellet. Red arrows indicate the corresponding height of bands found for tubulin presence in (A).*

3.11 Approach of chromatographic purification of the interacting protein – exploiting ultrafiltration

In the context of chromatographic approaches, the ability to track the fraction of interest is of paramount importance. In this experiment, the method of ultrafiltration was employed in an attempt to develop a drug-target binding assay. Protein extracts of tobacco BY-2 wild-type cells were subjected to affinity chromatography using Icafolin coupled to agarose beads and subsequently eluted by ionic pressure delivered by salt addition to the elution buffer (**Chapter 2.8**). In order to ascertain the approximate range of elution in which the protein of interest can be detected, protein extracts were fractionised by their affinity to Icafolin against salt concentrations of 1M, 2M and 3M KCl. The eluates were mixed with 10 µM Icafolin, incubated for 10 minutes, and subsequently transferred into a 2 ml ultrafiltration device. Following filtration, the respective retentates and flowthrough samples were subjected to MS/MS analysis in order to quantify the concentration of Icafolin. If Icafolin can be bound by its target protein present in the respective fraction, an increase in Icafolin concentration in the retentate should be observable. Unfortunately, the results revealed no significant change to the negative control, which consisted of the washing buffer only (**Fig. 28**). In all measured samples, a higher Icafolin concentration was observed for the retentate compared to its respective flowthrough which might be related to unsufficient elution from the column as discussed later (**Chapter 3.12**).

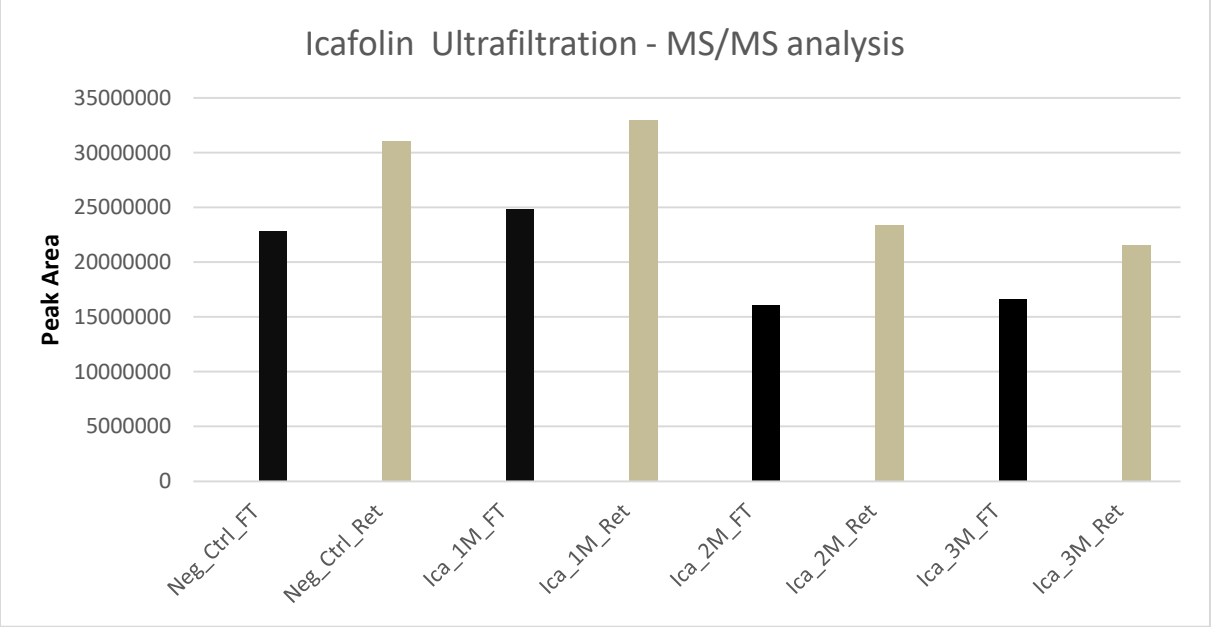

Fig. 28: MS/MS-Measurement of Icafolin ultracentrifugation samples. *Results show a similar pattern for all measured samples, including the no protein-containing negative control. The shown graph represents only one replication of the experiment.*

3.12 Nile-Blue Icafolin as a Sensor for Protein Fractionation

In this experiment, the objective was to utilise the properties of the Nile-Blue Icafolin construct to track potential binding events in SEC-derived fractions of a tobacco BY-2 protein extract. In its unbound state, the molecule's fluorescence is quenched, the quenching effect is hypothesized to be released after successful binding to the interaction partner of Icafolin, resulting in an amplification of fluorescence intensity. To validate this hypothesis, extracts of the soluble protein fraction of Tobacco BY-2 wild-type cells were prepared and diluted, then transferred to a 96-well plate. The fluorescence intensity was determined by a plate reader device after the addition of different concentrations of the Nile-Blue Icafolin construct to each well. The results demonstrated a correlation between an increase in fluorescence intensity and the concentration of both, protein and Nile-Blue Icafolin, in each respective well (**Fig. 29**).

Following the proof of concept, protein fractions were created by size exclusion chromatography using FPLC. 100 µl of the obtained fractions were transferred into a 96 well plate and mixed with 300 nM of NB-Icafolin in order to identify the fraction containing the potential interaction partner (**Fig. 30**). The results demonstrated an increase in fluorescence intensity at fraction 16 for all investigated cell lines. The controls were composed of either the chromatography mobile phase buffer (**Fig. 30 A/B, H1-5; C, H1-2**), and 100 nM, 200 nM, 300nM or 400nM NB-Icafolin as negative control, or the respective unfractionated extract of the soluble protein fraction of the investigated cell lines containing the same set of Nile-Blue Icafolin concentrations (**Fig. 30, A/B, H7-11; C, H7-8**). While negative controls exhibited a slight increase in fluorescence intensity, dependent on the concentration of NB-Icafolin, positive controls demonstrated a significant elevation in signal. Fractions of interest were submitted for mass spectrometry analysis; however, due to the low protein content within the samples, no definitive results could be obtained.

Raising fluorescent construct concentration

Raising protein concentration

Protein Extract	Nile Blue-Icafolin											
	0nM	5nM	10nM	20nM	30nM	40nM	50nM	60nM	70nM	80nM	90nM	100nM
no Protein	665	3000	3064	4734	7746	7024	8965	10124	13286	18116	14957	18133
(1:100)	622	1802	2530	3517	5047	9591	7574	8254	9526	10221	10701	14170
(1:32)	670	1765	3181	3746	5245	6284	8388	9934	11568	13004	12933	17264
(1:16)	959	2139	2582	4056	7408	7531	9098	10005	12267	12607	12329	21477
(1:8)	703	1671	2748	3978	6170	8038	9173	10815	14822	14561	15832	22745
(1:4)	709	2023	3084	4641	7001	8785	11350	13105	14310	18417	20036	13254
(1:2)	841	2353	3205	5964	8126	10046	12466	14642	18513	20368	20972	37601
Undiluted Protein	933	2700	3811	6666	8843	10683	13917	16582	18456	21395	23666	40795

Fig. 29: Nile-Blue sensor dilution series. *A dilution series of the soluble protein fraction of Tobacco BY-2 cells was created and transferred into a 96-well plate. Fluorescence intensity is raising drastically if the interaction partner of the Nile-Blue Icafolin construct is present in a sufficient concentration.*

A **Wildtype**

	1	2	3	4	5	6	7	8	9	10	11	12
A	18979	19464	14412	20944	22257	23267	21984	15325	21992	19037	18912	15523
B	14400	15767	30437	72072	56306	43066	38702	22896	23252	26743	25335	20470
C	15675	11006	12189	12972	11855	10282	9838	10620	12038	9683	9925	9843
D	20670	21707	23066	30463	26767	20693	16037	14355	11076	8767	9353	11176
E	8403	11589	12711	10707	10836	9976	7976	13269	11635	15151	14997	10041
F	5409	9412	5157	11237	8138	7414	6761	8596	8266	9221	9854	6339
G												
H	631	10932	21236	22445	26536		2823	55830	84865	121157	150311	

B **TuA3**

	1	2	3	4	5	6	7	8	9	10	11	12
A	1028	956	30963	25746	30659	32596	29245	31166	34224	14994	24934	29838
B	31800	32707	34778	92256	85904	74533	63386	53889	45393	45425	43106	50582
C	43215	52579	44809	49906	48788	43058	50091	38700	39402	34734	36020	34735
D	28628	23608	21215	23731	31015	40675	41819	27846	31931	25037	26758	26512
E	34493	29961	33036	27058	25743	19639	26734	14298	22671	21544	23127	26599
F	19212	22637	15596	14967	16518	21294	22364	17877	21556	23477	15699	527
G												
H	498	14411	9442	17916	27690		4241	105583	185600	208406	260000	

C **TuB6**

	1	2	3	4	5	6	7	8	9	10	11	12
A	4905	5916	5046	9491	5389	5702	7298	7592	11908	4728	5272	2951
B	9160	9321	6973	23506	18893	17575	14543	12136	12894	12826	11785	10087
C	6291	6577	6042	4992	4293	4060	3205	5045	4409	5658	6774	5699
D	6816	8137	7393	5543	3229	4161	6127	4939	4977	5148	5096	5474
E	4285	5745	4317	5002	4941	5032	4347	3593	3876	3715	5575	5646
F	3375	2664	2459	3398	2590	2844	4857	3072	2827	2333	2766	2677
G												
H	496	16325					1237	41590				

Fig. 30: Nile-Blue sensor fractionation experiment. *The soluble protein fraction of either Wildtype (A), TuA3 (B) or TuB6 (C) were fractionized by FPLC driven size exclusion chromatography. Obtained fractions were transferred on a 96 well plate represented as table in this figure. After addition of 300nM Nile-Blue Icafolin, fluorescence intensity was measured by a plate reader device. A strong increase in fluorescence signal can be observed in fraction 16 for all investigated cell lines (A,B,C). Negative controls contain the chromatography mobile phase buffer containing 0 nM,100 nM,200nM,300 nM or 400 nM Nile-Blue Icafolin located at H1-5 for (A) and (B) and 0 nM and 300 nM Nile Blue Icafolin located in H1-2 for (C). Positive controls contain the unfractionized soluble protein fraction containing 0 nM,100 nM,200 nM,300 nM or 400 nM Nile-Blue Icafolin located in H7-11 for (A) and (B) and 0 nM and 300 nM Nile-Blue Icafolin located in H7-8 for (C).*

3.13 Affinity chromatography reveals a set of Microtubule-associated Proteins as possible targets

In order to obtain fractions of greater purity in higher concentrations, an affinity chromatography approach was employed. To this end, the identical linker-Icafolin construct employed for the Nile-Blue Icafolin molecule was coupled to agarose, thus creating an affinity matrix. The obtained gravity column was loaded with the soluble protein fractions of either wild-type, TuA3 or TuB6 cells. Following washing, 1 ml fractions were obtained by gradient elution with a KCl solution ranging from 0 M to 3 M in 0.1 M steps. The proteins in the resulting fractions were concentrated by TCA precipitation, separated by SDS-PAGE, stained, and the obtained bands were sent for MALDI-MSI analysis (**for an example, see Fig. 31**). The results revealed five potential interaction candidates, all of which are related to microtubules and involved in microtubule-regulating mechanisms (**Table 5**).

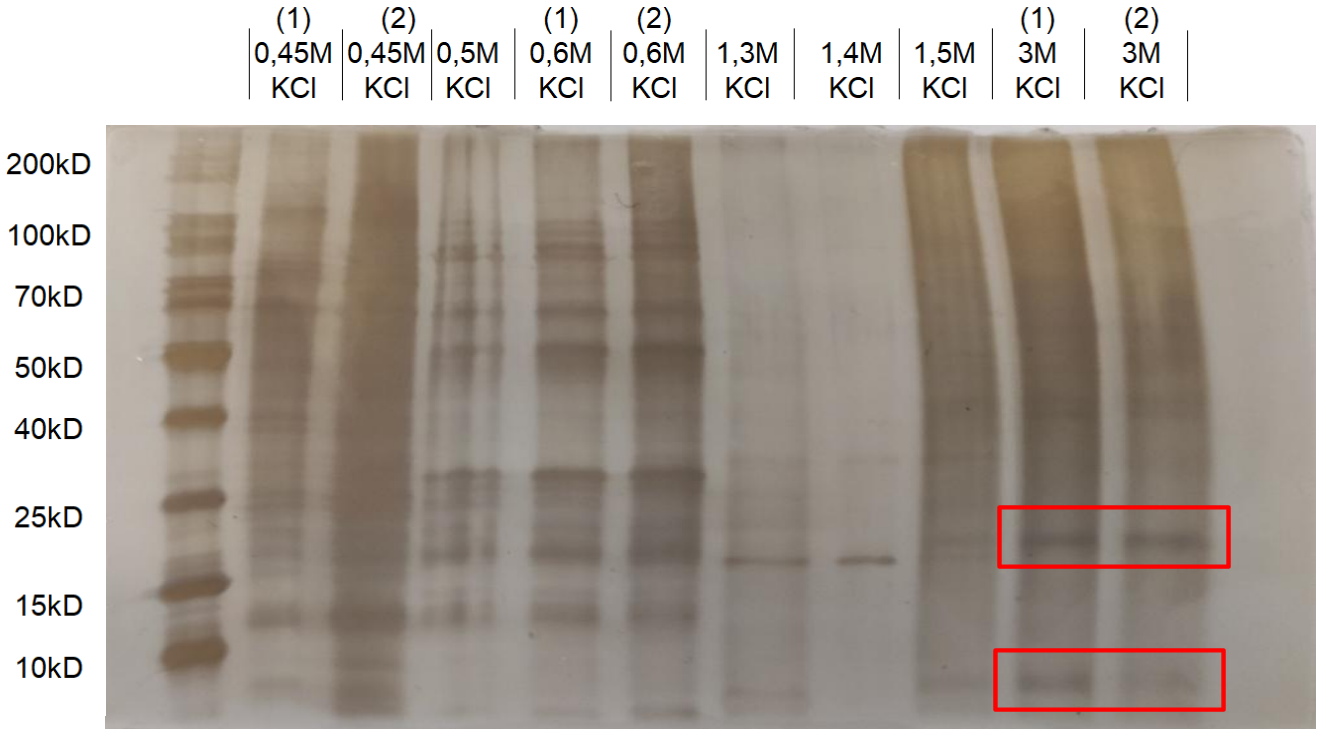

Fig. 31: Exemplary SDS-PAGE result of affinity chromatography fractions. *After affinity chromatography fractionation, obtained protein fractions were separated by SDS-PAGE. The resulting gel was stained by the silver staining technique. Since a higher affinity of a protein to the column matrix requires a higher salt concentration, proteins contained in the high salt fractions are more likely to harbour the interaction partner of Icafolin. Therefore, bands originating from high salt fractions were preferably cut and sent for mass spectrometry analysis. Numbers in clamps indicate replications load on the gel; the red rectangle indicates exemplary interesting bands obtained from high salt fractions.*

3.14 Icafolin might bind irreversibly

Following the previous described affinity chromatography approach, the column matrix exhibited a fluorescence signal under UV excitation (**Fig.32**). As the experiment was conducted with cell lines containing GFP-tagged subpopulations of tubulin, it was necessary to ascertain whether the observed fluorescence of the matrix was due to the tagged tubulin adhering to the column despite elution with a salt solution of high molarity, autofluorescence of the matrix or if the GFP tag itself exhibited a high affinity for the column. To address this issue, a new column was created and tested for autofluorescence prior to use in the experiment. To ascertain whether the GFP-tag is binding, a protein extract from an additional cell line, which harbours a GFP-tagged FABD2 (an actin-associated protein), was loaded, eluted and examined for residual fluorescence signal on the column. Finally, the same procedure was repeated with a protein extract of the TuA3 cell line.

The results demonstrate that agarose-Icafolin itself does not exhibit autofluorescence behaviour (**Fig. 32, A**). Following the loading and elution of an extract derived from the GFP-FABD2 cell line, only minor fluorescence was observable following the replication of three cycles (**Fig. 32, B**). In contrast, the loading and elution of an extract derived from the TuA3 cell line demonstrated a robust binding of fluorescent molecules to the column, which could not be eluted even with a 3 M salt solution (**Fig. 32, C; D**).

Consequently, the column matrix was removed and boiled at 98°C in protein extraction buffer for 10 minutes to denature bound proteins and achieve release from the column matrix. The resulting samples were either separated by SDS-PAGE according to the previous experiment or sent directly for MS analysis. The results confirmed the candidates obtained from experiment in Chapter 3.12 and additionally identified further microtubule-associated proteins involved in the regulation of microtubule nucleation (**Table 5**).

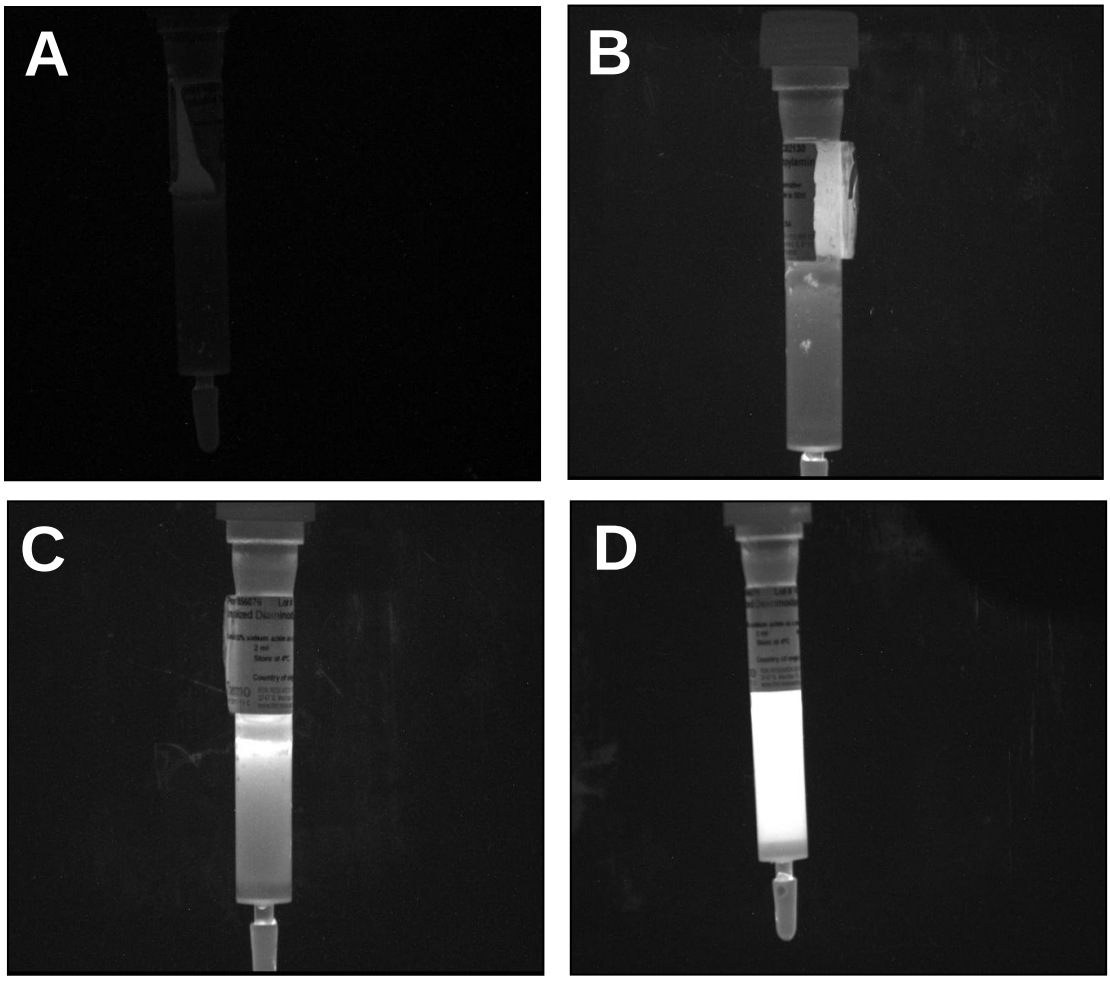

Fig. 32: Fluorescence remaining on the column after elution. *A: Fresh column before experimental usage. B: Fluorescence after loading and elution with an extract containing GFP-FABD2 for three times. C: Fluorescence after loading and elution of a TuA3 protein extract once. D: Fluorescence after full saturation of the column matrix due to repeated TuA3 loading. For each loading and elution cycle, samples were washed with 10 ml TBS before elution with 10 ml 3 M KCl solution.*

Protein ontology	Predicted function
Nucleation related protein 1	Involved in microtubule nucleation
Nucleation related protein 2	Involved in microtubule nucleation
Nucleation related protein 3	Involved in microtubule nucleation
Nucleation related protein 4	Involved in microtubule nucleation
Nucleation related protein 5	Involved in microtubule nucleation
ATP synthase	ATP synthesis
Microtubule associated protein 1	Function unknown, covers microtubules
Microtubule associated protein 2	Microtubule bundling
α-tubulin3	Part of microtubules
β-tubulin6	Part of microtubules

Table 5: List of interaction candidates obtained by affinity chromatography.

4 Discussion

The discovery of herbicides in the 1940s constituted a revolutionary development in the field of weed control management, transforming modern agriculture. The considerable success of these herbicides prompted the development of a multitude of substances that employ a vast array of different modes of action, which were subsequently released in the subsequent decades. Nevertheless, the market reached saturation in 1991, and no herbicide with a novel mode of action was introduced for three decades. In the present day, the continued excessive use of herbicides by farmers is promoting the evolution of herbicide-resistance in weeds. The current situation is therefore characterised by an increasing number of weeds developing resistance to one or multiple herbicide modes of action, while there are no novel modes of action to counter this.

In the present study, a promising novel substance to be released by Bayer Crop Science, Icafolin, was investigated for its cellular mode of action. The findings can be differentiated into two experimental Chapters, which contribute to a model for the mode of action at the end of this discussion. The first Chapter addresses the following areas:

1) Phenotype, Cytoskeleton and Microtubules

The second Chapter addresses the following areas:

2) Method development and target protein

4.1 Phenotype, Cytoskeleton and Microtubules

4.1.1 Icafolin is active at a low threshold. What does this mean?

The initial trial was designed to verify the hypothesis proposed by Bayer Crop Science that Icafolin acts on microtubules. The impact of Icafolin on microtubules was confirmed using tobacco BY-2 cell culture and *A. thaliana* seedlings expressing GFP-tagged tubulin α3 or β6 for microtubule visualization or GFP-tagged FABD2 for actin visualization. Furthermore, the threshold of Icafolin could be determined to be as low as 50 nM for short-term experiments and even 30 nM for long-term exposure, which is a surprisingly low concentration in comparison to other anti-microtubule agents such as Oryzalin or Propyzamide. The lowest observable effect of Oryzalin is 300 nM, while Propyzamide requires 2 µM (Akashi, Izumi et al. 1988, Baskin, Wilson et al. 1994, Baskin, Beemster et al. 2004). This is consistent with the specific mode of action of these compounds, which is thought to involve binding to free tubulin dimers, preventing further incorporation into growing microtubules, and ultimately leading to microtubule depolymerisation due to the dynamic nature of (Hugdahl and Morejohn 1993, Young and Lewandowski 2000). Given that tubulin can be considered a bulk protein, present in a relatively high copy number in a healthy cell as evidenced by various studies (Gard and Kirschner 1987, Goldmacher, Audette et al. 2015, Loiodice, Janson et al. 2019), the extremely low threshold suggests a potential target in the area of microtubule regulation or even signalling. The microtubule stabilising drug Taxol was unable to rescue the phenotype; however, it was demonstrated that it was slowing down the process, indicating that microtubule dynamics may be an additional mechanism factor.

4.1.2 Icafolin shows herbicidal activity. But why is death coming late?

The exposure of tobacco BY-2 cells to Icafolin throughout the cultivation period has been observed to effectively suppress growth, as evidenced by the reduction in sugar consumption in the cultivation media. Upon closer examination, cells exposed to Icafolin demonstrate a preliminary loss of cell axis following a 24 h exposure. This is evidenced by lateral bulging at the terminal cells of a cell filament, which progressively increases over the course of day 2, ultimately resulting in complete rounding up of cells by day 3. Following the day 4, the percentage of dead cells is increasing, and radial cell swelling is becoming evident. Given that mitotic activity typically reaches its peak on day 4 after subcultivation in tobacco BY-2 cell cultures, and that the cultivation cycle subsequently transitions into the elongation phase (Huang, Maisch et al. 2017), it can be postulated that the observed increase in mortality is linked to the mitotic process or the elongation of cells. The diverse superstructures of microtubules influence the proliferation process, rendering mitotic cells incapable of completing a successful mitosis when inhibitied. This phenomenon is often exploited to create polyploidy through the use of anti-microtubule agents (Ascough, Van Staden et al. 2008, Miguel and

Leonhardt 2011, Bharati, Fernández-Cusimamani et al. 2023). Conversely, the increase in mortality may be attributed to programmed cell death, which is initiated by the cell in response to incomplete cell division. Although this process, which is commonly referred to as mitotic catastrophe, has not yet been empirically demonstrated to occur in plant cells, it is a topic of active theoretical speculation within the scientific community. Furthermore, the progressive loss of cell axis and radial cell swelling is a well-described phenomenon that occurs when microtubules are lost (Baskin, Wilson et al. 1994, Baskin, Beemster et al. 2004, Domozych, Sørensen et al. 2013). The phenomenon is linked to the interaction of cortical microtubules with the cellulose synthase complex, which is guided along microtubule tracks during cellulose synthesis (Paredez, Somerville et al. 2006). The orientation of cellulose fibres around the cell defines the cell axis through reinforcement of the lateral cell wall, resulting in increased rigidity. The cell then expands perpendicular to the cellulose fibres (Nick 1998). In the absence of microtubules, this mechanism cannot be maintained, leading to progressive defects in cell axis and resulting in cell swelling when water uptake raises the turgor pressure required for cell expansion.

4.1.3 Icafolin enters the cell and localizes in small accumulations. Can there be any conclusions?

The labelling of Icafolin with the fluorescent dye Nile-Blue enabled the performance of localisation experiments *in vivo*. Following treatment, NB-Icafolin was observed to invade the cytoplasm, forming small dot-like accumulations within the cell. It was postulated that these punctate accumulations could be endocytic vesicles, which could be rapidly dislodged by a straightforward experiment utilising the endocytosis blocker Ikarugamycin. Although the dye Synaptored, which requires endocytosis to stain membranous cellular compartments, was excluded from the cell, NB-Icafolin was still able to penetrate. This suggests that either the membrane permeability of Icafolin is altered, or active transport mechanisms are involved. Furthermore, it was observed that there was no discernible colocalisation with microtubules. This further suggests that tubulin is not the interaction partner of Icafolin. If free tubulin dimers were to be targeted (by sequestration), one would anticipate the presence of a diffuse signal within the cell cytoplasm, in accordance with the location of free tubulin dimers. If tubulin, which is incorporated in established microtubules, were the target, a clear colocalisation should be observable either at the entire remaining microtubule residue or at least at one specific location along the microtubule structure. Therefore, it can be concluded that the mode of action affects microtubule regulation. Nevertheless, these findings should be interpreted with caution, given that the fluorophore attached to Icafolin, Nile Blue, is known to bind to hydrophobic molecules and accumulate in lysosomes (Martinez and Henary, 2016). While the molecule's activity has been demonstrated, its localisation may be influenced by the fluorophore's affinity, potentially leading to misinterpretation. To ensure accurate results, the experiment should be repeated with a control of untagged Nile Blue, excluding the possibility of fluorophore-induced localisation issues.

4.1.3 Removal of Icafolin results in complete microtubule recovery. But why the delay?

The results of the experiments demonstrated that if Icafolin is removed from the system, microtubules are capable of recuperating fully, contingent on the initial concentration of Icafolin and the duration of the incubation period. This phenomenon can also be observed in the case of anti-microtubule agents such as Propyzamide, which binds reversibly to tubulin (Akashi, Izumi et al. 1988). A notable distinction between Icafolin and other agents is the time required for complete recovery. In the case of Propyzamide, recovery times of approximately 15 minutes have been reported following the washing out event (Akashi, Izumi et al. 1988), which can be attributed to the high dynamic nature of microtubules. To get comparable results, cells treated with Icafolin should be observed for a minimum of 24 hours, or longer if higher concentrations or extended exposure times are employed. Given the delay in recovery, it was postulated that complete sequestration of the target protein by Icafolin might

occur, necessitating *de novo* synthesis. This would account for the delayed but successful reestablishment of the microtubular network. This hypothesis could be falsified by the addition of Cycloheximide, a translation blocker, to the experimental setup. It can thus be demonstrated that the return of microtubules is not dependent on translation. One potential explanation for this delayed phenomenon is affinity-guided targeting of microtubule-regulating complexes. If Icafolin exhibits a higher affinity for its target while it is incorporated in a complex, it may successfully sequester the complex, leading to microtubule destabilisation. Furthermore, if the complex components are also part of additional complexes, the turnover of these complexes may allow for the reestablishment of functional complexes after Icafolin removal, resulting in a delayed microtubule recovery. One illustrative example of a complex is the γ-TuSC and γ-TuRC complexes, whose components are proposed to participate in different derivative complexes. This participation may be dependent on factors such as phosphorylation status or post-translational modifications, which are necessary for fulfilling location and/or cell cycle-specific functions (Cuschieri, Nguyen et al. 2007, Teixidó-Travesa, Roig et al. 2012).

4.2 Method development and target protein

4.2.1 Approaches of tubulin isolation

In order to assess experiments designed to ascertain information regarding direct tubulin interaction, attempts were made to isolate tubulin. Although both tested approaches are viable for the isolation of tubulin in a fraction, it was not possible to obtain a sample free of microtubule-associated proteins or other contamination. To exclude the possibility of interference from MAPs, a more rigorous methodology is required. In view of the observed indications that Icafolin does not act as a direct interaction partner with tubulin, no further attempts at tubulin purification were made during the course of this study. Should this prove to be a more significant factor in future research, it may be necessary to refine the methodologies employed in this study, for instance through repeated *in vitro* polymerisation and depolymerisation events of microtubules in order to remove as many MAPs as possible. An alternative approach could be the forced denaturation and renaturation of tubulin. If tubulin can be purified to a sufficient degree, it may be possible to develop assays that provide evidence for direct tubulin interaction through titration experiments. If tubulin is indeed the interaction partner, the addition of Icafolin to a sample of purified tubulin and subsequent addition of viable tobacco BY-2 cells should result in a significant reduction in the observed effect due to the sequestering effect of free tubulin in the sample.

4.2.2 Exploiting Ultrafiltration

The objective of the method developed in this Chapter was to facilitate the tracking of fractions of interest following chromatographic approaches to fractionise protein extracts obtained from tobacco BY-2 cell cultures. Ultrafiltration is a commonly employed technique for concentrating protein content in a given sample by utilising filter membranes with a specific cutoff in the kD range. In this approach, the characteristics of ultrafilters were investigated with the objective of separating excess Icafolin following incubation in protein fractions after affinity chromatography. It was found that this approach was not functional for Icafolin. The results demonstrated a comparable elevation in Icafolin levels for the retentate in all sampled specimens, including the negative control comprising solely of washing buffer and no proteins. This suggests a moderate binding affinity to the filter membrane, and furthermore, no binding event in the respective fractions. In conclusion, the results may be explained by the properties of the affinity matrix. Subsequently, it was demonstrated that complete elution of the affinity column could not be achieved by ionic pressure. The highest salt concentration of 3 M KCl proved ineffective. As this was not known at the stage this method was applied, it is possible that the column was saturated with the actual target protein, which may have resulted in the loss of the potential target protein during the initial washings steps of the column after sample loading. The results obtained from the control, which did not contain any protein

but only washing buffer, demonstrated a comparable concentration discrepancy between the retentate and flowthrough as observed in fraction samples, thereby corroborating the conclusion. For alternative approaches to chromatographic fractionation, such as size exclusion or ion exchange chromatography, this methodology may offer a reliable indicator for monitoring the fraction of interest in the context of drug-protein interactions, and it may be subjected to further testing in future endeavours.

4.2.3 NB-Icafolin as sensor

In addition to the methodology outlined in Chapter 4.2.2, a further approach for the tracking of protein fractions following chromatographic processing has been developed. Given that the design of NB-Icafolin results in a quenching effect of Nile Blue, which was postulated to be released following binding, the addition of NB-Icafolin to fractions containing the interaction partner of Icafolin should result in a significant increase in fluorescent intensity compared to fractions lacking an appropriate binding partner. To obtain a rapid result, the fractions were transferred into a 96-well plate, 300 nM NB-Icafolin was added, and the subsequent measurement of the fluorescence signal was performed using a plate reader device. The results demonstrated a significant increase in fluorescence for certain fractions. Furthermore, the results were reproducible for all tested tobacco BY-2 cell lines. The fractions indicating binding events were subjected to MS/MS analysis, and the results are still pending until the end of this study.

4.2.4 Affinity chromatography reveals potential candidates for Icafolin interaction

The initial attempts at purifying tubulin by means of EPC-affinity chromatography gave rise to the notion of conducting a parallel experiment with Icafolin. Therefore, Icafolin was supplemented with a linker molecule. Following verification of the integrity of the phenomenon, coupling to agarose beads was achieved. The fragmentation process was conducted over an increasing salt gradient, and the proteins present in each fraction were subsequently separated by SDS-PAGE. It can be reasonably assumed that the protein with the highest affinity for Icafolin would require the highest anionic pressure to be released. Consequently, it seems logical that fractions eluted in high salt molarity would contain the protein of interest in a higher probability. Consequently, protein bands derived from higher salt concentrations were subjected to MS analysis. The results indicated the presence of a promising set of potential Icafolin interaction candidates, all of which were identified as being microtubule-associated. The inability to achieve complete elution with the maximum salt concentration of 3M KCl suggests the presence of an unusually strong affinity. The analysis of the ineluteable column remaining demonstrated consistency with the previously obtained results from KCl elution, and revealed the presence of additional proteins with an even tighter binding affinity, which belong to the microtubule nucleation apparatus. Once more, it was demonstrated that

it is not possible to obtain a single candidate by affinity chromatography, despite the apparent high affinity. This finding aligns with the previously obtained results, suggesting that Icafolin does not act on a single protein, but rather on a protein as part of a larger protein complex

4.3 Conclusion

4.3.1 Mode of action: targeting microtubule regulation

In light of the obtained results, it can be concluded that the mode of action of Icafolin is distinct from that of other anti-microtubular agents, such as Oryzalin, Propyzamide, and Colchicine, which act as tubulin dimer sequestrators. While the threshold for named agents is in the range of µM, the threshold for Icafolin in experiments conducted during this study was found to be 30 nM. Given that tubulin can be considered a bulk protein, omnipresent in the cell, positing Icafolin as an additional sequesterer is inconsistent with stoichiometry. The findings of this study indicate that the mode of action may be localised in the regulatory mechanism, including the control of microtubule dynamics. This is evidenced by the ability to slow down the process by the addition of Taxol. While the phenomenon can be reversed by removing Icafolin from cell culture samples, the time required for the cell to fully reestablish the microtubule network does not align with the findings of previous studies investigating reversible binding agents like Propyzamide (Akashi, Izumi et al. 1988). This finding is consistent with the results obtained through Icafolin affinity chromatography. While α-tubulin bound to an EPC-Sepharose column can be eluted in a range of 0.2-0.3 M KCl, elution of proteins bound to an Icafolin-Agarose matrix cannot be achieved even with 3 M KCl. This suggests that the binding of Icafolin to its target is almost irreversible. Consequently, reversible binding of Icafolin does not appear to be the mechanism by which microtubules recover. Furthermore, inhibition studies have demonstrated that *de novo* synthesis is not necessary for microtubule recovery, indicating that this process is not dependent on translation. In conclusion, it is recommended that the target be bound to Icafolin on a permanent basis. It has been demonstrated that the phenotype can be rescued by already present proteins, while the time needed for full recovery is dependent on the concentration and exposure time of the Icafolin impulse. In light of these findings, it can be postulated that a protein complex may serve as the target in this process. The analysis of proteins obtained from affinity chromatography, including those that remained on the column, revealed a set of microtubule-associated proteins that may constitute part of a complex whose functionality is crucial for regulating microtubule dynamics with regard to microtubule nucleation and catastrophe events. Although contractual provisions prohibit the disclosure of the identity of the obtained affinity chromatography candidates, it can be reasonably inferred that the majority are related to the microtubule nucleation machinery. Complexes comprising these proteins were identified in a range of protein

combinations or modifications within the cell. This was evidenced by the discovery of a diverse range of complex sizes, containing components of the identified candidates. These were hypothesised to fulfil a variety of functions, including the recruitment of nucleation factors and the regulation of microtubule dynamics through the binding of factors involved in the control of microtubule stability (Oakley, Paolillo et al. 2015). If Icafolin targets a specific complex isotype containing the target protein, while other complexes present in the cell contain different proteins, the microtubule destabilising effect may be due to the inhibition or sequestration of a complex involved in regulating microtubule stability (**Figs. 33, 34**). Once Icafolin has been removed, the remaining complexes may undergo turnover, potentially releasing the actual binding partner of Icafolin. This could allow for reestablishment of the sequestered complex and subsequent microtubule recovery without the need for *de novo* synthesis of additional proteins. This would also be consistent with the observation of time- and concentration-dependent effects. If Icafolin is present for a longer period of time, the turnover of complexes that shield the binding partner may result in the release of the interaction partner and subsequent sequestration by Icafolin. This could potentially slow down the recovery process by reducing the available target concentration in the cell. In the event of exceedingly high concentrations of Icafolin within the experimental setup, the complete removal of the substance may prove challenging. Consequently, residual Icafolin may potentially engage with complex components that remain available following isotype complex turnover. Given the extremely low threshold exhibited by Icafolin, effects may be observable until the intracellular concentration of free Icafolin falls below the threshold concentration. One potential approach to test this hypothesis would be to block translation and perform multiple Icafolin impulses. The threshold required should decrease after each successful microtubule recovery due to the progressively sequestered target.

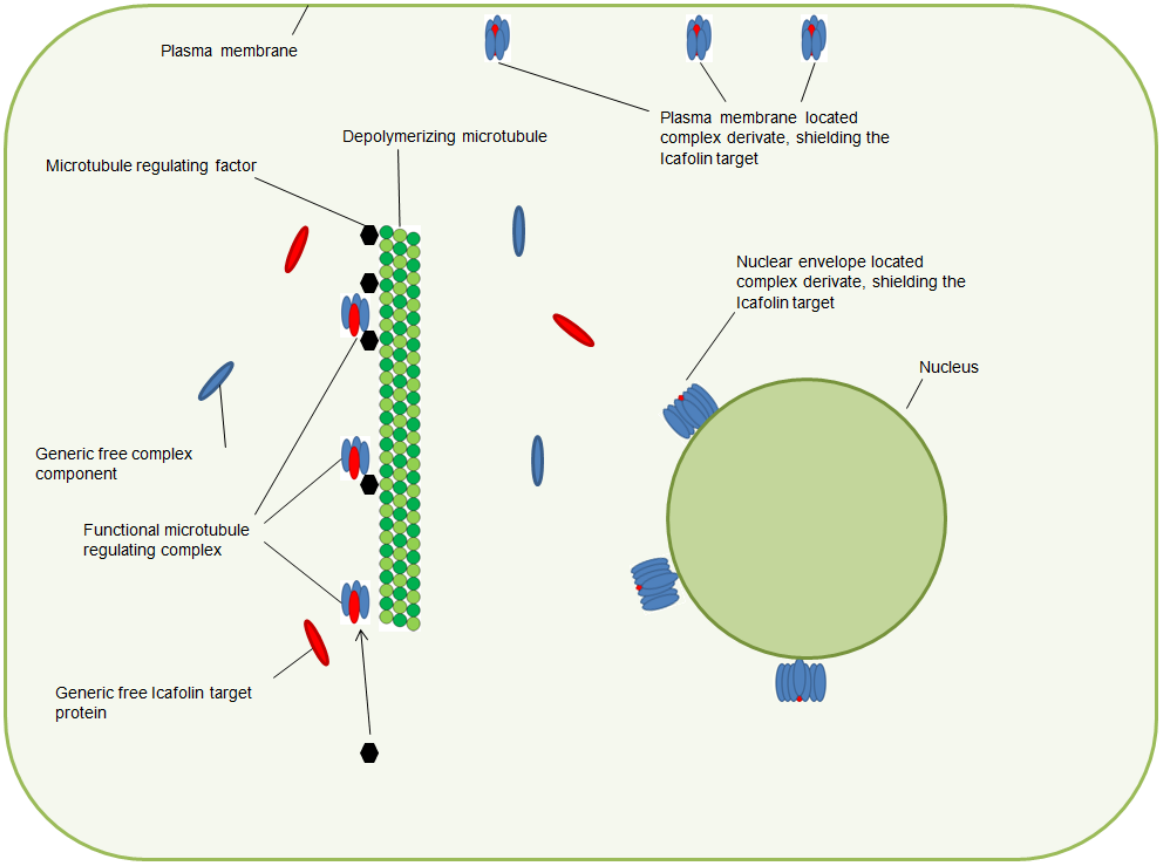

Fig. 33: Model – Icafolin targets a regulating complex: Before Icafolin exposure. *In the hypotezised model, Icafolin acts as sequesterer of a specific protein complex, important for microtubule regulation. The complex might be location along the microtubule lattice and might be able to stabilize the microtubule either by itself, or by recruitment or binding of microtubule regulating factors. The actual interaction partner of Icafolin might be also part of other complexes including modified isotypes of the original microtubule regulating complex.*

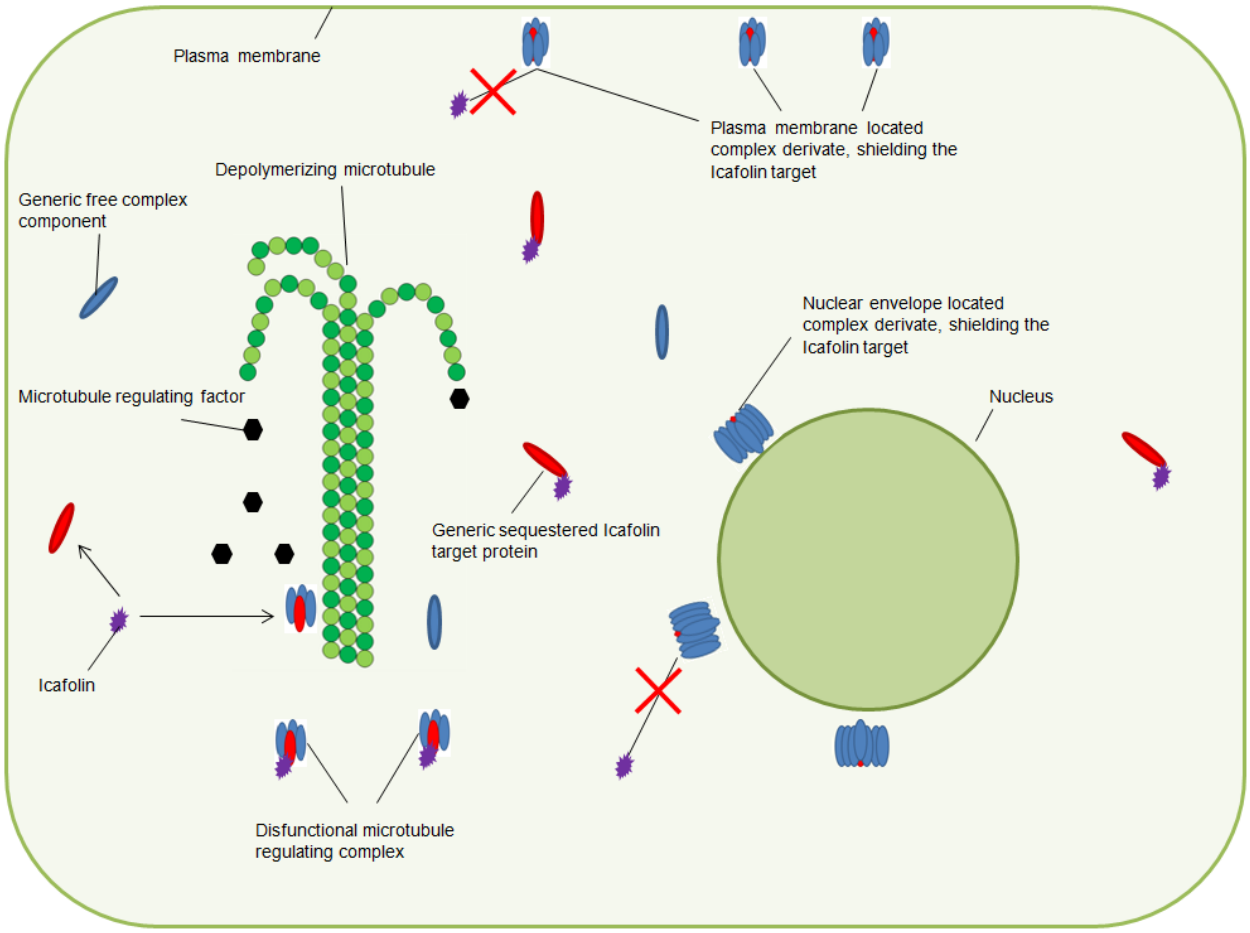

Fig. 34: Model – Icafolin targets a regulating complex: During Icafolin exposure. *In this model, if Icafolin is applied in a sufficient concentration, the regulating complex might be inhibited leading to loss of its stabilizing effect or loss of further recruitment of microtubule regulating factors required for microtubule stability resulting in microtubule catastrophe. The actual binding partner of Icafolin present might be protected by other complex components or modifications.*

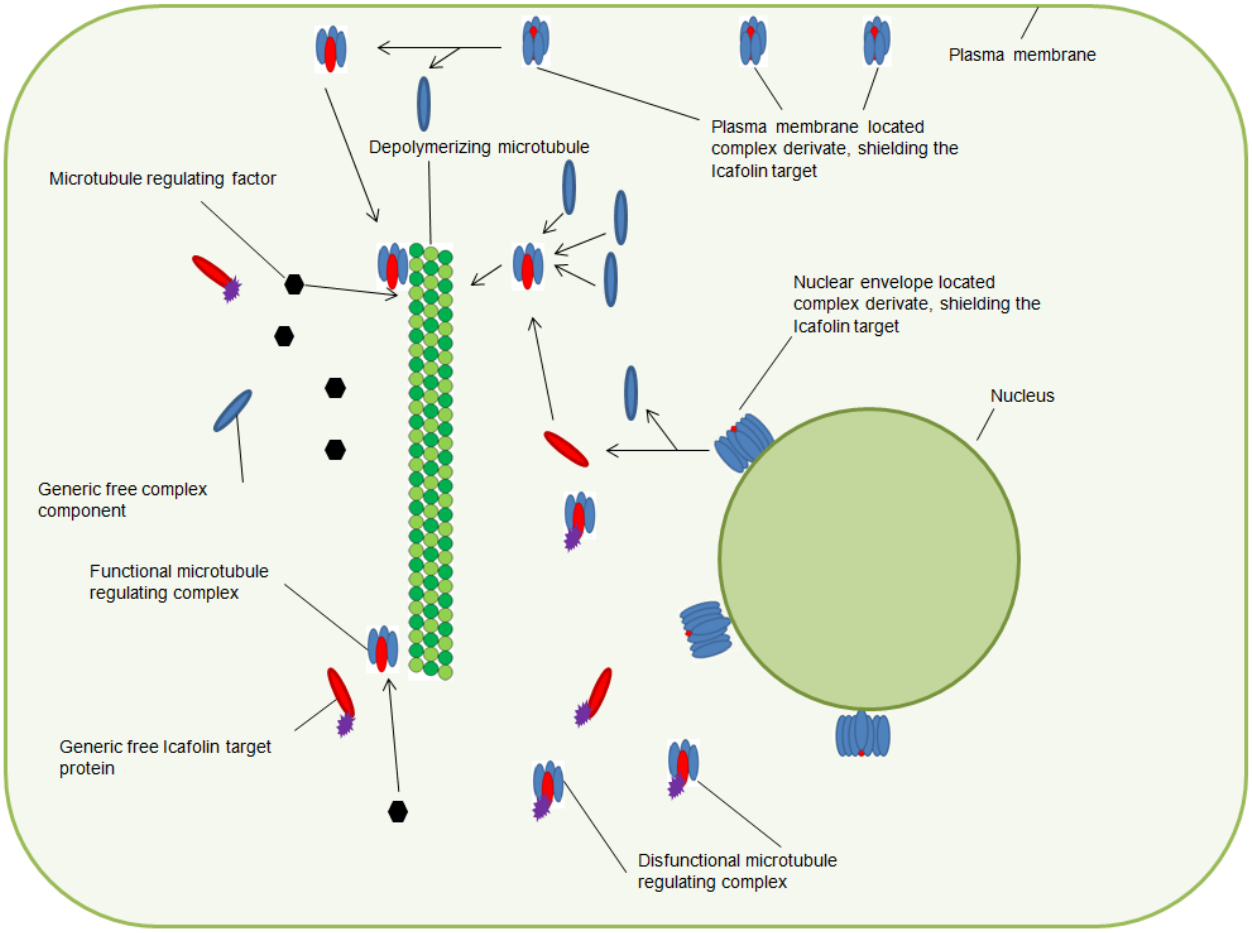

Fig. 35: Model – Icafolin targets a regulating complex: Microtubule recovery after Icafolin removal. *Target complexes and free binding partners might be sequestered, but the turnover or modification of other complexes containing parts of the target complex might lead to release and reformation to functional microtubule regulating complexes over time without the necessity of de novo synthesis of additional proteins.*

4.3.2 Alternative model: targeting tubulin

Although the targeting of tubulin dimers is unlikely to have occurred, the results obtained in this study do not allow to exclude this possibility. This is because tubulin itself could also be detected during affinity chromatography approaches. In order to create a working model for the mode of action of Icafolin, one could hypothesise that tubulin is an interaction partner. This would entail considering a different affinity of Icafolin to free tubulin dimers versus polymerised tubulin at the plus end of a growing or established microtubule. The stability of microtubules is contingent upon the cycle of guanosine triphosphate (GTP) hydrolysis to guanosine diphosphate (GDP). It is established that GTP-tubulin is permanently incorporated into growing plus ends, exhibiting a more linear structure and thereby supporting the stability of the entire microtubule. However, the hydrolysis of GTP-tubulin to GDP-tubulin results in a conformational change, which is widely regarded as the cause of structural tension within the microtubule, thereby promoting microtubule catastrophe. Given that the hydrolysis of GTP is delayed in comparison to the incorporation of additional GTP-tubulin at the plus end, the

region of GTP-containing tubulin is referred to as the GTP cap. If Icafolin demonstrates a markedly enhanced affinity for tubulin as part of the GTP cap and induces a conformational alteration to GDP-tubulin, it may potentially destabilise the microtubule, resulting in depolymerisation. The specific binding to polymerised GTP-tubulin may explain the low threshold needed for efficacy. This finding is consistent with the results of the cell mortality study, which demonstrated that tobacco BY-2 cells overexpressing the endogenous tubulin α3 isotype, which is one amino acid shorter than the typical isotype, exhibited enhanced resistance compared to the wild-type cell line. It may be the case that the difference in the single amino acid is responsible for a reduction in affinity. Furthermore, the enhanced incorporation of this specific isotype in microtubules, caused by overexpression, may result in a higher occurrence of the protein. This hypothesis does not, however, account for the delay in microtubule re-establishment following an Icafolin impulse. One would expect rapid microtubule recovery, as observed with the reversible binding microtubule polymerisation inhibitor Propyzamide, which reports microtubule recovery after approximately 15 minutes following the removal of the substance.

4.4 Outlook

Despite the presentation of indices for the illustrated models created in Chapter 4.3, this study was unable to provide definitive clarification regarding the mode of action of Icafolin. It is recommended that future investigations focus on the Icafolin target candidates obtained from affinity chromatography approaches in this study, as they may prove instrumental in expanding knowledge about the mode of action. To obtain further information regarding the effects of Icafolin on the potential interaction candidates, *A. thaliana* mutants containing T-DNA inserts in the respective coding sequence of the obtained candidate proteins were ordered. The initial experiments did indeed demonstrate resistance phenomena, and thus further investigation is recommended in the follow-up project. As a second approach, an attempt was made to determine the exact candidate protein. This involved coupling Icafolin to a photoaffinity molecule (PA-Icafolin) and additionally radioactive labelling for detection. The molecule is capable of irreversibly binding to proteins in close proximity after an impulse in a specific wavelength, thereby serving as a sensor for interactions by detection of radioactivity. The proposed experiment would entail incubating a cell lysate in the presence of PA-Icafolin in the dark, followed by the application of a light impulse to trigger the photoaffinity reaction after a sufficient incubation period. Subsequently, a denaturation step followed by SDS-PAGE would facilitate the separation of potential complex components, and the obtained bands could be investigated for radioactivity. Should the radioactive band be identified, subsequent MS analysis may reveal the true interaction partner of Icafolin. Furthermore, additional digestion by proteases may even reveal the specific binding site. Following approaches of genome editing, and alteration of the Icafolin binding site, may lead to Icafolin resistance. This could be performed by using the the CRISPR-Cas9 system in an appropriate model organism like Tomato for a first proof of concept. If successful, implementation of this in major crop systems would open the possibility of applying Icafolin on fields during the growing phase of crops.

Furthermore, the identification of the binding partner of Icafolin may facilitate a more profound understanding of microtubule regulation. The presence and functionality of this interaction partner appear to be pivotal for microtubule integrity. Consequently, a more comprehensive investigation into the role of this interaction partner within the microtubule regulatory system may prove highly beneficial for future research projects.

5 Appendix

5.1 Verfication of biological activity of the Icafolin-linker intermediate molecule

The molecule employed in the synthesis of either the affinity matrix (**Chapter 2.15; 3.12**) or the NB-Icafolin construct (**Chapter 2.8; 3.11**) was subjected to preliminary biological activity testing prior to undergoing further processing. A 1 ml sample of a TuA3 cell culture was exposed to 10 µl of the intermediate molecule, incubated for one hour at 25°C under continuous shaking, and the effects on microtubules were then observed via live cell imaging.

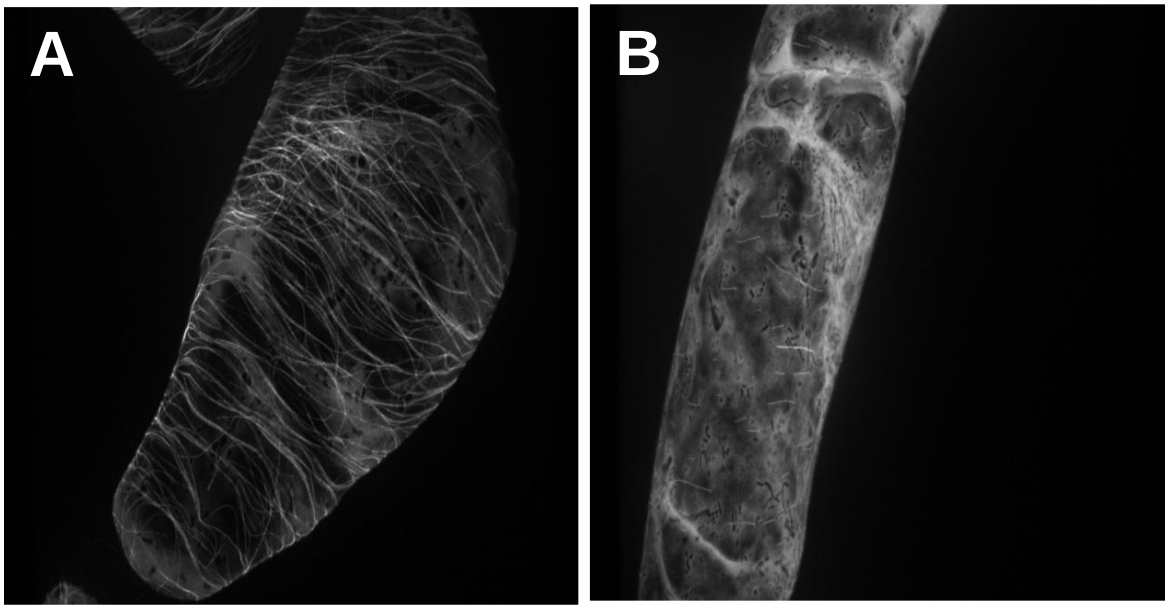

Fig.S1 : TuA3 cells exposed to linker-Icafolin. *A: Untreated TuA3 cell. Microtubules are intact. B: TuA3 cell under influence of linker-Icafolin at 10 µM for 1 h. Microtubules are depolymerised.*

The results demonstrated the efficacy of the linker-Icafolin molecule. While microtubules in untreated TuA3 cells remained intact (**Fig. S1, A**), treatment with 10 µM linker-Icafolin resulted in a clear depolymerisation of microtubules (**Fig. S1, B**).

6 References

Akashi, T., et al. (1988). "Effects of Propyzamide on Tobacco Cell Microtubules In Vivo and In Vitro." Plant and Cell Physiology **29**(6): 1053-1062.

Ambrose, C. and G. O. Wasteneys (2014). "Microtubule Initiation from the Nuclear Surface Controls Cortical Microtubule Growth Polarity and Orientation in Arabidopsis thaliana." Plant and Cell Physiology **55**(9): 1636-1645.

Ambrose, J. C. and R. Cyr (2007). "The kinesin ATK5 functions in early spindle assembly in Arabidopsis." The Plant Cell **19**(1): 226-236.

Ascough, G. D., et al. (2008). "Effectiveness of colchicine and Oryzalin at inducing polyploidy in Watsonia lepida NE Brown." HortScience **43**(7): 2248-2251.

Avila-Garcia, W. V., et al. (2012). "Target-site mutation associated with glufosinate resistance in Italian ryegrass (Lolium perenne L. ssp. multiflorum)." Pest Management Science **68**(9): 1248-1254.

Ballowitz, E. (1888). "Untersuchungen über die Struktur der Spermatozoën, zugleich ein Beitrag zur Lehre vom feineren Bau der contraktilen Elemente." Archiv für mikroskopische Anatomie **32**(1): 401-473.

Baskin, T. I. (2001). "On the alignment of cellulose microfibrils by cortical microtubules: A review and a model." Protoplasma **215**(1): 150-171.

Baskin, T. I., et al. (2004). "Disorganization of Cortical Microtubules Stimulates Tangential Expansion and Reduces the Uniformity of Cellulose Microfibril Alignment among Cells in the Root of Arabidopsis." Plant Physiology **135**(4): 2279-2290.

Baskin, T. I., et al. (1994). "Morphology and Microtubule Organization in Arabidopsis Roots Exposed to Oryzalin or Taxol." Plant and Cell Physiology **35**(6): 935-942.

Beckie, H. J. and F. J. Tardif (2012). "Herbicide cross resistance in weeds." Crop Protection **35**: 15-28.

Benbrook, C. M. (2012). "Impacts of genetically engineered crops on pesticide use in the U.S. -- the first sixteen years." Environmental Sciences Europe **24**(1): 24.

Bharati, R., et al. (2023). "Oryzalin induces polyploids with superior morphology and increased levels of essential oil production in Mentha spicata L." Industrial Crops and Products **198**: 116683.

Blum, H., et al. (1987). "Improved silver staining of plant proteins, RNA and DNA in polyacrylamide gels." ELECTROPHORESIS **8**(2): 93-99.

Böhm, K. J., et al. (1984). "Effect of microtubule-associated proteins on the protofilament number of microtubules assembled in vitro." Biochimica et Biophysica Acta (BBA) - General Subjects **800**(2): 119-126.

Breviario D, Linss M, Nick P (2001). A-tubulins from tobacco: gene cloning and expression studies. NCBI accession CAD13176.

Burgess, J. and D. H. Northcote (1968). "The relationship between the endoplasmic reticulum and microtubular aggregation and disaggregation." Planta **80**(1): 1-14.

Carl Zeiss Microscopy GmbH. (2023). arivis Cloud. www.apeer.com

Chrétien, D. and R. H. Wade (1991). "New data on the microtubule surface lattice." Biology of the Cell **71**(1-2): 161-174.

Cuschieri, L., et al. (2007). "Control At The Cell Center: The Role Of Spindle Poles In Cytoskeletal Organization And Cell Cycle Regulation." Cell Cycle **6**(22): 2788-2794.

Dallai, R. and B. A. Afzelius (1990). "Microtubular diversity in insect spermatozoa: Results obtained with a new fixative." Journal of Structural Biology **103**(2): 164-179.

Dallai, R., et al. (2006). Unusual Axonemes of Hexapod Spermatozoa. International Review of Cytology, Academic Press. **254:** 45-99.

Délye, C., et al. (2013). "Deciphering the evolution of herbicide resistance in weeds." Trends in Genetics **29**(11): 649-658.

Desai, A. and T. J. Mitchison (1997). "Microtubule polymerization dynamics." Annual review of cell and developmental biology **13**(1): 83-117.

Dimitrov, A., et al. (2008). "Detection of GTP-tubulin Conformation in Vivo Reveals a Role for GTP Remnants in Microtubule Rescues." Science **322**(5906): 1353-1356.

Domozych, D. S., et al. (2013). "Disruption of the microtubule network alters cellulose deposition and causes major changes in pectin distribution in the cell wall of the green alga, Penium margaritaceum." Journal of Experimental Botany **65**(2): 465-479.

Duke, S. O. and S. B. Powles (2008). "Glyphosate: a once-in-a-century herbicide." Pest Management Science **64**(4): 319-325.

Field, J. J., et al. (2013). "The binding sites of microtubule-stabilizing agents." Chemistry & biology **20**(3): 301-315.

Gaff, D. and O. Okong'O-Ogola (1971). "The use of non-permeating pigments for testing the survival of cells." Journal of Experimental Botany **22**(3): 756-758.

Gaillard, J., et al. (2008). "Two Microtubule-associated Proteins of Arabidopsis MAP65s Promote Antiparallel Microtubule Bundling." Molecular Biology of the Cell **19**(10): 4534-4544.

Gard, D. L. and M. W. Kirschner (1987). "Microtubule assembly in cytoplasmic extracts of Xenopus oocytes and eggs." J Cell Biol **105**(5): 2191-2201.

Gardiner, J. (2013). "The evolution and diversification of plant microtubule-associated proteins." The Plant Journal **75**(2): 219-229.

Goldmacher, V. S., et al. (2015). "High-affinity accumulation of a maytansinoid in cells via weak tubulin interaction." PLoS One **10**(2): e0117523.

Goodwin, S. S. and R. D. Vale (2010). "Patronin regulates the microtubule network by protecting microtubule minus ends." Cell **143**(2): 263-274.

Goshima, G. and A. Kimura (2010). "New look inside the spindle: microtubule-dependent microtubule generation within the spindle." Current Opinion in Cell Biology **22**(1): 44-49.

Goshima , G., et al. (2008). "Augmin: a protein complex required for centrosome-independent microtubule generation within the spindle." Journal of Cell Biology **181**(3): 421-429.

Granger, C. L. and R. J. Cyr (2001). "Use of abnormal preprophase bands to decipher division plane determination." Journal of Cell Science **114**(3): 599-607.

Green, J. M. (2014). "Current state of herbicides in herbicide-resistant crops." Pest Management Science **70**(9): 1351-1357.

Green, P. B. (1962). "Mechanism for Plant Cellular Morphogenesis." Science **138**(3548): 1404-1405.

Hachisu, S. (2021). "Strategies for discovering resistance-breaking, safe and sustainable commercial herbicides with novel modes of action and chemotypes." Pest Management Science **77**(7): 3042-3048.

Hashimoto, T. (2013). "A ring for all: γ-tubulin-containing nucleation complexes in acentrosomal plant microtubule arrays." Current Opinion in Plant Biology **16**(6): 698-703.

Hashimoto, T. (2015). "Microtubules in plants." Arabidopsis Book **13**: e0179.

Heap, I. (2014). "Global perspective of herbicide-resistant weeds." Pest Management Science **70**(9): 1306-1315.

Heap, I. and S. O. Duke (2018). "Overview of glyphosate-resistant weeds worldwide." Pest Management Science **74**(5): 1040-1049.

Heap I. The International Herbicide-Resistant Weed Database (2024). Available from: www.weedscience.org.

Ho, C.-M. K., et al. (2011). "Interaction of Antiparallel Microtubules in the Phragmoplast Is Mediated by the Microtubule-Associated Protein MAP65-3 in Arabidopsis " The Plant Cell **23**(8): 2909-2923.

Hohenberger, P., et al. (2011). "Plant actin controls membrane permeability." Biochimica et Biophysica Acta (BBA)-Biomembranes **1808**(9): 2304-2312.

Horio, T. and H. Hotani (1986). "Visualization of the dynamic instability of individual microtubules by dark-field microscopy." Nature **321**(6070): 605-607.

HRAC (Herbicide Resistance Action Committee) (2024). "2024-HRAC-Global-Herbicide-MoA-Classification-Master-List. https://hracglobal.com/tools/2024-hrac-global-herbicide-moa-classification

Huang, X., et al. (2017). "Sensory role of actin in auxin-dependent responses of tobacco BY-2." Journal of Plant Physiology **218**: 6-15.

Hugdahl, J. D. and L. C. Morejohn (1993). "Rapid and Reversible High-Affinity Binding of the Dinitroaniline Herbicide Oryzalin to tubulin from Zea mays L." Plant Physiol **102**(3): 725-740.

Hutchins, J. R. A., et al. (2010). "Systematic Analysis of Human Protein Complexes Identifies Chromosome Segregation Proteins." Science **328**(5978): 593-599.

Ishida, T., et al. (2007). "Helical microtubule arrays in a collection of twisting tubulin mutants of Arabidopsis thaliana." Proceedings of the National Academy of Sciences **104**(20): 8544-8549.

Jabran, K., et al. (2015). "Allelopathy for weed control in agricultural systems." Crop Protection **72**: 57-65.

Janski, N., et al. (2012). "The GCP3-Interacting Proteins GIP1 and GIP2 Are Required for γ-tubulin Complex Protein Localization, Spindle Integrity, and Chromosomal Stability " The Plant Cell **24**(3): 1171-1187.

Kaźmierczak, A., et al. (2023). "Kinetin induces microtubular breakdown, cell cycle arrest and programmed cell death in tobacco BY-2 cells." Protoplasma **260**(3): 787-806.

Kennard, J. L. and A. L. Cleary (1997). "Pre-mitotic nuclear migration in subsidiary mother cells of Tradescantia occurs in G1 of the cell cycle and requires F-actin." Cell Motility **36**(1): 55-67.

Kimmy Ho, C.-M., et al. (2011). "Augmin Plays a Critical Role in Organizing the Spindle and Phragmoplast Microtubule Arrays in Arabidopsis." The Plant Cell **23**(7): 2606-2618.

Kollman, J. M., et al. (2015). "Ring closure activates yeast γTuRC for species-specific microtubule nucleation." Nature Structural & Molecular Biology **22**(2): 132-137.

Kollman, J. M., et al. (2011). "Microtubule nucleation by γ-tubulin complexes." Nature Reviews Molecular Cell Biology **12**(11): 709-721.

Kraehmer, H. (2012). "Innovation: Changing Trends in Herbicide Discovery." Outlooks on Pest Management **23**(3): 115-118.

Krtková, J., et al. (2012). "Hsp90 binds microtubules and is involved in the reorganization of the microtubular network in angiosperms." Journal of Plant Physiology **169**(14): 1329-1339.

Kumagai, F., et al. (2001). "Fate of nascent microtubules organized at the M/G1 interface, as visualized by synchronized tobacco BY-2 cells stably expressing GFP-tubulin: time-sequence observations of the reorganization of cortical microtubules in living plant cells." Plant and Cell Physiology **42**(7): 723-732.

Ledbetter, M. C. and K. R. Porter (1963). "A "MICROTUBULE" IN PLANT CELL FINE STRUCTURE." J Cell Biol **19**(1): 239-250.

Ledbetter, M. C. and K. R. Porter (1964). "Morphology of Microtubules of Plant Cell." Science **144**(3620): 872-874.

Lee, Y.-R. J. and B. Liu (2013). "The rise and fall of the phragmoplast microtubule array." Current Opinion in Plant Biology **16**(6): 757-763.

Leterrier, J. F., et al. (1990). "How do microtubules interact in vitro with purified subcellular organelles?" Biochem J **269**(2): 556-558.

Liu, T., et al. (2014). "Augmin triggers microtubule-dependent microtubule nucleation in interphase plant cells." Current Biology **24**(22): 2708-2713.

Loiodice, I., et al. (2019). "Quantifying tubulin Concentration and Microtubule Number Throughout the Fission Yeast Cell Cycle." Biomolecules **9**(3).

Maisch, J. and P. Nick (2007). "Actin is involved in auxin-dependent patterning." Plant Physiology **143**(4): 1695-1704.

Manton, I. (1950). "Demonstration of Compound Cilia in a Fern Spermatozoid by Means of the Ultra-violet Microscope." Journal of Experimental Botany **1**(1): 69-70.

Manton, I. (1957). "Observations with the Electron Microscope on the Cell Structure of the Antheridium and Spermatozoid of Sphagnum." Journal of Experimental Botany **8**(3): 382-400.

Manton, I. and B. Clarke (1952). "An Electron Microscope Study of the Spermatozoid of Sphagnum." Journal of Experimental Botany **3**(9): 265-275.

Masuda, H., et al. (2013). "Fission yeast MOZART1/Mzt1 is an essential γ-tubulin complex component required for complex recruitment to the microtubule organizing center, but not its assembly." Molecular Biology of the Cell **24**(18): 2894-2906.

Mesnage, R., et al. (2021). Herbicides: Brief history, agricultural use, and potential alternatives for weed control.

Miguel, T. P. and K. W. Leonhardt (2011). "In vitro polyploid induction of orchids using Oryzalin." Scientia Horticulturae **130**(1): 314-319.

Mitchison, T. and M. Kirschner (1984). "Dynamic instability of microtubule growth." Nature **312**(5991): 237-242.

Mizuno, K., et al. (1981). "Isolation of plant tubulin from azuki bean epicotyls by ethyl N-phenylcarbamate-Sepharose affinity chromatography." J Biochem **89**(1): 329-332.

Mohan, R. and A. John (2015). "Microtubule-associated proteins as direct crosslinkers of actin filaments and microtubules." IUBMB Life **67**(6): 395-403.

Morejohn, L., et al. (1987). "Oryzalin, a dinitroaniline herbicide, binds to plant tubulin and inhibits microtubule polymerization in vitro." Planta **172**: 252-264.

Mortz, E., et al. (2001). "Improved silver staining protocols for high sensitivity protein identification using matrix-assisted laser desorption/ionization-time of flight analysis." PROTEOMICS **1**(11): 1359-1363.

Murata, T., et al. (2013). "Mechanism of microtubule array expansion in the cytokinetic phragmoplast." Nature Communications **4**(1): 1967.

Nagata, T., et al. (1992). Tobacco BY-2 cell line as the “HeLa” cell in the cell biology of higher plants. International review of cytology, Elsevier. **132:** 1-30.

Nakamura, M., et al. (2004). "Low concentrations of Propyzamide and Oryzalin alter microtubule dynamics in Arabidopsis epidermal cells." Plant and Cell Physiology **45**(9): 1330-1334.

Nakamura, M., et al. (2012). "Arabidopsis GCP3-interacting protein 1/MOZART 1 is an integral component of the γ-tubulin-containing microtubule nucleating complex." The Plant Journal **71**(2): 216-225.

Nick, P. (1998). Signaling to the microtubular cytoskeleton in plants. International review of cytology, Elsevier. **184:** 33-80.

Nick, P. (2013). "Microtubules, signalling and abiotic stress." The Plant Journal **75**(2): 309-323.

Nogales, E., et al. (1998). "Erratum: Structure of the αβ tubulin dimer by electron crystallography." Nature **393**(6681): 191-191.

Noodén, L. D. (1971). "Physiological and developmental effects of colchicine." Plant and Cell Physiology **12**(5): 759-770.

Oakley, B. R., et al. (2015). "γ-tubulin complexes in microtubule nucleation and beyond." Mol Biol Cell **26**(17): 2957-2962.

Oerke, E.-C. (2006). "Crop losses to pests." The Journal of agricultural science **144**(1): 31-43.

Oerke, E.-C., et al. (2012). Crop production and crop protection: estimated losses in major food and cash crops, Elsevier.

Ofosu, R., et al. (2023). "Herbicide Resistance: Managing Weeds in a Changing World." Agronomy **13**(6): 1595.

Orlando, F., et al. (2020). "Participatory approach for developing knowledge on organic rice farming: Management strategies and productive performance." Agricultural systems **178**: 102739.

Paredez, A. R., et al. (2006). "Visualization of Cellulose Synthase Demonstrates Functional Association with Microtubules." Science **312**(5779): 1491-1495.

Paschal, B. M., et al. (1989). "Interaction of brain cytoplasmic dynein and MAP2 with a common sequence at the C terminus of tubulin." Nature **342**(6249): 569-572.

Peterson, G. E. (1967). "The Discovery and Development of 2,4-D." Agricultural History **41**(3): 243-254.

Powles, S. B. and Q. Yu (2010). "Evolution in Action: Plants Resistant to Herbicides." Annual Review of Plant Biology **61**(Volume 61, 2010): 317-347.

Pratley, J., et al. (1999). "Resistance to glyphosate in Lolium rigidum. I. Bioevaluation." Weed Science **47**(4): 405-411.

Qu, R.-Y., et al. (2021). "Where are the new herbicides?" Pest Management Science **77**(6): 2620-2625.

Rajcan, I. and C. J. Swanton (2001). "Understanding maize–weed competition: resource competition, light quality and the whole plant." Field crops research **71**(2): 139-150.

Rasmussen, C. G., et al. (2011). "Determination of Symmetric and Asymmetric Division Planes in Plant Cells." Annual Review of Plant Biology **62**(Volume 62, 2011): 387-409.

Rüegg, W. T., et al. (2007). "Herbicide research and development: challenges and opportunities." Weed Research **47**(4): 271-275.

Ryan, G. (1970). "Resistance of common groundsel to simazine and atrazine." Weed Science **18**(5): 614-616.

Sammak, P. J. and G. G. Borisy (1988). "Direct observation of microtubule dynamics in living cells." Nature **332**(6166): 724-726.

Schulte, M. (2005). "Transgene herbizidresistente Kulturen." Gesunde Pflanzen **57**(2-3): 37-46.

Shaner, D. L. (2014). "Lessons Learned From the History of Herbicide Resistance." Weed Science **62**(2): 427-431.

Smith, A. E. and D. M. Secoy (1975). "Forerunners of pesticides in classical Greece and Rome." Journal of Agricultural and Food Chemistry **23**(6): 1050-1055.

Sui, H. and K. H. Downing (2010). "Structural basis of interprotofilament interaction and lateral deformation of microtubules." Structure **18**(8): 1022-1031.

Sweeney, H. L. and E. L. Holzbaur (2018). "Motor proteins." Cold Spring Harbor Perspectives in Biology **10**(5): a021931.

Teixidó-Travesa, N., et al. (2012). "The where, when and how of microtubule nucleation – one ring to rule them all." Journal of Cell Science **125**(19): 4445-4456.

Twell, D., et al. (2002). "MOR1/GEM1 has an essential role in the plant-specific cytokinetic phragmoplast." Nature Cell Biology **4**(9): 711-714.

Umeyama, T., et al. (1993). "Dynamics of microtubules bundled by microtubule associated protein 2C (MAP2C)." Journal of Cell Biology **120**(2): 451-465.

UN. Population Division (2001). Department of economic, social affairs. Population, Environment and Development: The Concise Report (Vol. 202): United Nations Publications.

Van Damme, D. (2009). "Division plane determination during plant somatic cytokinesis." Current Opinion in Plant Biology **12**(6): 745-751.

Voigt, B., et al. (2005). "GFP-FABD2 fusion construct allows in vivo visualization of the dynamic actin cytoskeleton in all cells of Arabidopsis seedlings." European journal of cell biology **84**(6): 595-608.

Weisenberg, R. C., et al. (1968). "Colchicine-binding protein of mammalian brain and its relation to microtubules." Biochemistry **7**(12): 4466-4479.

Whittington, A. T., et al. (2001). "MOR1 is essential for organizing cortical microtubules in plants." Nature **411**(6837): 610-613.

Young, D. H. and V. T. Lewandowski (2000). "Covalent Binding of the Benzamide RH-4032 to tubulin in Suspension-Cultured Tobacco Cells and Its Application in a Cell-Based Competitive-Binding Assay." Plant Physiology **124**(1): 115-124.

Yuan, J. S., et al. (2007). "Non-target-site herbicide resistance: a family business." Trends in Plant Science **12**(1): 6-13.

Zeng, C. J. T., et al. (2009). "The WD40 Repeat Protein NEDD1 Functions in Microtubule Organization during Cell Division in Arabidopsis thaliana " The Plant Cell **21**(4): 1129-1140.

Zimdahl, R. (2013). Fundamentals of Weed Science. Fourt Edition, London: Elsevier Inc.